UNIVERSITY OF CALIFORNIA,
IRVINE

A Renewable and Clean Energy Solution for Microgrid Reliability and Resiliency in Novel Operational Scenarios

DISSERTATION

submitted in partial satisfaction of the requirements
for the degree of

DOCTOR OF PHILOSOPHY

in Electrical and Computer Engineering

by

Weixi Wang

Dissertation Committee:
Professor Jack Brouwer, Co-Chair
Professor Pramod Khargonekar, Co-Chair
Professor Keyue Smedley

2024

DEDICATION

To

my parents and friends

LIST OF CONTENTS

LIST OF FIGURES

LIST OF TABLES

Nomenclature

ACPF – AC Power Flow

CPUC - California Public Utilities Commission

DER – Distributed Energy Resource

DG – Distributed Generation

ESS - Energy Storage System

EV – Electric Vehicle

NEM – Net Energy Metering

NHTS - National Household Travel Survey

NREL - National Renewable Energy Laboratory

PSPS - Public Safety Power Shutoff

PNNL - Pacific Northwest National Laboratory

PV System – Photovoltaic System

MG - Microgrid

OVMG Project – Oak View Microgrid Project

SCE – Socal Edison

URBANopt - Urban Renewable Building and Neighborhood optimization

ACKNOWLEDGEMENTS

I would like to express the deepest appreciation to my committee Chair, Professor Jack Brouwer, whose brilliant mentorship has provided me with incredible research ideas and led to this research work.

I would also like to thank my committee Co-chair, Professor Pramod Khargonekar and committee member Professor Keyue Smedley, for serving on my doctoral committee and furthering the committee's ability to evaluate and instruct.

In addition, I would like to thank Dr. Robert Flores, who has been incredibly helpful all the time to me on optimization process, electric vehicle as well as microgrid system modeling.

I would also like to thank Dr. Ghazal Razeghi, Dr. Laura Novoa, Dr. Jennifer Lee, Victor Klumper for their help during my PhD study.

I would like to specially thank my mom for her wonderful support during my time at University of California, Irvine. To mom: You are the reason I am able to study abroad and make it happen.

VITA

Weixi Wang

University of California, Irvine

Doctor of Philosophy, Electrical and Computer Engineering 09/2019-06/2024

University of California, Irvine

Master of Science, Electrical and Computer Engineering 09/2019-12/2022

Southeast University, Nanjing, China

Bachelor of Engineering, Electrical Engineering 08/2015-06/2019

FIELD OF STUDY

Electrical Engineering with a focus on microgrid systems.

PUBLICATIONS

- Wang W, Flores R, Razeghi G, Brouwer J. Quantifying Transformer and Cable Degradation in Highly Renewable Electric Distribution Circuits. 2023 IEEE PES Grid Edge Technol Conf Expo Grid Edge 2023 2023:1–5. https://doi.org/10.1109/GridEdge54130.2023.10102733.
- Flores R, Houssainy S, Wang W, Joseph R, Cu KN, Polly B, et al. Developing and Tuning a Community Scale Energy Model for a Disadvantaged Community. Energy Build 2023:112861. https://doi.org/10.1016/j.enbuild.2023.112861.
- Jilin C, Min Z, Zhonghua G, Weijiang Q, Yong C, Weixi W. The application of douglas-peucker algorithm in collaborative system for power grid operation mode calculation. MATEC Web Conf 2018;175. https://doi.org/10.1051/matecconf/201817503041.
- Ding P, Zhao M, Tian P, Wang W, Xu X, Cai J. An electromechanical transient simulation method based on frequency-dependent network equivalent and time-varying dynamic phasor DC model. Power Syst Technol 2019;43:1658–65.

• GUO Z, WANG Y, GUO Y, WANG W. Full Time Domain Storage Method for Power Grid Data. DEStech Trans Comput Sci Eng 2019:309–15. https://doi.org/10.12783/dtcse/ammms2018/27279.

• Flores R, Houssainy S, Wang W, Cu KN, Nie X, Woolfolk N, et al. Addressing Building Related Energy Burden, Air Pollution, and Carbon Emissions of a Low-Income Community in Southern California. Adv Appl Energy 2024;14:100169. https://doi.org/10.1016/j.adapen.2024.100169.

ABSTRACT OF THE DISSERTATION

A Renewable and Clean Energy Solution for Microgrid Reliability and Resiliency in Novel Operational Scenarios

by

Weixi Wang

Doctor of Philosophy in Electrical and Computer Engineering

University of California, Irvine, 2024

Professor Jack Brouwer, Co-chair

Professor Pramod Khargonekar, Co-chair

Growing negative impacts from climate change have increased the popularity of microgrid systems. However, novel and developing microgrid scenarios have brought uncertainty to the reliable operation and resiliency of the grid systems. This dissertation is concerned with using renewable, clean energy sources to enhance microgrid reliability and resiliency in novel grid operational scenarios.

The dissertation starts with the modeling of an AC Power Flow (ACPF) model for a disadvantaged community, the Oak View Community, located in Huntington Beach, CA, based on OpenDSS. The model's computing ability is then enhanced with a MATLAB-OpenDSS interface before the model is tested with a cross-platform comparison to confirm accuracy.

The community ACPF model is then integrated with renewable and clean energy systems through four distinct operational scenarios. The initial scenario involves EV adoption within the community by employing a stochastic approach to generate and assign discrete EV charging events using the Monte Carlo algorithm. Subsequently, this scenario is

extended to encompass the broader region of Southern California. The second operational scenario focuses on islanding strategies during Public Safety Power Shutoff (PSPS) events. An optimal algorithm is developed utilizing multilevel graph partitioning techniques. Then, the dissertation explores the deployment of Distributed Energy Resources (DERs) with NEM 3.0 ratings for cost optimization. A Mixed Integer Linear Programming (MILP) algorithm is employed to determine the optimal sizing and dispatch of DERs while adhering to infrastructure degradation constraints. Ultimately, the dissertation introduces a novel microgrid design framework inspired by and abstracted from the author's work on the project.

Following the power quality and degradation evaluations of the scenarios under consideration, it is shown that the current electric infrastructure in Southern California, especially distribution and transmission transformers, lacks the capacity to support the increasing electric demand driven by the EV market. Addressing this issue necessitates significant investments in transformer upgrades and/or the implementation of additional load management measures. The simulation results also find that DER/ESS solution with transformer limit constraint emerges as approximately ten times larger on average in TDV cost compared to the highest average cost incurred by infrastructure upgrade solutions.

1 INTRODUCTION

With increasing awareness of global warming and its devastating effect on human life by the general public, clean and renewable energy solutions are catching the attention of more and more researchers. Distinguished by its by-design adoption of distributed generation (DG) and Net Zero Emissions (NZE) compatibility, microgrid systems have been widely considered good platforms to deploy sustainable energy resources and thereby combating global warming. Due to the traits mentioned above, microgrids have been funded for R&D activities, subsidized for development, tested with case studies throughout the US with federal and statewide level, and sometimes even municipal support. As early as the 1990s US lawmakers started to consider microgrid applications. In 1992 the US congress has passed microgrid related regulation in 1992 US Energy Policy Act [1], and the effort was further amended in 2004 with 2004 US Energy Policy Act [2]. Most recently, president Joe Biden's administration have passed a series of laws to fund and boost the use of microgrids throughout the nation [3][4]. State level microgrid work has also become increasingly common. One well-known effort is California's incentivized microgrid deployment support as stated in CA Senate Bill No. 1339 [5][6], which is administered by California Public Utilities Commission (CPUC) [7] [8]. Several municipal level microgrid projects have also taken place. The City of Santa Barbara, CA has established its own solar power plants through mass use of microgrid systems [9], and the city of Hunting Beach and Irvine in California have also spent extensive effort on building their own local microgrids [10]. Further local development of microgrid systems throughout US can be found in [11].

While initially powered by fossil fuels, microgrid systems in recent years have been relying increasingly on renewable energy. The main driving forces for the transition include the significant cost reduction of renewable energy infrastructure technologies, their appropriate use in distributed applications, and their preference for sustainability [12]. By deploying a high penetration of on-site distributed energy resources (DER) and energy storage systems (ESS), most commonly Photovoltaic (PV) systems, electricity demands throughout a microgrid system are able to remain to a certain extent and in some cases, completely, self-sufficient. Therefore, less energy import is needed from macro-grid and thus centralized generators, which mainly operate on fossil fuels [13], resulting in an overall reduction of greenhouse gas (GHG) emissions.

In addition to the ability to bring down GHG emissions, microgrid systems also mitigate consequences from existing GHG emissions and enhance the overall grid reliability by keeping the power on during macro-grid interruptions such as public safety power shutoff (PSPS), wildfire, earthquake, hurricanes, storms and other extreme weather events. While remaining able to work with grid-connected operation mode in normal situations, during the emergency times when either the centralized macro-grid can no longer provide the grid customers the power with acceptable power quality or when power is intentionally interrupted (as in PSPS events), a microgrid systems can work in islanded mode and isolate itself from the main grid with the help of DER, ESS and appropriate switchgear. With enough DER penetration rate and proper control from the energy management system (EMS), it is possible for a microgrid systems to power itself independently for a considerable amount of time until the macro-grid interruption is fixed.

However, development and changes in electrical consumption by utility customers are posing challenges on the reliable operation and design of microgrid systems. One of the biggest changes in daily domestic electrical use is the growing market of electric vehicles (EV) [14]. Incentivized and looking for a less expensive way to commute, more people are adopting EV over the increasing cost of gasoline [15]. The way EV changes the energy consumption habit and challenges microgrid operational reliability is mainly threefold. First, EV charging increases daily electric demand and therefore puts extra pressure on macro-grid abilities to produce, transmit and distribute the power. For many existing US communities, key electrical infrastructures including distribution transformers and power cables were only built to support traditional power demands, and a very high penetration of EV in a disadvantaged community may very well make the mentioned infrastructure degrade significantly in a short period of time and crash the entire system, as seen in [16]. Secondly, the magnitude and diversity of EV charging types is reshaping the power consumption map. With more EV deployed, not only will the electric demand in residential sectors increase which is a result of Home Level 1 and Home Level 2 charging, the commercial and industrial (C&I) sectors will also see an increase as people charge their EVs during work or out in public charging stations. The major challenge of EV charging of different type is that the synchronicity of them in terms of time and location, which creates issues for microgrid control. Thirdly, the growing development of Vehicle-to-Grid (V2G) technology complicates microgrid dispatch. Using the EV battery as an additional form of DER, V2G technology enables the bidirectional charging of EV and eventually increases the challenges for grid and microgrid operators/controllers.

Other significant changes in recent years that help forge novel electric scenarios include the policymakers' openness to individual sell-back of excess power from renewable DER. As a pioneer in novel power markets, the California Public Utilities Commission (CPUC) established the framework for net energy metering (NEM) back in 1995 in accordance with the legislation of California senate bill (SB) 656 [17] that encourages and allows customers to use their self-installed renewable generators to reduce energy dependance on the macro-grid and to even sell back any excess power. These net metering policies and tariffs have been updated over time leading up to the most recent program changes included in NEM 3.0 of 2023 for CA customers, which comes along with even more viable long-term support for renewable DER and ESS and detailed guidance [18]. Many other states in US and throughout the world have followed to implement policies in support of DER and ESS similar to those of California. The question by the increasing openness of energy trading to microgrid operators and designers is that the whole new concept is challenging the existing framework on how traditional microgrid works and new techniques are much needed for it to work reliably.

Many technical and policy challenges must be overcome before microgrid systems can be widely deployed to reliably integrated with the macro-grid and coupled with renewable and clean energy systems. Although the idea of widespread use of 100% renewable microgrid systems seems desireable for GHG emission reduction, close to 90% of installed US microgrids are currently fossil fuel powered [19]. The novel yet steadily developing operations in electrical markets mentioned above are also making it challenging to operate and dispatch microgrids. The current work contributes to the development of reliable and

resilient microgrid design using renewable and clean energy resources and is accomplished by:

1. Constructing the baseline alternating current (AC) power flow (ACPF) model in OpenDSS based on the Oak View Community located in Huntington Beach, California for the Oak View Microgrid (OVMG) Project as testbed for microgrid development.
2. Validating the simulation capabilities of the OpenDSS based OVMG ACPF model.
3. Extending the computing methods of OVMG ACPF model to support high speed computing and operating and to support multi-interface collaboration.
4. Adopting renewable and clean energy systems into the OVMG system under various novel operational scenarios.
5. Evaluating the electrical and financial impacts of novel operational scenarios as well as that of renewable and clean energy resources on the OVMG system as well as the entire Southern California area.

1.1 Literature Review

1.1.1 Microgrid and Topology Design Overview

A successful microgrid system is always the key to quality microgrid design. With the promise of microgrids in mind, the popularity of microgrid design has been skyrocketing in recent years. Normally, existing microgrid design can be divided into three general categories: microgrid control design, microgrid topology design and hybrid of both.

Microgrid control design or planning focuses on optimization of microgrid operation. Several control design strategies have been published. In 2015, a distributed cooperative control strategy for ESS in regards of local power balance related to charging/discharging efficiency was proposed [20]. A control strategy on various layers of hierarchical control architecture of microgrids on par with traditional power system also proved economically efficient in 2016 [21]. It is worth mentioning that a model predictive control approach based on a mixed integer linear programming (MILP) algorithm was presented to optimize time-variable goals such as optimum charge/discharge schedule [22].

Microgrid topology design, on the other hand, can be categorized into two kinds, one being planning and building from scratch to get desired conditions, the other being refurbishment and upgrade from existing topology. Some relevant studies are found and listed in accordance with the first criteria mentioned for microgrid topology design. Based on survivability schemes, one topology design involves a reconnection of a few small microgrid network communities which changes over time, aiming at reliability by optimized harness of renewable energy

sources [23] . Topology design in [24] and [25] efficiently combines graph partitioning algorithm with MILP to reach local energy equilibrium when generating islands and remaking connections for mesh circuits. Multi-Objective Substrate Layer Coral Reefs Optimization Algorithm (Mo-SL-CRO) was applied by Jiménez-Fernández, S et al. to decide distribution of DERs and optimal connection of different nodes [26]. A viable restructuring of existing microgrids using phase angle measurements of the swing equations was announced by S. Talukdar et al. based on multivariate Wiener filtering to reconstruct operating radial power grids [27].

Fewer research efforts for designing the microgrid from existing grid systems have been initiated compared to the first one. One interesting probabilistic reliability index based topology design has been proposed to partition the grid system into microgrids after optimizing reliability or a combination of reliability and supply-security [28]. A novel robust optimization approach suggested by F. S. Gazijahani et al. enables researchers to determine allocation and parameters of key elements of microgrids such as DG and ESS before island existing grid into reconfigurable microgrids with profit and reliability considered [29]. Another option to optimally add and configure DG on existing grid circuits without changing original connections was proposed by M. V. Kirthiga et al. using sizing algorithm for an autonomous operation [30].

Normal aspects considered for microgrid design are assorted, usually depending on the design task the researchers are given. Reliability is probably the most considered factor. For instance, Erol-Kantarci et al. and Cortes et al. all depict reliability as optimization goal in their papers, with one using renewable energy occupation maximization and the other using cooperation of loop design and performance index to reach the goal [23] [25]. Local power balance within islands is also popular. One topology design in [24] describes how efficient

partitioning of grid can influence power supply/demand balance within each island generated. In [31] a supervision design to predict DC microgrid power flow with multiple factors considered using ILP algorithm was developed. Financial profit is another point commonly seen for consideration. Nguyen DT et al, and Gazijahani et al, illustrate the increase of grid profit by risk-constrained stochastic programming and game theory in [32] and [33], respectively. A novel block-chain involved microgrid design proposed by Tsao, Y et al. optimizes the use of renewable energy units to gain network profit along with reduced risk by robust type-2 fuzzy programming [34].

Some papers also take into consideration special requirements along with the normal aspects mentioned above. First to mention, some paper specially aims at a certain type of circuit type. For instance, as discussed in [35], Qin, M et al. applied extended DistFlow model of AC-OPF to the problem and an MILP algorithm involved method was proposed to solve operation of ESS specifically in radial networks; the coordinated control of radial grid system with multi-agent system (MAS) was investigated in [36]. On the contrary, Almadhor A discussed the availability of using small mesh circuits in the grid as control route for PV monitoring [37], while another scenario including small scale mesh connections is discussed in [38] using modified L1 Adaptive control method. [24] and [25] are designed for mesh grids as well.

Also, grid type in terms of special types of electricity is another special feature that is sometime considered for research purposes. While most research exploits AC grids, such as [39] [40] [41] [42] [43], several papers have set their focus upon DC microgrid topology design. Chen YK et al. presents a fuzzy control method for DC microgrids by design an energy management system (EMS) in [44]. Kumar M et al. proposes a control strategy involving two Synchronous

Reference Frames for a DC microgrid [45]. Some research even goes as far as AC/DC hybrid microgrids, such as that designed and evaluated in [46], [47] and [48].

1.1.2 Renewable and Clean Energy Resources and Measures in Microgrids

With a microgrids' inherent ability to use DERs as the primary energy resources, increasing use of sustainable energy sources are seen in recent microgrid development as the awareness of climate change and air pollution and their negative effects are becoming more widely recognized. While common renewable energy sources are clean energy sources, not all of them are necessarily clean. Common renewable and clean energy resources include solar energy, wind energy, bioenergy.

The integration of renewable and clean energy resources and their associated technologies can be generally categorized into two overarching approaches [49]. The first approach centers on enhancing energy efficiency, exemplified by the increased conversion efficiency of photovoltaic (PV) systems, driven by advances in solar cell and layer materials [49]. This improvement has significantly boosted the effectiveness of solar energy capture and utilization.

The second approach encompasses decarbonization [50], which can be further subdivided into the use of alternative fuels and electrification. Within the domain of alternative fuels, the focus is on replacing traditional fossil fuels with lower-carbon energy sources, such as employing clean hydrogen. This shift contributes to a reduction in carbon emissions while maintaining energy output. Electrification, on the other hand, involves the transition from conventional energy sources to electric-based systems and can be broken down into three

principal sectors: industrial electrification, transportation electrification, and domestic electrification. In industrial electrification, a key example is the substitution of conventional industrial energy sources with electric alternatives. In transportation and domestic electrification, efforts are directed toward promoting electric vehicles (EVs) and transitioning from fossil-fuel-based systems to electric-based infrastructure, such as building electrification.

By adopting these two overarching approaches, renewable and clean energy resources can be more effectively integrated into the energy landscape, promoting sustainability and reducing carbon footprints. The author has selected several key topics in renewable and clear energy measures for further literature review.

1.1.2.1 Electrical Vehicle and V2G Technology in Microgrids

Electrical vehicles (EV) have gained much popularity these days. One of the biggest advantages of the electrical vehicle, be it Plug-in Hybrid Electric Vehicle (PHEV) or fully electric Battery Electric Vehicle (BEV), is that exhaust emissions can be reduced. Executive Order B-16-2012 signed by Governor Brown Jr. has stated that a CA statewide electrification of transportation be met by 2025 and 1.5 million Zero Emission Vehicles (ZEVs) be on road. Executive Order B-48-18 later reaffirms the former Order and set a new goal of 5 million ZEVs on California road [51].

The mass adoption of EV into microgrid systems, however, has potential negative impacts. Possible negative electrical impact on grid system from large scale EV adoption was discussed in [52–55], including load instability and power quality disturbance. Possible charging peaks with regional fleet charging where distribution infrastructure may be affected the most were

researched and determined in [56–58]. The possibility of overloading of key distribution components was discussed by case studies in [59] and [60]. A thorough review of EV integration into grid system by Garwa N et al. and Hussain MT et al. not only discussed the adverse power quality issued from EV, but also talked about the decrease of transformer lifecycle from it, in [52] and [61] respectively. While existing studies have extensively deliberated on the impact of EV charging on the electric grid system, a limited number have quantified these effects, especially on electric infrastructure. This underscores the necessity for more in-depth and quantitative investigations to comprehensively understand the implications of EV adoption on the existing electric grid infrastructure.

To quantitatively assess the impact of EV charging on power grids, usually EV charging models need to be developed first. Such models are generally categorized into two classes: static models and dynamic models. The static models typically address the aggregate charging characteristics associated with fleet charging, without considering individual charging events. In [62], a fuzzy-logic inference system was employed by Shahidinejad S et al. to simulate the initiation of bulk charging events. Another approach, detailed in [63], utilized a non-Gaussian probabilistic decision-making algorithm and a Monte Carlo algorithm to determine State of Charge (SOC) and daily charging schedules, respectively. Additionally, Cao Y et al. proposed a generation method that incorporates time-of-use (TOU) pricing to optimize bulk charging algorithms. On the other hand, dynamic models are usually spatial-temporal and involve the concept of vehicular travel [64]. In a closely related study, traffic topology data was leveraged to formulate a vehicle travel model for generating dynamic EV charging demands [65]. Employing cooperative game theory in conjunction with National Household Travel Survey

(NHTS) travel data, Flores RJ et al. determined EV charging demands for various purposes in [66]. Moreover, Bae S et al. explored the prospect of employing fluid dynamic traffic models and queuing theory to predict individual EV arrival rates and associated charging demands in [67].

Another significant derivative technology from EV in the field of the power grid is Vehicle-to-Grid (V2G) technology. Interacting with the power between the vehicles and the grid, V2G technology achieves demand response services for the two platforms [68]. It is argued that a special kind of single-phase PEV charger can support the utility grid network by providing reactive power, meanwhile still successfully functioning as a battery-charger [69]. It is also argued that not only a great percentage decrease on CO2 emission can be achieved, a bigger amount of wind power can be incorporated into the grid system because of V2G application [70].

Apart from the friendliness towards various renewable energy adoption in microgrids as mentioned above, V2G can also fill in the regulative role in the microgrid systems. Khan SU et al. and Mets K et al. discussed the possibility and potential control strategy of coordinating various EVs to charge/discharge to partially achieve the strategy known as “Peak Shaving and Valley Filling” for the Demand Response (DR) to relieve grid peak load pressure while reducing the cost of energy for utility customers, in [71,72]. More specifically, it is argued that sufficient amount of bidirectional charging of EV/PEV can completely achieve the peak-shaving strategy alone [73]. Also, It is further demonstrated using experiments that, along with the capability to support distribution load, V2G technology can also provide ancillary services, namely regulation, which is most expensive [74].

However, several challenges are affecting the practical implementation of V2G technology. It has been known that intermittent or even regular charging and discharging behavior can reduce battery life onboard the vehicle and incur faster replacement [75]. It is also mentioned by researchers about how challenging it is to meet the need of strong interaction between vehicles and the grid [76]. Even though the challenges have not been overcome for now, researchers are optimistic about the future of V2G technology as intelligent control strategies are being developed and experimental results showed a reduction of 17% of peak demand compared to business-as-usual (BAU) scenarios if V2G charging is smartly used [72]. Also, although the lifespan of onboard battery in PEVs could be lowered for using V2G, it may still be considered more economical for both vehicle owners and grid companies to deploy V2G and possible battery changes accordingly [76].

1.1.2.2 Peak Load Shaving

Scientists have come up with a few peak load shaving strategies. Some of the most popular ones include: using of on-site energy storage system, demand side management (DSM), and use of EV [77].

The idea of using on-site energy storage systems (ESS) for peak load shaving involves reducing or managing the highest levels of electricity demand during specific periods. The first step of this strategy is usually to find out when peak demand occurs in the local facility or grid before implementing anything. Typically, there are certain hours of the day when electricity usage is at its highest. The second step is to size the ESS, which is to determine the appropriate

size of the energy storage system based on peak load requirements. This usually involves analyzing historical data of electricity consumption to identify the peak demand level and duration. The last step is to implement the charging/discharging algorithm. During off-peak hours when electricity demand is lower, the energy storage system can be charged using cheaper electricity or renewable energy sources, such as solar panels. This ensures that the ESS has sufficient stored energy to supply power during peak demand periods. When peak demand occurs, the energy stored in the ESS can be discharged to supplement the power supply from the grid. By doing so, the facility can reduce its reliance on expensive electricity from the grid during peak hours, thereby lowering electricity costs.

A coordinated peak shaving strategy using Neural Network on Energy-intensive load (EIL) to estimate ESS capacity is shown in [78] to minimize overall system operation costs. Nikolovski S et al. discuss the possibility of forecasting BESS and PV capacity based on adaptive neuro-fuzzy inference system (ANFIS) for maximum peak load reduction in [79]. An accuracy-enhanced load forecast algorithm is proposed in [80] to reduce peak load level and electricity cost at the same time considering real-time electricity price. A simple but powerful real-time scheduling algorithm of BESS is described in [81] to optimally shave peak load. In [82], a distribution circuit specific model predictive control (MPC) strategy is proposed to forecast the day-ahead energy consumption to optimally control the ESS for peak load reduction. A optimal strategy of ESS dispatch to adjust the optimal peak shave level is present in [83] so that peak level can be reduced the most and no undesired power peak would be generated from ESS discharging process. A quick estimate algorithm of optimal ESS capacity is shown in [84] using historical

aggregated load profiles. Hong et al. developed an optimized BESS operation schedule using back propagation (BP) neural network to eliminate load peaks as shown in [85].

Similar in goal of the first strategy, DSM also manages the consumption of electricity by influencing when and how much electricity consumers use, which is usually achieved by incentives. Nasir T et al. summarizes popular ways of DSM to reduce peak to average ratio (PAR) in [86]. A DSM framework that optimizes both ESS and appliance scheduling schemes are discussed in [87]. In [88], deferrable loads are scheduled using an autonomous energy consumption scheduling algorithm to optimally reduce peak load level and prevent power backflow from PV system. An economically optimized DSM scheduling of vanadium redox flow battery (VRFB) and PV system is demonstrated in [89]. A novel DSM strategy of coupling thermal energy storage (TES) with solar PV system is developed and implemented in [90] to reduce peak load power considering electric tariff period. Game theory is considered in [91] and [92] to optimally reduce peak load as well. Two rescheduling algorithms of existing domestic electric consumption is mentioned in [93] and [94]to reduce peak energy power cost.

The use of EV to achieve peak load shaving can be further divided into two categories. The first category is the coordination of EV charging, without the possibility of bi-directional charging from the EV battery. The other category is V2G, which is discussed in the previous section as well. A two-layer non-linear MILP optimization algorithm is proposed in [95] to maximally shave peak load while considering charging availability. A few coordinated EV charging strategies are discussed in [96–98] for various optimization goals including peak load reduction in community and distribution grid circuits. The second category, V2G, has been a popular research topic. Two V2G control algorithms by coordinating with real-time electric

demand are discussed in [99] and [73]. A few V2G control problem turned ILP-based optimizations are discussed in [100,101]. A few others even considered using Predictive Control strategies to take into account the uncertainty of vehicle trip and charging events to optimally control EV discharging into the grid system [102,103].

While all three peak shaving has very similar ultimate goal, which is to reduce peak load, the scope of each method, however, is different. DSM is usually by on a larger scale, usually by system operators or of higher level, while on-site ESS is always on a smaller level due to its unique distributed way of deployment. EV integration, on the other hand, can involve both small- and large-scale applications.

1.1.2.3 Net Energy Metering

Originally offered as an alternative billing method to utility customers, Net Metering or Net Energy Metering (NEM) has been increasingly valued for its ability to further promote the adoption of renewable energy resources in daily life. One fundamental difference of NEM to the DER/ESS is that the former has no storage capacity and extra power gets exported back to the main grid while the latter has the option to store up extra generated power.

While NEM policies differ greatly throughout the world, the basic algorithm is similar—self-generated power is first harnessed by the ratepayers' household needs, and the extra power will be sent back to the main grid and will show up on electric bills as credit. In USA, NEM policies are different in each state or area with metering options and export rates. The original way to charge is a 1:1 ratio as average retail rate, which was first introduced in Minnesota in early 2000s [104]. One of the most well-known state policy supporting the ratio is California's

NEM 2.0, which was first introduced in 2016 [105]. The most common export rates, however, is Time-Of-Use (TOU) rate and the so-called avoided cost rate, as used by California's NEM 1.0 and NEM 3.0 respectively [106].

1.2 Goal

The goal of this effort is to develop a methodology, apply techniques and provide solutions for optimal design, dispatch and reliable and resilient operation of renewable energy sources and clean energy systems in a disadvantaged community microgrid.

1.3 Objectives

1. Develop Baseline AC power flow (ACPF) model for Oak View microgrid (OVMG) system to analyze novel smart microgrid systems.

2. Validate and extend the OVMG ACPF Baseline model to evaluate various electric demand profiles, energy efficiency practicality and demand response effectiveness in the OVMG.

3. Model and generalize the abilities of the OVMG system for supporting high renewable penetration and clean energy system adoption.

4. Further the reliability and resiliency of the OVMG system to support the Southern California Edison (SCE) macro-grid system by optimizing existing infrastructure and the smart addition of clean energy system in novel operational scenarios.

5. Evaluate the impact of electrification, energy efficiency measures, renewable and clean energy techniques, and EV charging on the OVMG and SCE systems.

2 Approach

Task 1: OVMG ACPF Model and Baseline Development

In this task, an AC power flow (ACPF) Model for Oak View microgrid (OVMG) system is first created in OpenDSS platform. Based on SCE's DERiM Project, a topological model of Oak View Community is created using OpenDSS platform. Real-life based coordinate system of each generator, transformer and load are determined to generate the map and potential field are accomplished. To determine the actual line and transformer parameters, data from American Wire Gauge (AWG) are harnessed to image the real impedance condition. For the load from different types of customers, which includes both residential and industrial load, URBANopt system as well as powerful electrical analytical toolkit E3 (Energy & Environmental Economics) platform are potentially used to reflect the real-time data profile.

Multiple test case scenarios are then developed based on the OVMG ACPF model to reflect on socioeconomically motivated needs as well as policy-induced pathway to a renewable future.

Task 2: Extension of Computing Methods

In this task the operation platform of OVMG ACPF is extended beyond OpenDSS. An OpenDSS-MATLAB interface is first developed to further enhance the operability and flexibility of the model and enhance the compute speed using parallel computing.

Task 3: OpenDSS Validation for Baseline Model

In this task, electrical profiles across platforms including URBANopt and DERopt, are first verified theoretically to ensure their feasibility. Profiles are simulated in OVMG ACPF model and electrical power quality index is calculated and compared with accepted limit. Theoretical verification of profiles is then followed by multi-platform comparison between OpenDSS/URBANopt and OpenDSS/DERopt to further confirm the viability of profiles.

Task 4: Renewable and Clean Energy System Integration

In this task several practical scenarios are paired with renewable and clean energy resources to further regional clean energy goal. The siting and sizing of these resources are determined using DERopt with MILP constraints. Certain level of PV/ESS, EV are considered and deployed.

Task 5: Optimal Renewable and Clean Energy System Adaption in Novel Operational Scenarios

In this task the optimal design and application of renewable energy resources and clean energy technologies are discussed and analyzed. Relatively novel and developing microgrid scenarios, including islanded operation during Public Safety Power Shutoff (PSPS) events, Demand Response, Net Energy Metering (NEM) 3.0, are considered and optimized with proposed design. The design aims at addressing and enhancing the reliability and resiliency of the microgrid systems, and the OVMG system is tested upon. Some optimal designs require rearrangement or upgrade of existing infrastructure, such as rewiring of power cable and replacement of distribution transformer.

Task 6: Impact Analysis of the Microgrid System

In this task the electrical and financial impact of novel scenarios as well as renewable and clean energy resources on the OVMG model is analyzed and quantified. The analysis is comprised of three parts: reliability and resiliency analysis, degradation analysis as well as cost and benefits analysis. All considered scenarios generated in previous tasks are analyzed under both normal and islanded operation mode.

3 OVMG Baseline OpenDSS ACPF Model Development

3.1 Baseline Buildup

The real-life example used in this effort is the Oak View Community located in Huntington Beach, California. The electric distribution model was developed using the alternating current (AC) power flow simulator OpenDSS [107]. The OpenDSS tool can capture the complete resolution of three-phase voltage and current through distribution power lines and transformers. The western section of the community consists of commercial and industrial plants and offices along with Oak View School. The rest of the community is primarily residential. The AC power flow steady state analysis calculates the active and reactive power flow of each active cable. The process is described in equation (1) and (2).

$$P_{ij} = \sum_{j=1}^{j \in N_i} |V_i||V_j|\left(G_{ij} \cos\left(\theta_i - \theta_j\right) + B_{ij} \sin\left(\theta_i - \theta_j\right)\right) \quad (1)$$

$$Q_{ij} = \sum_{j=1}^{j \in N_i} |V_i||V_j|\left(G_{ij} \sin\left(\theta_i - \theta_j\right) - B_{ij} \sin\left(\theta_i - \theta_j\right)\right) \quad (2)$$

Where i,j are actives buses in topology N, G_{ij} and B_{ij} are line conductance and susceptance from bus i to j. V_i and θ_i are bus vontage and angel between bus i and j, respectively. P_{ij} and $Q_{ij}$are line active and reactive power flow from bus i to j.

The distribution system topology of Oak View Community in OpenDSS was developed in three steps. The first step is to outline Oak View Community electric grid connection from SCE's DRPEP tool [108][109].

Secondly, on-site inspections were made to record and verify circuit connections, transformer types, ratings, locations and belongings, single phase existence and usage, and to revise them if necessary. Underground transformers and cables were believed to exist on the western commercial and industrial side of the community. In the case of both underground and unmarked or unobservable transformers above ground, estimated ratings were given and will be discussed later. Wire rating and gauge were unobtainable as well, therefore discuss and assumptions will be made on them.

The last step is to combine the outlined grid topology and information gained from field walks and a preliminary OpenDSS topology was made and then refined. This model was exercised using the tuned electrical demand results from the Oak View community energy simulation developed in URBANopt [110]. In instances where wire ampacity limits were violated in the power flow simulation, wire diameter size was increased to avoid over-ampacity issues. In instances where transformer power limits were exceeded, building – transformer connections were first examined to ensure correct linkages. If overloads continued to occur after any changes to the model, transformer ratings were increased to the proper kVA rating. Wires were also sized using OpenDSS results. Complete transformer rating and revision have been attached in Appendix A.

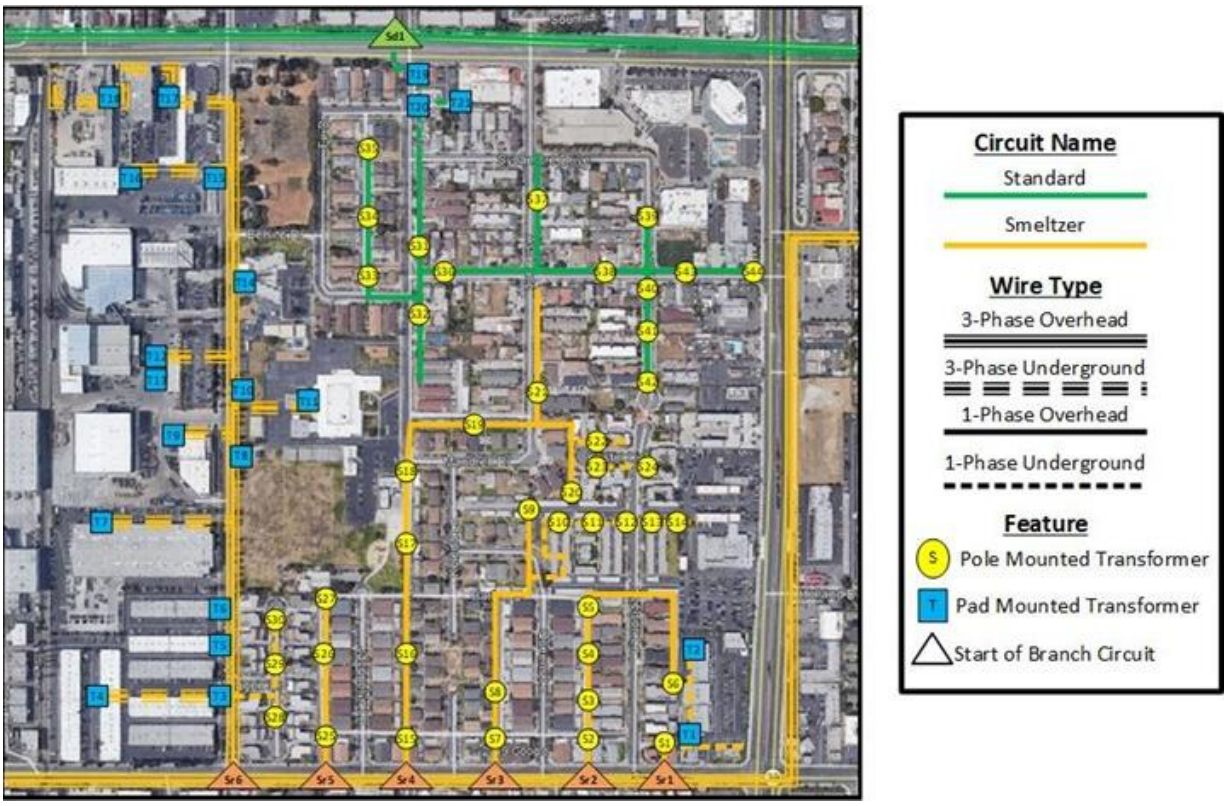

Figure 1. Oak View Community topology (not showing Beach 12 KV Distribution Circuits and Oceanview Substation

Gauge selection occurred on an ampacity basis, ensuring that the baseline model would produce no over-ampacity conditions across all circuits. American Wire Gauge (AWG)[111] standards were used to select from. Wire conductor material is not known but is assumed to be copper. Sizing wires based on copper cable ampacity limits show that all residential circuits can receive utility service using 6-gauge wire. The commercial and industrial circuit, however, requires 2-gauge wire at the start of the circuit, followed by 6-gauge wire sizes along the remainder of the length of the circuit. Only 6% of length of total commercial branched circuit is comprised of 2-gauge wire.

Existing topology of the Oak View Community is depicted in Figure 1. Branch SR1-SR5 and SD1 are all residential branches, whereas SR6 is the only commercial and industrial branch. Oceanview Substation (not present in **Error! Reference source not found.**) is located in the

Northeast corner Oak View Community and powers multiple local areas, including the Oak View Community. The Oak View Community consists of approximately 1,100 utility customers.

3.2 Extension of Computing Methods

Aiming to enhance the efficiency of power flow analysis within OpenDSS and fostering enhanced compatibility with prevalent operational platforms, a novel interface has been meticulously developed. Presently, one useful interface has been devised: the OpenDSS-MATLAB interface, primarily geared towards enriching result demonstration functionalities, as well as tailored for adept data formatting purposes. The interface represents pivotal advancements aimed at fortifying the analytical capabilities and interoperability of the OpenDSS framework within diverse operational contexts.

3.2.1 MATLAB-OpenDSS Interface

The first interface to be developed is between OpenDSS and MATLAB. Renowned globally for its adaptability across diverse disciplines, MATLAB shares a vast user base hailing from varied backgrounds [112]. Nonetheless, within the domain of ACPF analysis, MATLAB's general-purpose framework and support for a range of components inadvertently obstruct streamlined usability. Conventionally, Simulink, an adjunct tool within MATLAB, has been the preferred avenue for conducting ACPF analysis [113]. While Simulink's graphical interface may ostensibly enhance the clarity of the design process, the exigency of constructing or revising ACPF models from the scratch within this environment may incur significant workload and effort compared to OpenDSS's expedient coding methodology. Conversely, OpenDSS's interface offers a potent

combination of robust functionality and user-centric design, notably facilitating swift and efficient result examination through its intuitive monitor and summary functions.

Nevertheless, when it comes to model revision, the comparative advantages of OpenDSS and MATLAB diverge. Minor modifications, such as the addition or deactivation of connections, or the adjustment of three-phase connection configurations, are markedly more straightforward within the OpenDSS framework. Conversely, for substantial alterations necessitating integration of external data sources, particularly Excel files, MATLAB's interface proves more accommodating.

It is noteworthy that MATLAB's compatibility engenders the occasional provision of more granular operational insights, including detailed harmonic analyses. However, in terms of computational efficiency, MATLAB may outpace OpenDSS thanks to its optimized parallelization algorithms, a feature yet to be assimilated within the latter.

Therefore, both platforms have unique traits, and an interface between them would combine them to generate a even more powerful ACPF analysis platform. A complete summary of review of OpenDSS and MATLAB in terms of ACPF analysis is listed below in Table 1.

Table 1. Comparison of OpenDSS and MATLAB in ACPF Analysis

Functionality Evaluation	OpenDSS	MATLAB
Ease of use for New Design	Generally true with simple coding method	More complicated, may take longer time

Ease of use for Revision	Generally true for small change, but change of core elements is not easy	More complicated for simple change but is easier for major revisions
Results Evaluation	Simply yet powerful	Could provide more detail but is not easy to operate
Operation Speed	Quick for simply operation	Quicker when paralleling algorithm is harnessed

The structure of OpenDSS-MATLAB interface is explained in Figure 2. The simulation commences with the execution of a MATLAB script tasked with initializing the Component Object Model (COM) interface between OpenDSS and MATLAB. Subsequently, a subset of predetermined MATLAB simulation parameters is invoked, followed by the extraction of grid equivalent parameters within the MATLAB environment. These parameters, along with the temporal instantiation of the simulation initialization code, are conveyed to OpenDSS, where a pre-written script undertakes real-time power-flow analysis and conveys the subsequent simulation time resolution back to MATLAB. This temporal information is then utilized by MATLAB to ascertain the completeness of the ongoing simulation. Should the simulation remain incomplete, the iterative process persists. When simulation is completed, the ACPF results can be further harnessed by MATLAB for detailed visualization and analytical purposes.

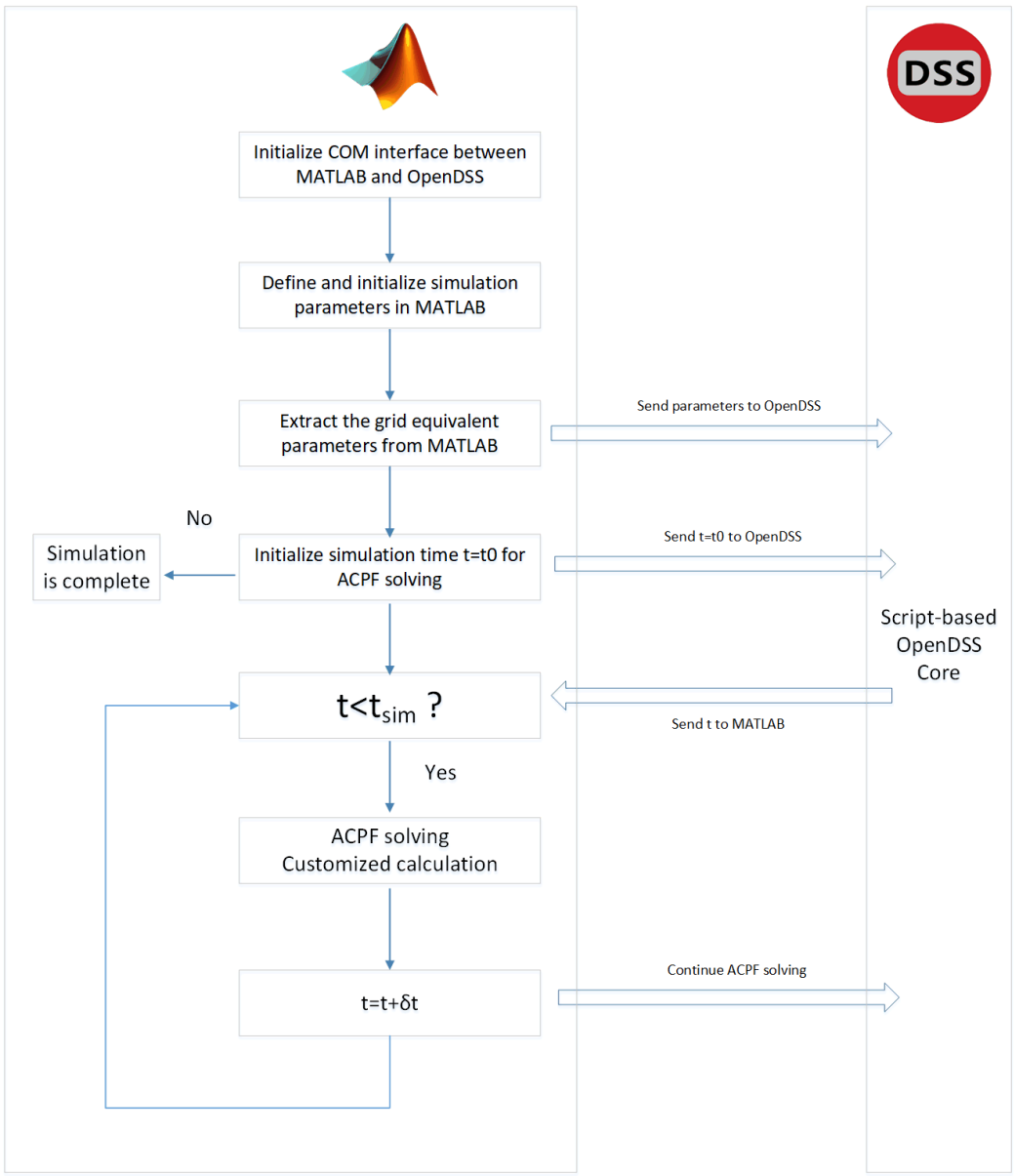

Figure 2. Structure and cross-platform implementation of the hybrid ACPF simulation with OpenDSS and MATLAB

3.3 Baseline Model Verification

To verify the accuracy of OVMG OpenDSS ACPF model, a cross-platform comparison is carried out. The baseline load is first run in both OpenDSS and DERopt, and a comparison of p.u. phase-to-phase voltage for all active distribution transformers. The baseline model is then installed with PV/ESS of different penetration rates to ensure lowest cost at resiliency level for each branch. Nine different scenarios aiming at ensuring normal operation of different levels of critical load in OVMG are eventually developed and tested in both OpenDSS and DERopt with

same parameters for each scenario. Details about each tested scenario is listed in Table 2. Details on parameters that was used as same input in OpenDSS and DERopt are shown in

Table 3. Details about UES scenarios can be found in previous published works by the author [110].

Table 2. Details about tested scenarios, including involved electrification technology, optimization goal and critical level rating.

Scenario	Scenario Feature	Critical Load Level
Baseline	N/A	N/A
UES 1A-CL6	No Cooling, Lowest Cost	6
UES 1A-CL7	No Cooling, Lowest Cost	7
UES 1B-CL6	No Cooling, Lowest TDV	6
UES 1B-CL7	No Cooling, Lowest TDV	7
UES 2A-CL6	With Cooling, Lowest Cost	6
UES 2A-CL7	With Cooling, Lowest Cost	7
UES 2B-CL6	With Cooling, Lowest TDV	6
UES 2B-CL7	With Cooling, Lowest TDV	7

Table 3. Parameters used for comparison by both OpenDSS and DERopt.

Parameters Used for Comparison	Category
Electric Demand	Individual Profile
Utility Import	Individual Profile
Solar Production	Individual Profile
Storage Charging	Individual Profile

Storage Discharging	Individual Profile
PV Capacity	System Capacity
ESS Capacity	System Capacity

Voltage results from the two platforms and a delta voltage percentage result will be shown for each scenario. The results are demonstrated using box plots, where the x-axis of those figures indicates the start of branch circuits. Active nodes are shown in order of proximity to start of branch circuit. The middle red line in each box plot indicates the median annual value. The 25th and 75th percentile values are shown as the bottom and top of each box, respectively. All regular data falls within the whiskers and extreme data points as red '+' markers.

To verify the accuracy of the model, all test case scenarios are run in the two platforms to generate two separate sets of power flow analysis, and results are then compared. The comparison for baseline is first accomplished.

From top to bottom in Figure 3, Line-Neutral voltage of OVMG and DERopt of Baseline Scenario respectively, the delta voltage percentage of results from two platform are shown. It is obvious that with a negligible maximum difference around 0.5% between voltage results from two platforms for the Baseline Scenario, the way OCMG OpenDSS ACPF model works in a very similar way to DERopt.

From top to bottom in Figure 4 and Figure 5, Line-Neutral voltage of OVMG and DERopt of UES 1A-CL6 and 1A-CL7 respectively, the delta voltage percentage of results from two platform are shown. It is obvious that with a negligible maximum difference around 4% between voltage

results from two platforms for both scenarios and the majority of the differences within 2%, the way OCMG OpenDSS ACPF model is considered to work in similar way as DERopt.

From top to bottom in Figure 6 and Figure 7, Line-Neutral voltage of OVMG and DERopt of UES 1B-CL6 and 1B-CL7 respectively, the delta voltage percentage of results from two platform are shown. It is obvious that with a negligible maximum difference around 5% of voltage results differences between the two platforms for both scenarios and the majority of the differences that are within 2%, we can conclude that the OCMG OpenDSS ACPF model is verified to work in a similar way as the microgrid simulations of DERopt.

From top to bottom in Figure 8 and Figure 9, Line-Neutral voltage of OVMG and DERopt of UES 2A-CL6 and 2A-CL7 respectively, the delta voltage percentage of results from two platform are shown. It is obvious that with a negligible maximum difference around 6% of voltage results between two platforms for both scenarios and the majority of the differences within 2%, the way OCMG OpenDSS ACPF model is once again considered to work in similar way as DERopt.

From top to bottom in Figure 10 and Figure 11, Line-Neutral voltage of OVMG and DERopt of UES 2B-CL6 and 2B-CL7 respectively, the delta voltage percentage of results from two platform are shown. It is obvious that with a negligible maximum difference within 6% between voltage results from two platforms for both scenarios and the majority of the differences within 2.5%, the way OCMG OpenDSS ACPF model is once again considered to work in similar way as DERopt.

In conclusion, for all nine considered scenarios, the cross-platform comparison of the Baseline Scenario works best, with an overall maximum 0.2% difference in Line-Neutral voltage.

For all UES scenarios, although occasional outliers in delta voltage percentage could go as high as 6%, the vast majority of the difference is usually blow 2%, which is well acceptable. Therefore it is believed that the OpenDSS-based OVMG ACPF model is reasonably accurate and good for future use.

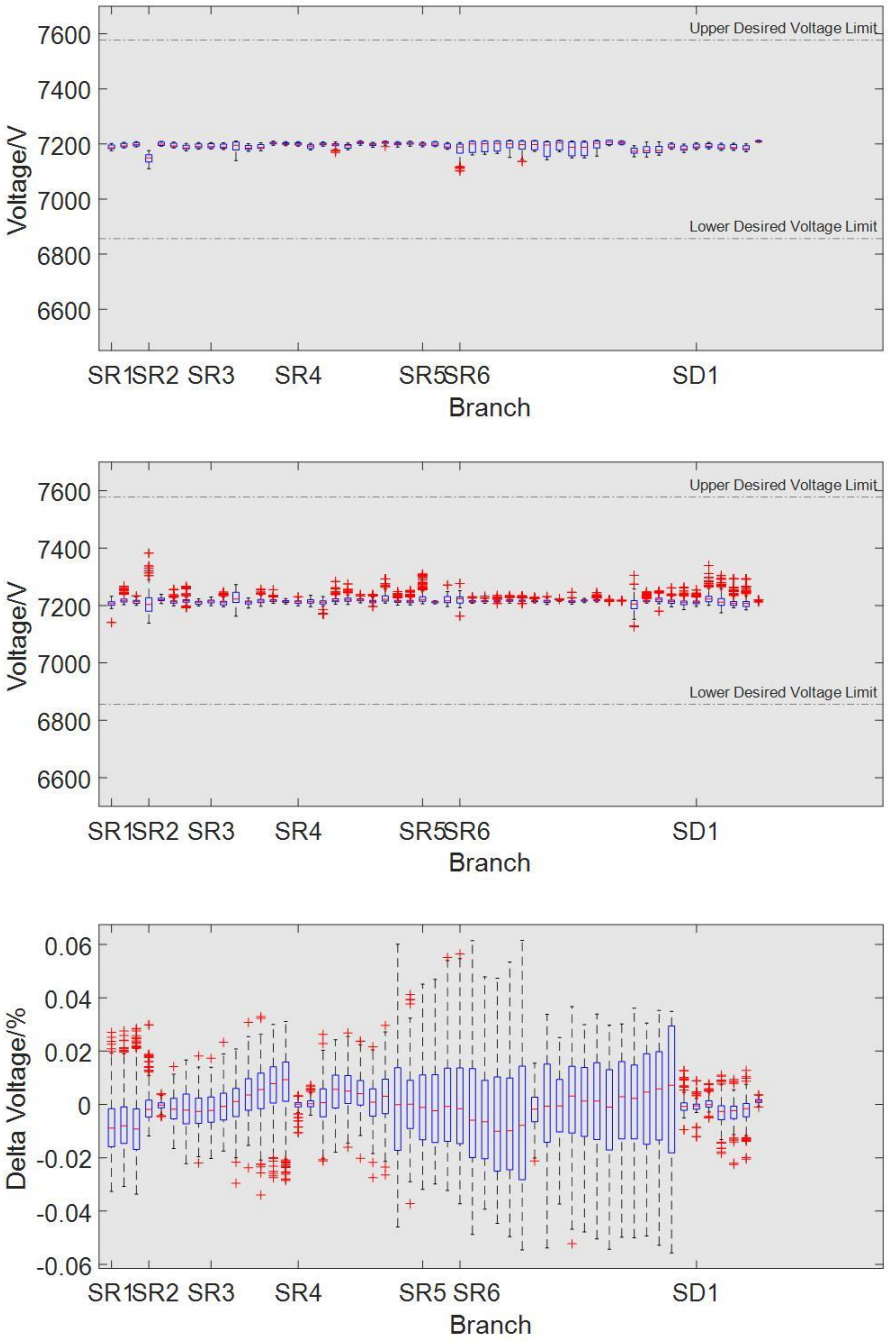

Figure 3. Cross-platform voltage comparison of OVMG Baseline Scenario. From top to bottom: Line-Neutral voltage of OVMG Baseline Scenario in OpenDSS, Line-Neutral voltage of OVMG Baseline Scenario in DERopt, delta voltage percentage of the two models above.

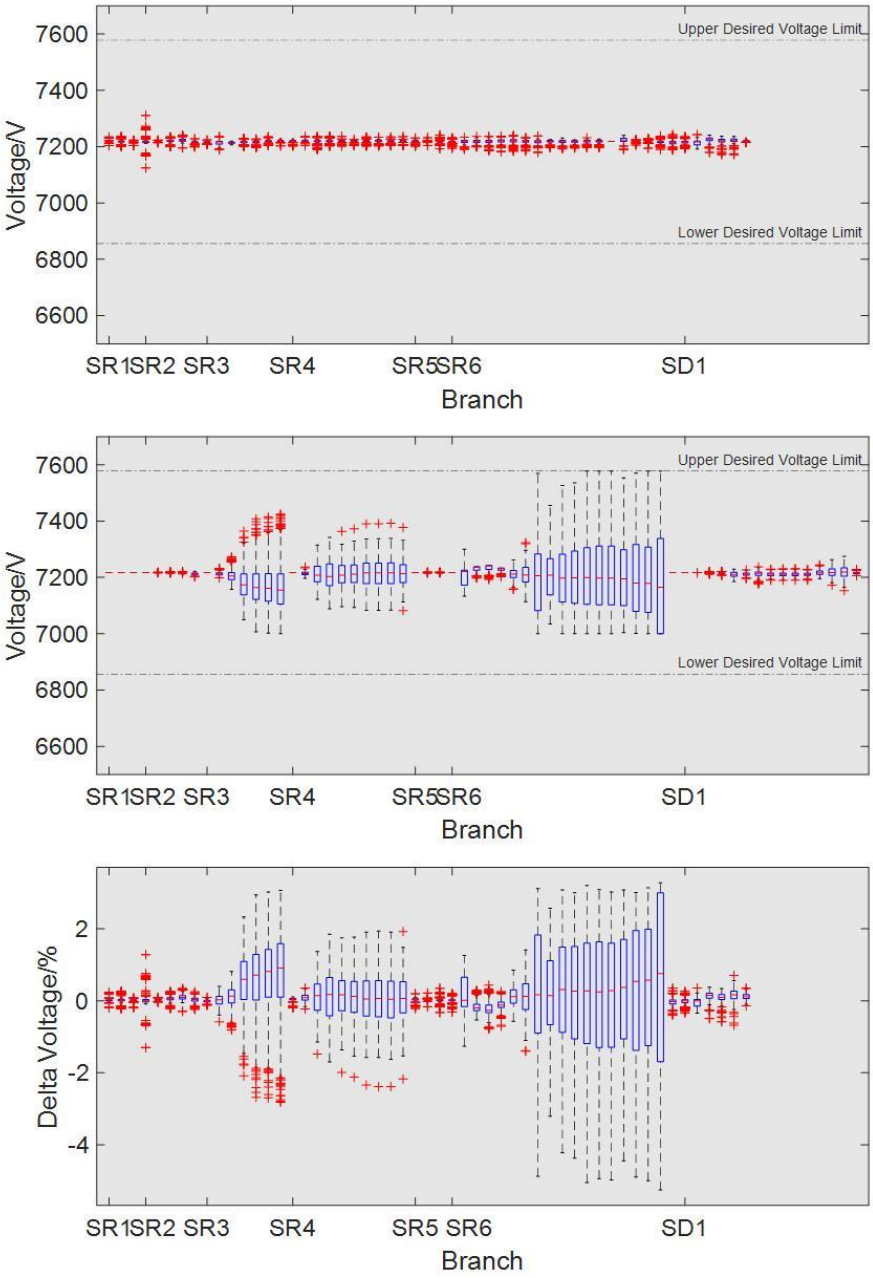

Figure 4. Cross-platform voltage comparison of OVMG UES 1A-CL6 Scenario. From top to bottom: Line-Neutral voltag of OVMG Baseline Scenario in OpenDSS, Line-Neutral voltage of OVMG Baseline Scenario in DERopt, delta voltage percentage of the two models above.

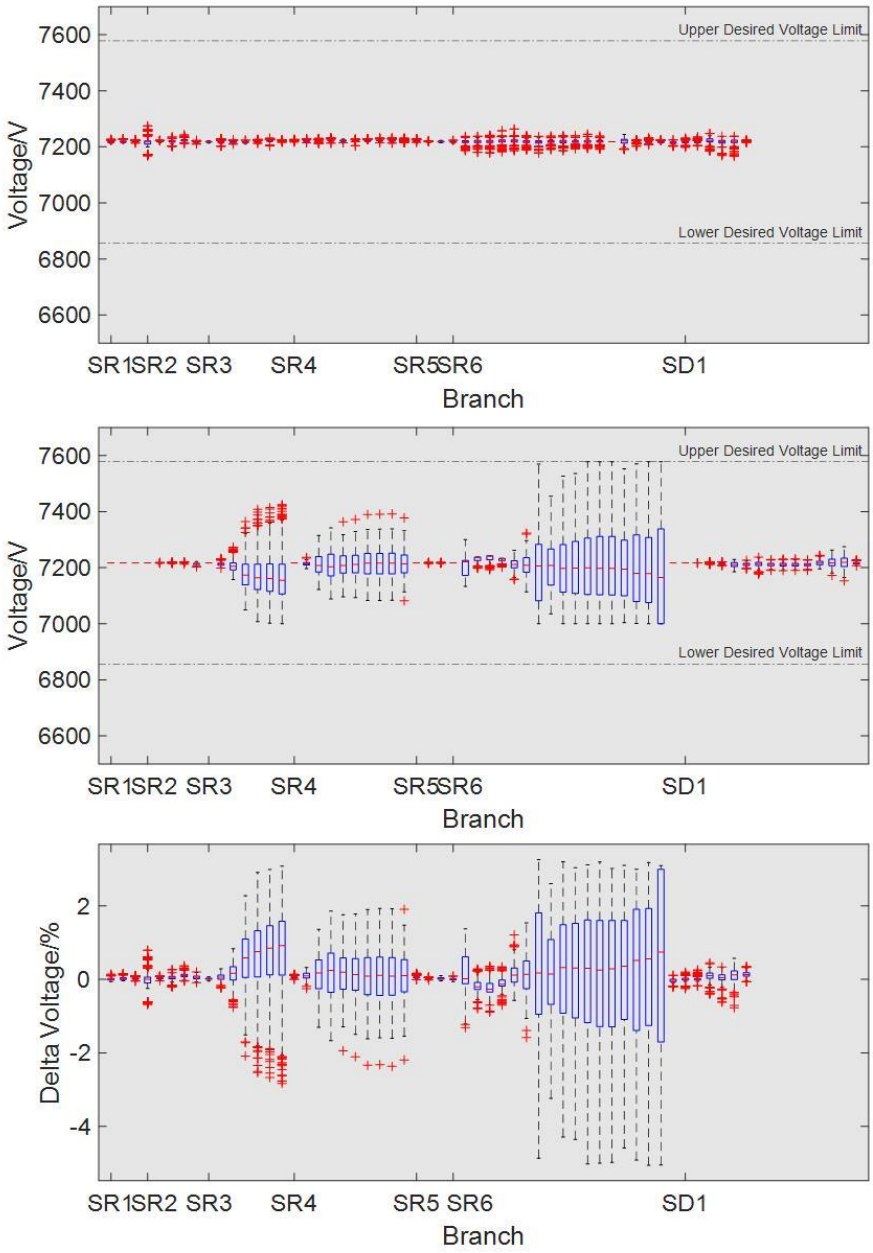

Figure 5. Cross-platform voltage comparison of OVMG UES 1A-CL7 Scenario. From top to bottom: Line-Neutral voltage of OVMG Baseline Scenario in OpenDSS, Line-Neutral voltage of OVMG Baseline Scenario in DERopt, delta voltage percentage of the two models above.

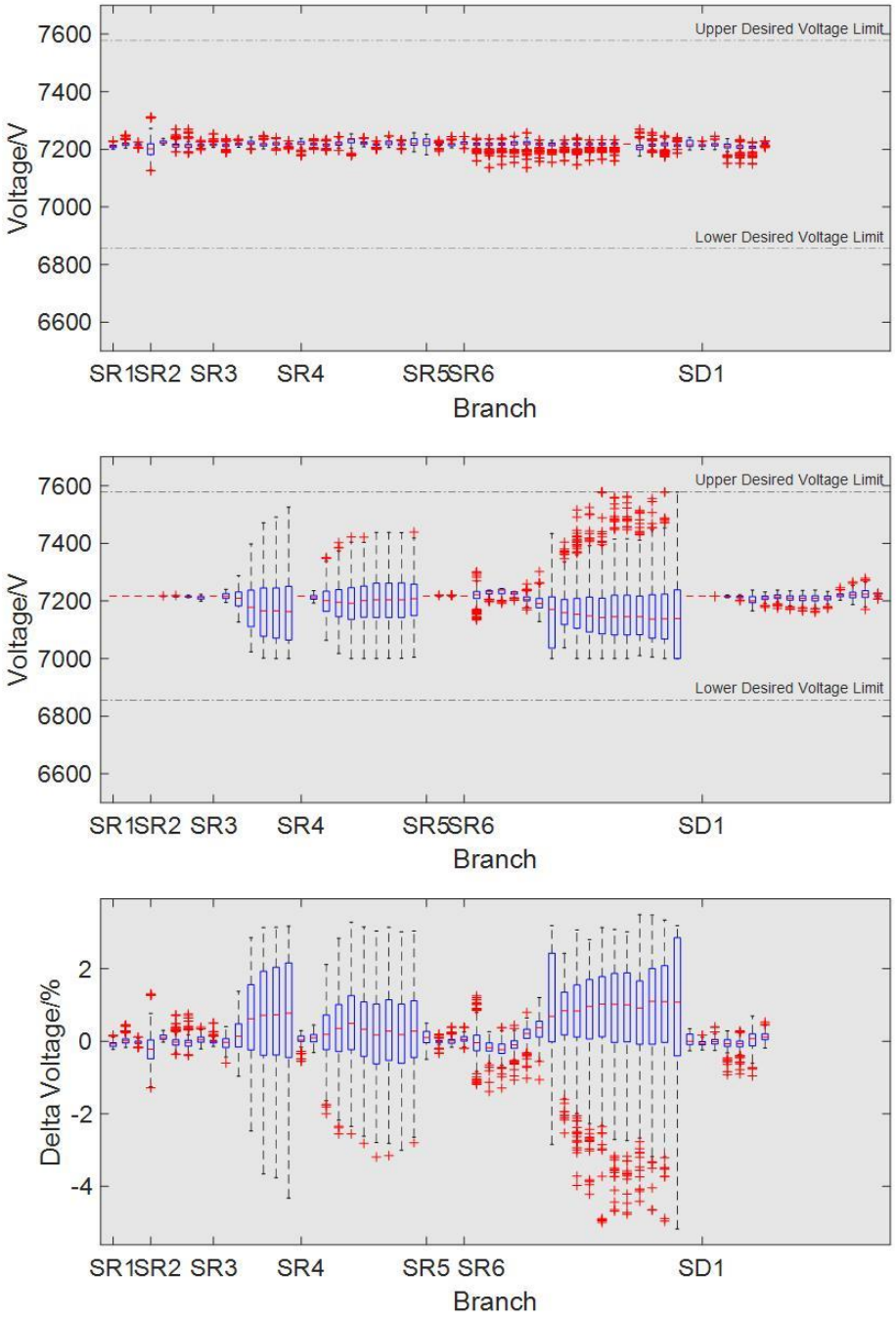

Figure 6. Cross-platform voltage comparison of OVMG UES 1B-CL6 Scenario. From top to bottom: Line-Neutral voltage of OVMG Baseline Scenario in OpenDSS, Line-Neutral voltage of OVMG Baseline Scenario in DERopt, delta voltage percentage of the two models above.

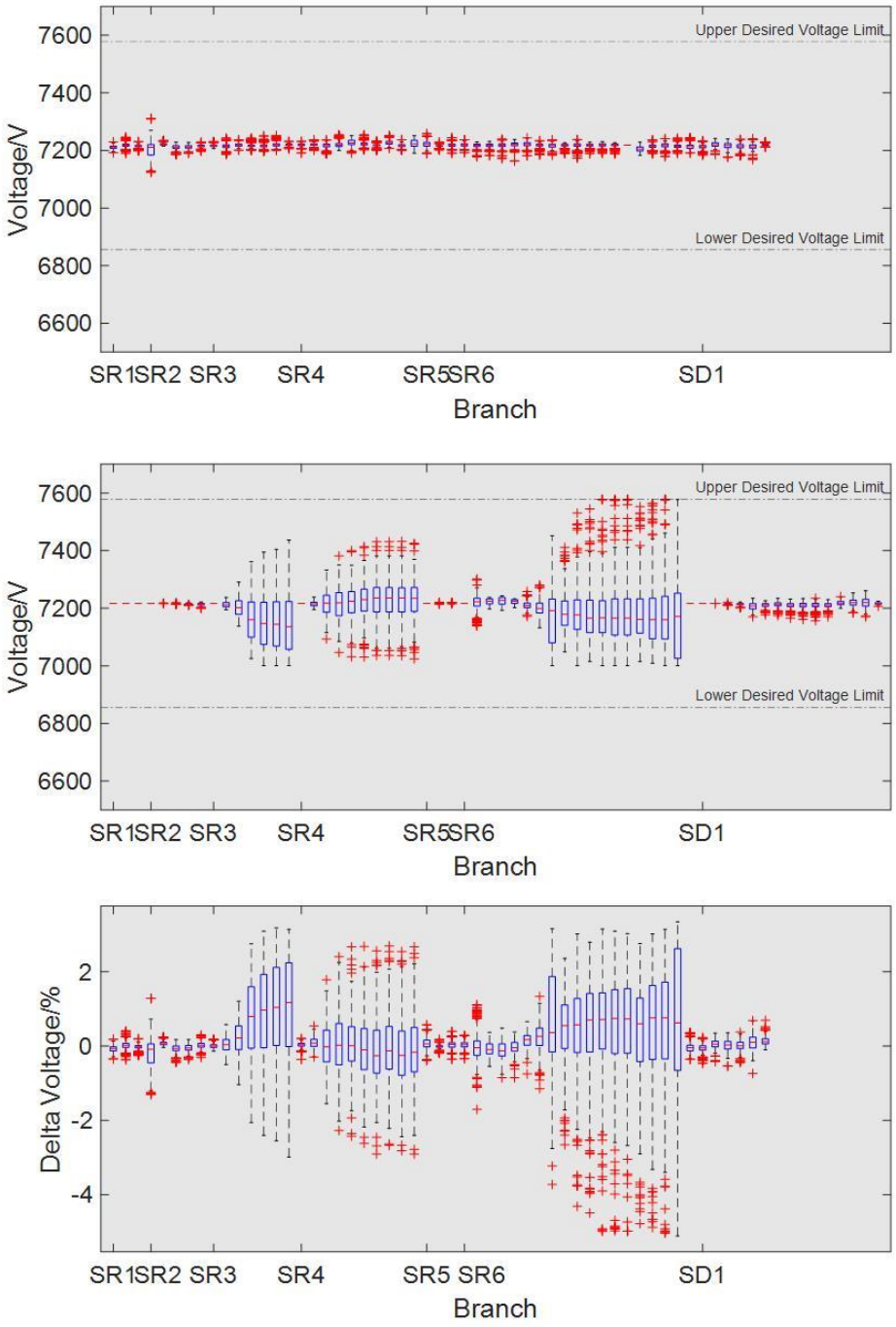

Figure 7. Cross-platform voltage comparison of OVMG UES 1B-CL7 Scenario. From top to bottom: Line-Neutral voltage of OVMG Baseline Scenario in OpenDSS, Line-Neutral voltage of OVMG Baseline Scenario in DERopt, delta voltage percentage of the two models above.

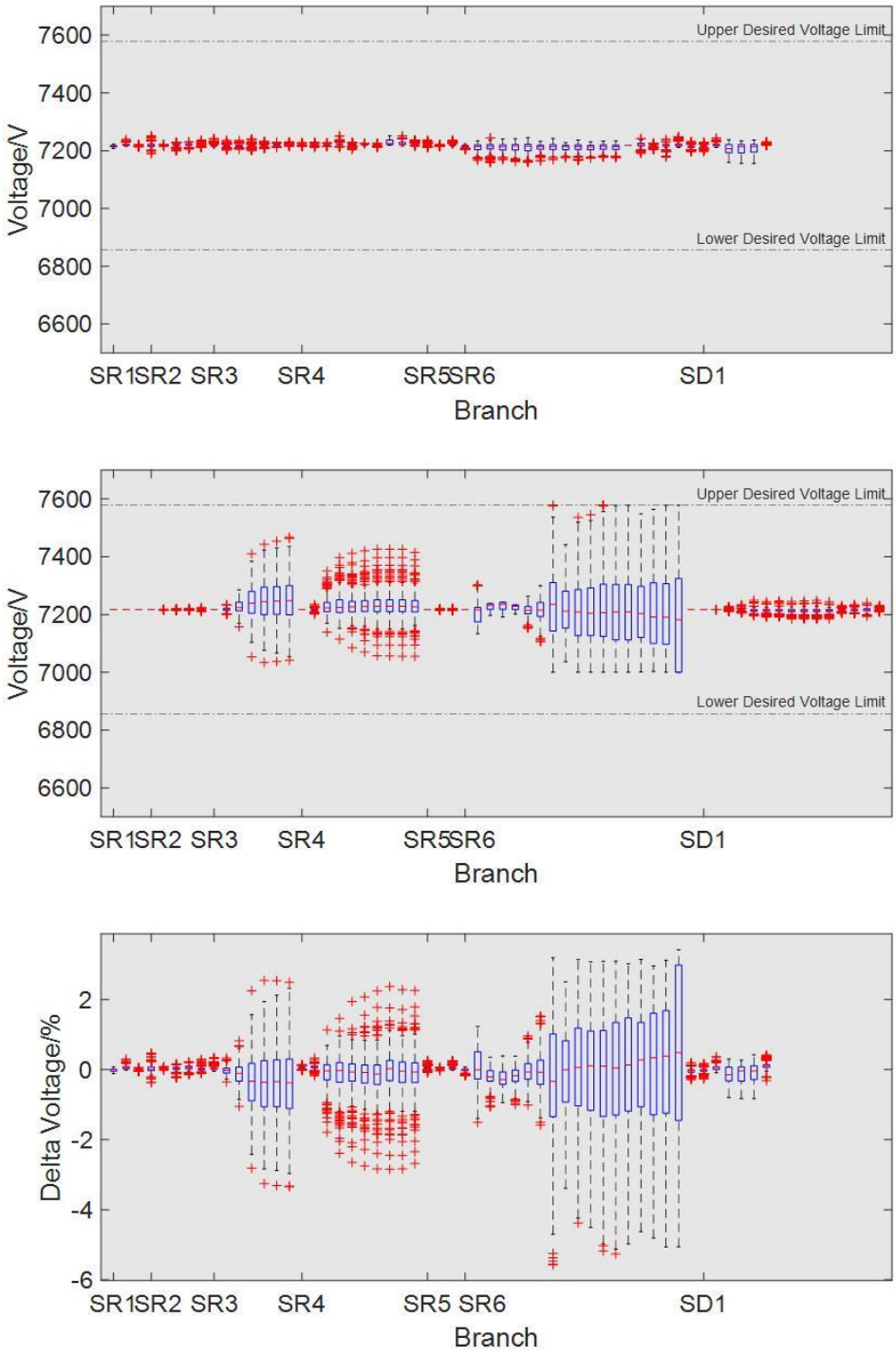

Figure 8. Cross-platform voltage comparison of OVMG UES 2A-CL6 Scenario. From top to bottom: Line-Neutral voltage of OVMG Baseline Scenario in OpenDSS, Line-Neutral voltage of OVMG Baseline Scenario in DERopt, delta voltage percentage of the two models above.

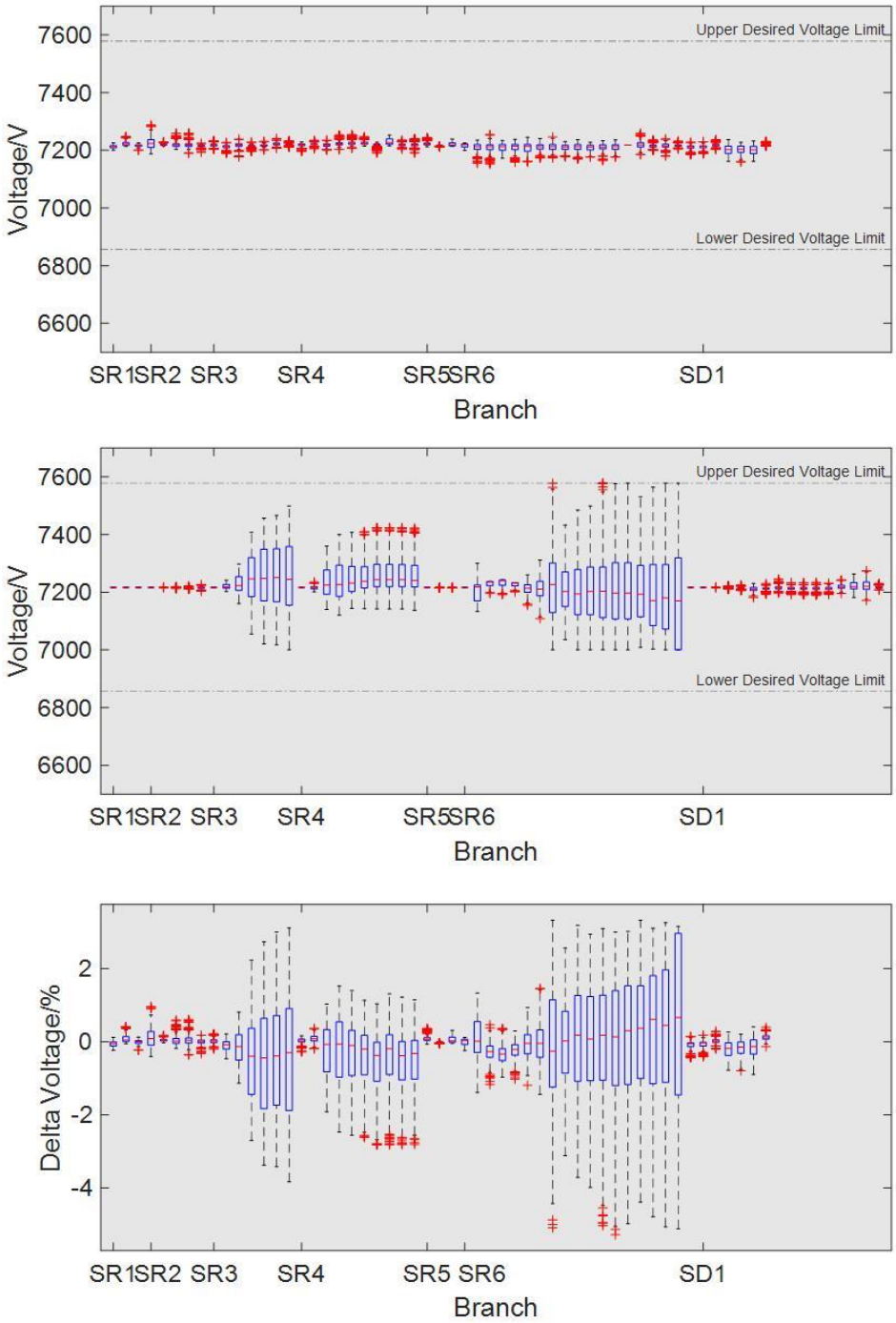

Figure 9. Cross-platform voltage comparison of OVMG UES 2A-CL7 Scenario. From top to bottom: Line-Neutral voltage of OVMG Baseline Scenario in OpenDSS, Line-Neutral voltage of OVMG Baseline Scenario in DERopt, delta voltage percentage of the two models above.

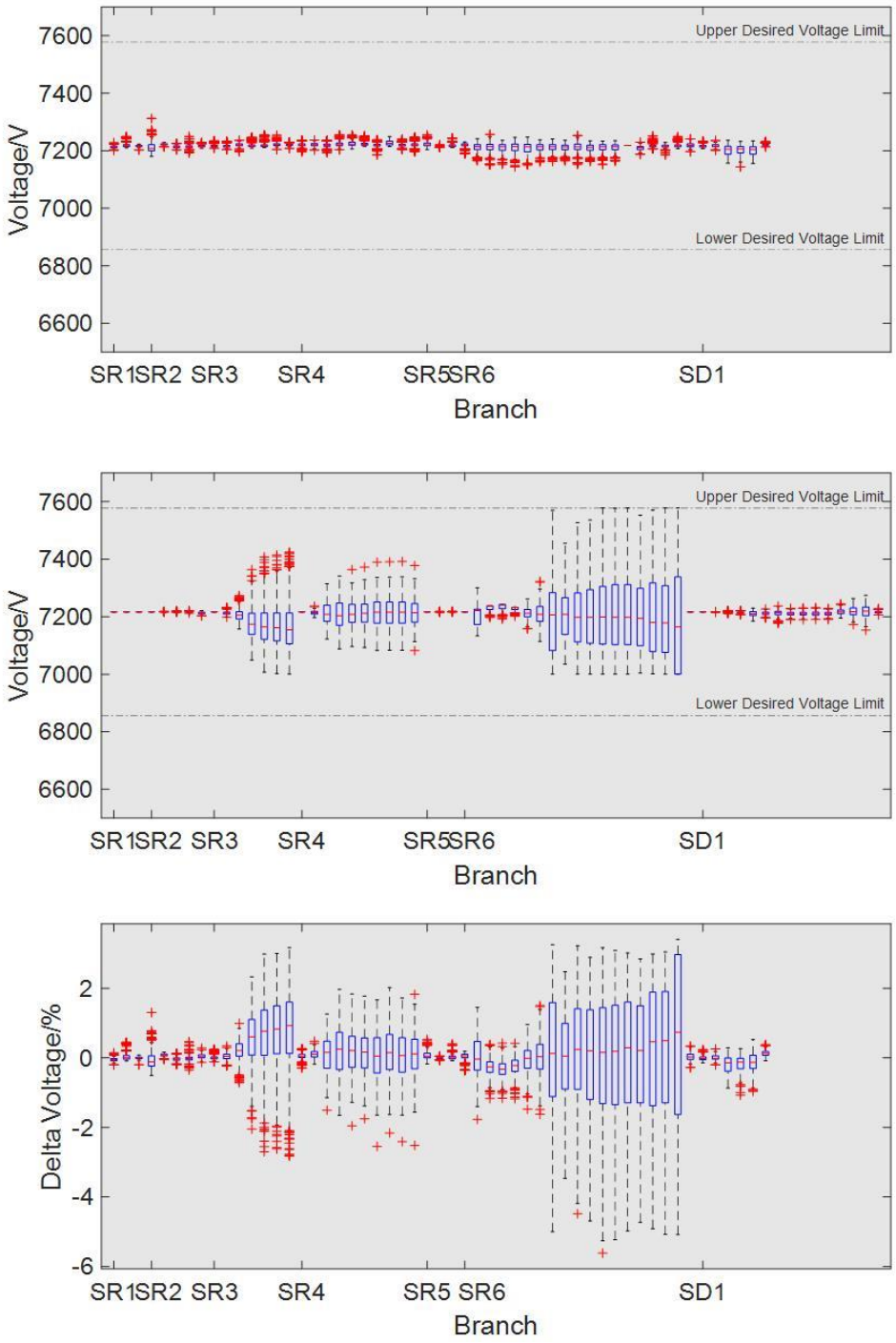

Figure 10. Cross-platform voltage comparison of OVMG UES 2B-CL6 Scenario. From top to bottom: Line-Neutral voltage of OVMG Baseline Scenario in OpenDSS, Line-Neutral voltage of OVMG Baseline Scenario in DERopt, delta voltage percentage of the two models above.

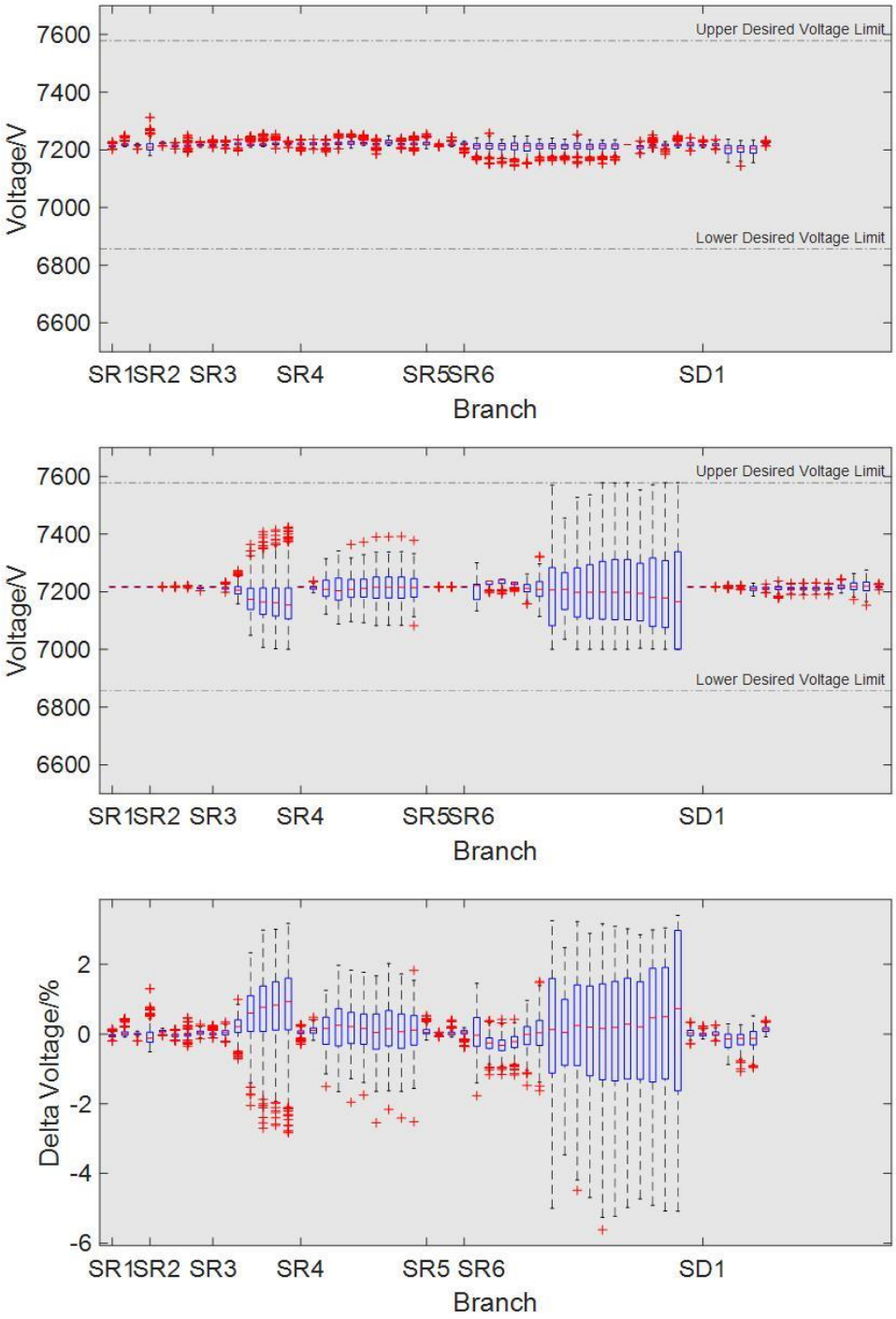

Figure 11. Cross-platform voltage comparison of OVMG UES 2B-CL7 Scenario. From top to bottom: Line-Neutral voltage of OVMG Baseline Scenario in OpenDSS, Line-Neutral voltage of OVMG Baseline Scenario in DERopt, delta voltage percentage of the two models above.

4 Renewable and Clean Energy System Integration into OVMG

After the completion of OVMG ACPF baseline model, renewable and clean energy resources and measures including EV are then adopted. The widespread adoption of EVs is impeded by several challenges. Foremost among these impediments is the populace's reluctance to transition from conventional vehicles to EVs. Additionally, inherent constraints associated with EVs, such as limited vehicle range and battery degradation, further contribute to the hindrances [114][115]. However, some pivotal challenges lie in the realm of infrastructure, encompassing both the availability of charging stations and the grid capacity to accommodate the heightened electric demand and demand dynamics arising from EV charging. Although numerous states have initiated or are in the process of formulating investment plans to establish extensive EV charging facilities, exemplified by California's commitment to deploying 250,000 EV charging stations by 2025 as mandated by Senate Bill 350 [116], there remains a gap of comprehensive research on the impacts and challenges of the increased electric demand, especially on electric infrastructure and its subsequent influence on stable and reliable electricity delivery.

The present section introduces an innovative approach for the generation of discrete EV charging profiles, integrating both static and dynamic methods for profile generation. A quantitative assessment of the impact of charging activities at various levels on key electric infrastructure will be conducted in the following section, utilizing empirical data obtained from a real-world community in Southern California, subsequently extended to encompass the entire Southern California (SoCal) region. The proposed profile generation methodology leverages National Household Travel Survey (NHTS) vehicle travel data specific to California. In contrast to

prior works like that of [65], which relies on traffic data that is not consistently available, our study first develops a stochastic model for individual EV travel, accounting for factors such as vehicle departure time, residence duration, and travel distance. The individual EV charging model is then implemented in a disadvantaged community within the SoCal region, employing the stochastic Monte Carlo algorithm. This deployment continues until a state of stable power quality and degradation is achieved, at which point a comprehensive report is generated. Subsequently, the methodology is extended to encompass the entire service territory of Southern California Edison (SCE), allowing for the generation of analogous reports for all residents within the SCE service territory.

4.1 Discrete EV Charging Profile Development

This section presents a methodology for the derivation of discrete electric vehicle (EV) profiles, with a particular emphasis on state-specific precision and potential applications. The principal objective of this process is to systematically generate a representative array of discrete EV charging profiles, tailored specifically to the state of California. These profiles are generated at a resolution that aligns with existing load profiles and incorporates associated allocation possibilities, which will be further elucidated in subsequent sections. This comprehensive methodology forms the foundation for subsequent discussions and applications in the forthcoming sections.

The methodology for generating discrete EV profiles specific to California comprises three distinct phases, each designed to ensure the accuracy and applicability of the profiles. The first phase in this methodology is data preparation and pre-processing. This stage is fundamental for

acquiring and transforming the requisite data sources into a format suitable for subsequent analysis. It includes activities such as data acquisition, data eligibility assessment, and data integration. It is imperative to ensure the reliability and representativeness of the data used in generating the discrete EV profiles. Additionally, the pre-processing step may involve data cleansing, normalization, and aggregation to prepare for subsequent phases. In the second phase, the EV charging and discharging profiles are estimated. This step involves the development of mathematical models to simulate the charging and discharging behavior of electric vehicles within the California region. The model accounts for factors including starting state of charge (SOC) and charging time. The final phase of the methodology focuses on the generation of discrete EV charging profiles. In this step, every possible EV charging profile is systematically created, taking into account the specific characteristics of California's electric vehicle market utilization. These profiles are generated at a level of detail that aligns with existing load profiles and can be applied to various scenarios. Importantly, the generation of these profiles also involves the calculation of associated probabilities to account for the likelihood of different charging behaviors, considering real-world uncertainties and variability.

4.1.1 Preparation and Pre-processing

When it comes to EV charging, key questions that every charging strategy needs to answer are to determine when to start charging and the state of charge of electric vehicles at the onset of charging. Acquiring pertinent information to address these pivotal questions necessitates the collection and analysis of two distinct sets of data. The first set of data pertains to the specifications of the EVs themselves, encompassing critical parameters such as the EV battery size and the nominal driving range achievable by the vehicle. The second set of data is EV travel

data, detailing the comprehensive driving patterns and behaviors of EV operators concerned with the travel patterns and behaviors of the EV drivers, encompassing various factors that significantly influence charging strategies. In this effort, we harnessed data from the National Household Travel Survey to gain insights into the overarching travel behaviors of EV users [117], and derived California-specific vehicle travel data, augmenting our dataset with valuable information such as the departure times of vehicle operators, the distances traveled, the time expended during travel, and the duration of dwelling time at destinations. The acquired EV data is categorized in Figure 12. The percentage of every possible daily vehicle dwelling hours and daily vehicle travel distances within 70 miles are included in Appendix B.

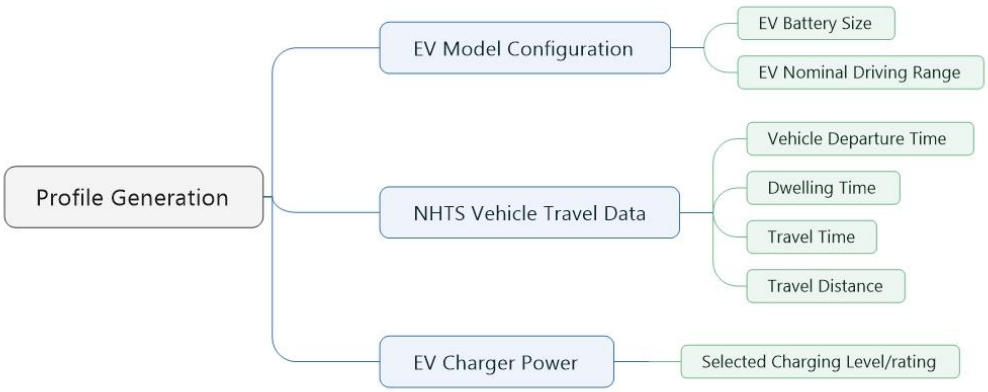

Figure 12. Data necessary for proposed methodology. The preparation process requires both EV characteristics and EV travel data.

Figure 13 shows the most popular EV model in CA based on state registrations in 2023 [118]. For the purpose of this analysis, the Tesla Model Y has been designated as the standard model, chosen based on its predominant share of the EV market in California, with a full charging time of 36 hours and maximum traveling distance per charge of 360 miles. The full charging time and maximum driving distance is crucial for the calculation in the following

sections. The analysis focuses on a maximum driving distance of 250 miles, restricting the daily travel distance of the vehicle to within this threshold as per the selected NHTS data.

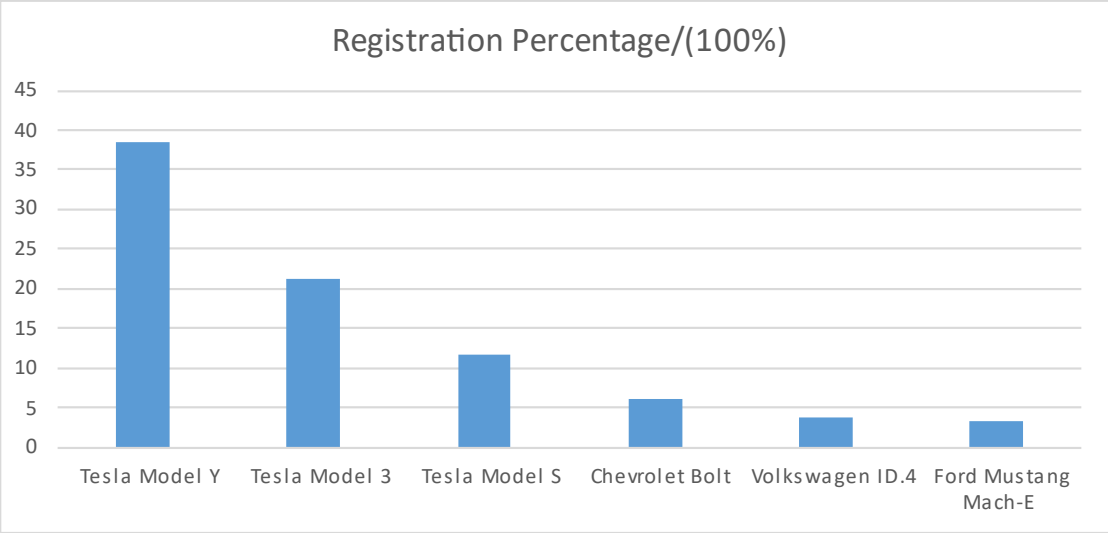

Figure 13. Most popular BEV models in the state of California from 2022-2023 Q3. Data source is California New Car Dealers Association.

4.1.2 Discreet EV Charging and Discharging Profile and Estimation and Trip Model Simplification

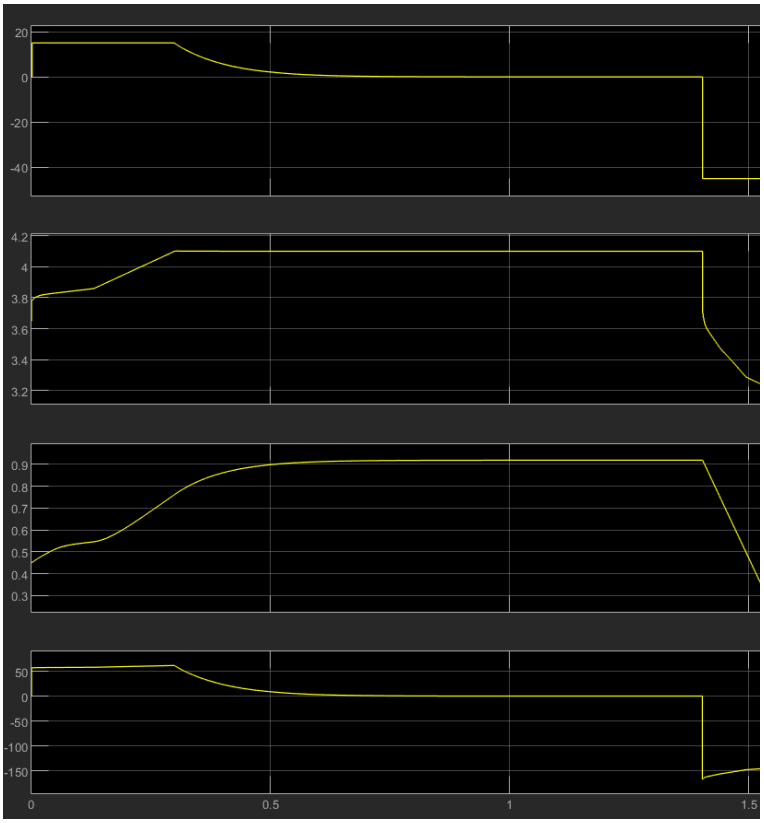

Figure 14. Charging profile of individual EV. From top to bottom are charging apmacity, charging voltage, SOC and charging power, respectively.

In our model, we used a near ideal individual EV level 1 charging profile based on a standard Lithium battery [119]. The charging profile of the characteristic EV is shown in Figure 14. The starting SOC of each individual EV is approximated by considering the ratio of trip distance to maximum driving mileage. Under the assumption that all EVs depart from home fully charged in our model, the computation of SOC and the subsequent derivation of the charging profile become straightforward.

An additional critical aspect of EV charging analysis pertains to the examination of vehicle trips. In coherence with the definition of vehicle trips provided by the NHTS, we herein establish

a simplified representation of a vehicle. In this representation, the EV's travel time encompasses both the duration taken from departure at home to the destination and the return journey from the destination to home. Moreover, the travel distance incorporates the combined distance of the entire trip. This simplification of EV travel and trips serves to facilitate a more straightforward implementation of bulk stochastic charging simulation, as elaborated in the subsequent sections.

4.1.3 Profile Generation and Possibility Calculation

To exploit the amassed data effectively, an initial methodology has been formulated. The process of profile generation is delineated in Figure 15. Primarily, the NHTS data underwent an initial screening to accommodate the maximum driving distance of the selected EV model. Subsequently, all conceivable combinations of EV departure time (from home), driving distance, travel time, and dwelling time (at the destination) were systematically considered, and their corresponding probabilities were computed.

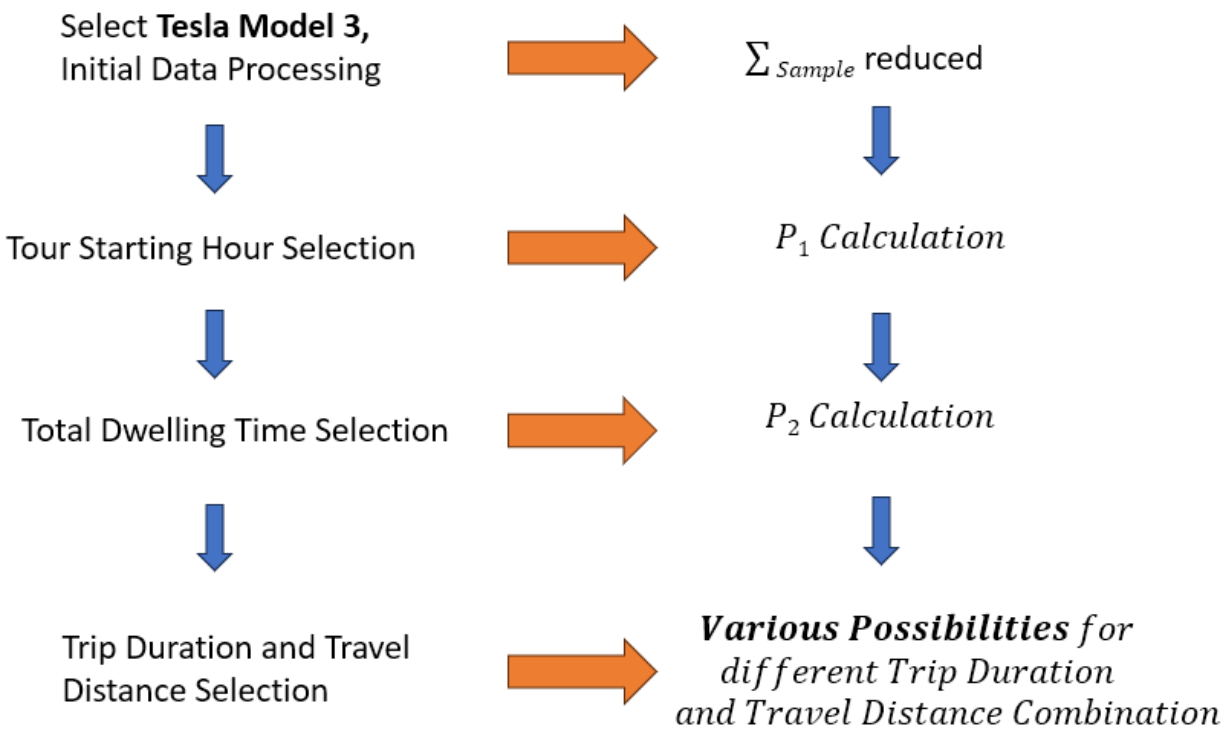

Figure 15. Preliminary EV charging profile generation and possibility calculation process.

A notable challenge arose, however, due to the inherent correlation between travel time data and travel distance, as shown in Table 4. To address this issue, we amalgamated the travel time data with EV departure time data (from home) and introduced what we term EV Arrival Time profiles. This integration aims to mitigate the influence of the travel time and travel distance correlation. The resultant correlation, calculated as 0.020202, indicates a minimal association between arrival time and travel distance. The EV Arrival Time profiles are visually represented in Figure 16. The revised generation process is shown in Figure 17. Based on information from California New Car Dealers Association in Figure 13, the EV considered in our model need 36 hours to get fully charged and can run up to 360 miles. An estimation for EV starting SOC is then developed. The calculations of possibilities of EV arrival time options, travel

distance options, dwelling time options as well as SOC estimation calculations are shown in equation (3)-(6).

$$P_{arrv\_t(i)} = \frac{\sum_1^{N\_arrv\_t(i)}}{\sum_1^{N\_arrv\_t}} \quad (3)$$

$$P_{trvl\_d(j)} = \frac{\sum_1^{N\_trvl\_t(j)}}{\sum_1^{N\_trvl\_d}} \quad (4)$$

$$P_{dwl\_t(i)} = \frac{\sum_1^{N\_dwl\_t(i)}}{\sum_1^{N\_dwl\_t}} \quad (5)$$

$$SOC_{i,j} = \left(1 - \frac{trvl_{d(j)}}{360/36}\right) \times 100\% \quad (6)$$

where $P_{arrv\_t(i)}$ is the possibility of EV arriving at the destination at hour i (i=0,1,…,23), $P_{trvl\_d(j)}$ is the possibility of EV traveling distance being j (j=10,20,…,180), $P_{dwl\_t(i)}$ is the possibility of EV dwelling at the destination for a total hour of i (i=0,1,…,23); $N\_arrv\_t(i)$ and N_arrv_t is the total number of samples that has an arrival time of i and the sum of total number of all possible arriving time in the sample. $N\_trvl\_d(j)$ and N_trvl_d is the total number of samples that has an traveling distance of j and the sum of total number of all possible traveling distances in the sample. $N\_dwl\_t(i)$ and N_dwl_t is the total number of samples that has a dwelling time of i and the sum of total number of all possible dwelling time in the sample.

The Monte Carlo operation details are listed in Table 5. The estimated quantity in the algorithm is the total infrastructure upgrade cost from EV integration, which will be illustrated

in the following sections. Note that if the results get below a standard deviation of 5% and converge within 500 iterations, then 500 iterations are run to ensure accuracy of the analysis.

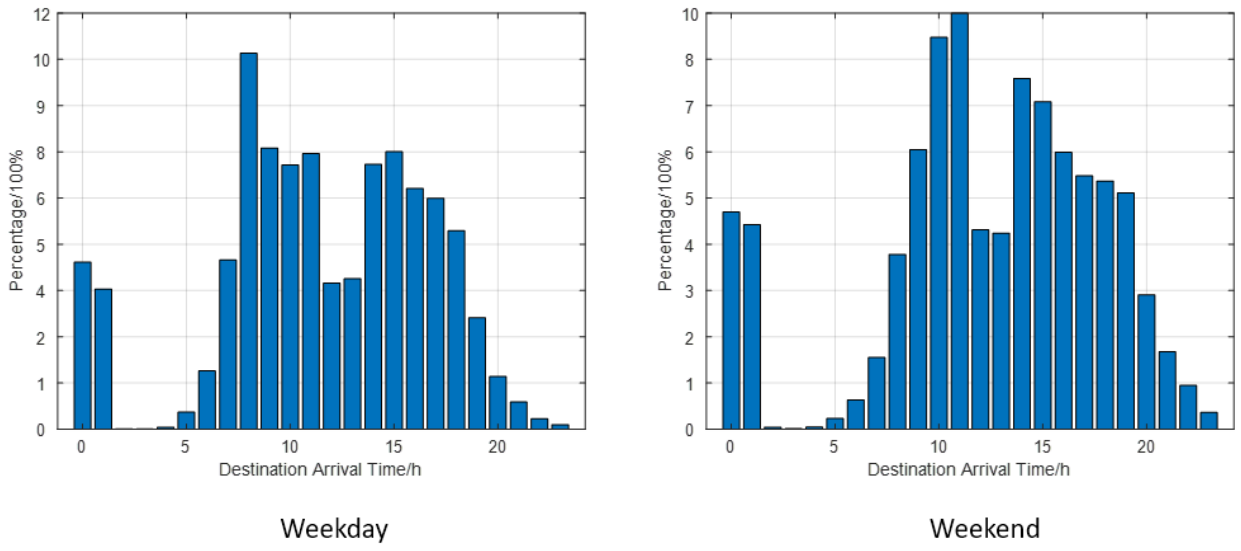

Figure 16. EV arrival time of weekdays and weekend. The figure is generated using NHTS data.

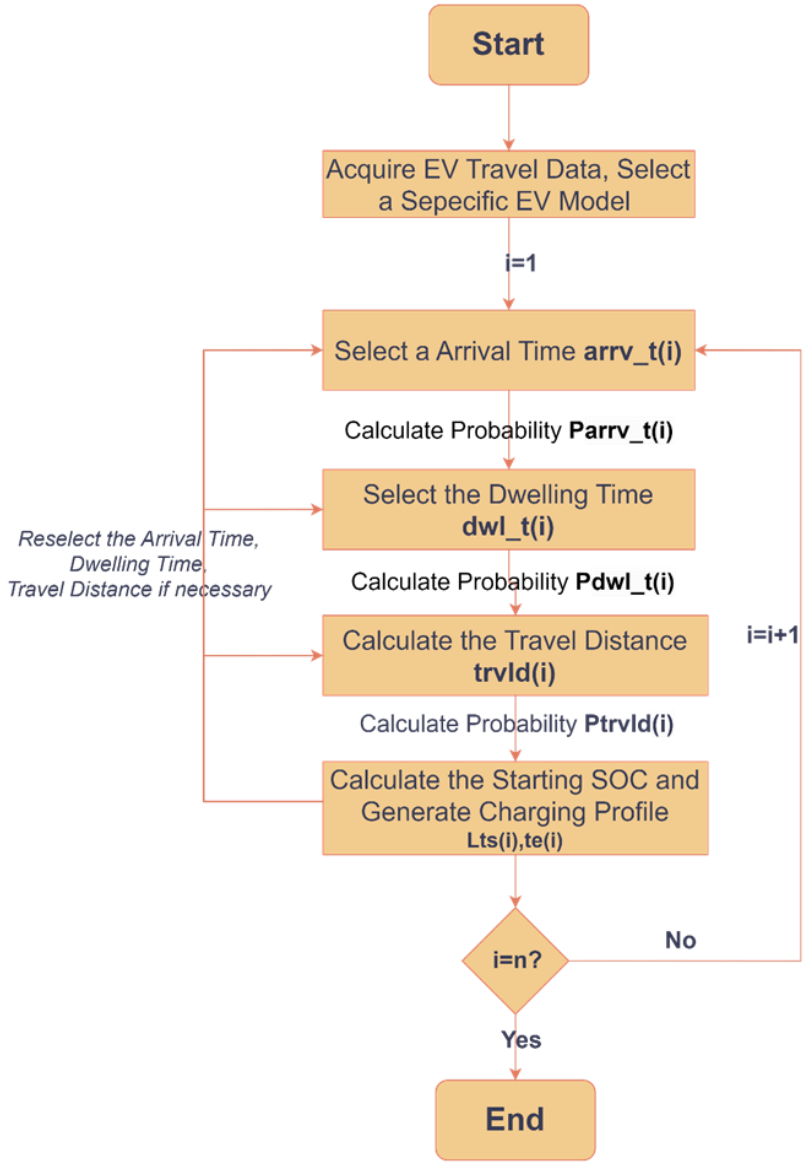

Figure 17. Final EV charging profile generation and possibility calculation process using EV Arrival Time.

Table 4. Correlations between each EV travel elements

	Starting Time	Travel Time	Travel Distance	Dwelling Time
Starting Time	N/A	-0.02190	-0.00017	0.052072
Travel Time	-0.02190	N/A	0.723092	0.123725
Travel Distance	-0.00017	0.723092	N/A	0.125907
Dwelling Time	0.052072	0.123725	0.125907	N/A

Table 5. Monte Carlo Algorithm Parameters.

Number of Iteration	Up to 500
Number of EVs in Each Iteration	Depending on EV Penetration Rate
Estimated Object	Total Infrastructure Upgrade Cost from EV Integration
Convergence Criteria	$\sigma<5\%$

4.1.4 EV Charging with Pseudo-Random Allocation in the Oak View Community

In this section, we address the allocation of discreet charging events facilitated by the available event generation. As noted earlier, the determination of these events takes into account the variables of vehicle arrival time, travel distance, and the duration of vehicle dwelling prior to the commencement of home charging. To comprehensively account for the inherent randomness in these factors, the Monte Carlo algorithm is employed, executing a predetermined number of iterations.

In accordance with the explicitly defined EV penetration rates stipulated by the California EV policy, each iteration follows a three-step process for the allocation of EV charging events. Firstly, a set number of residential units is randomly selected, with the ratio of the selected units to the total number of units corresponding to the EV percentage specified in the policy. This selection is predicated on the assumption that each residential unit is equipped with a single vehicle, and adherence to the policy's mandated EV penetration rate is rigorously maintained. The second step involves the allocation of vehicle arrival time, travel distance, and vehicle dwelling time for each EV or residential unit, guided by probability considerations. This step is termed "Pseudo-random allocation," as it prioritizes likelihood over purely random

assignment of these parameters. In the third step, the charging load profile is integrated with the existing electric demand, and a power flow simulation is executed to assess the impact of the added EV charging load on the electrical network. This iterative process encapsulates the intricate dynamics of real-world EV charging occurrences, providing a robust framework for evaluating the implications of different EV penetration rates as mandated by the CA EV policy.

In consideration of the established residential unit density within the Oak View Community, as previously delineated by the authors, the primary challenge in effectuating varying EV penetration rates within the Oak View community lies in the random selection of a specific percentage of residential units by Monte-Carlo Algorithm. For each iterative process, residential units within the same building are treated as independent entities, and the stochastic nature of random selection may lead to disparate EV ownership distributions among units within a given building, aligning with real-world scenarios. The residential population density is graphically presented in Figure 18.

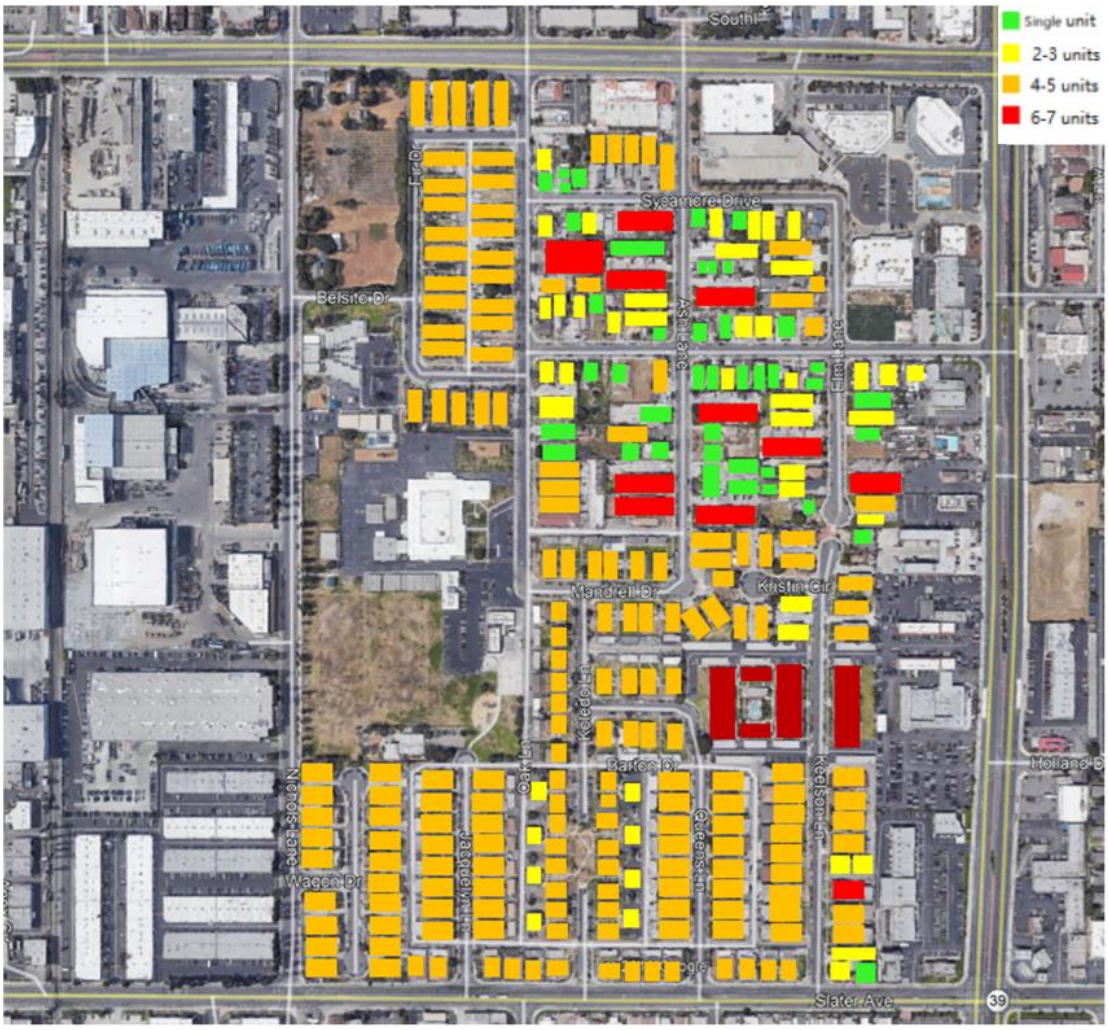

Figure 18. Population density of Oak View Community. Note that most units are multifamily housing.

4.2 Community Scale Vehicle Electrification Scenarios

4.2.1 Policy-driven EV Adoption Scenarios

California has emerged as a trailblazer in the domain of vehicle electrification. In accordance with Governor Newsom's Executive Order N-79-20, the progression of electric vehicle (EV) adoption in California is delineated through a three-step plan. By the year 2025, it is anticipated that 35% of the total new vehicle sales will comprise EVs. Subsequently, by the year 2030, this proportion of new vehicle sales is expected to escalate to 68%. The ultimate milestone in this

trajectory is the realization of 100% EV sales by the year 2035. Of course, many years of new vehicle sales are required to turn over the entire vehicle fleet. Nonetheless, inspired by California's ambitious EV goals which will eventually turn over the entire light duty vehicle fleet, we have constructed three EV scenarios as shown in Table 6 where the actual EV market share corresponds to the three levels of EV new sales percentages. According to California State Portal [120], the 35% EV market share will be achieved in 2040, with 68% EV market share achieved in 2045 and 100% share realized in 2055.

Table 6. California EV penetration rates considered as inspired by Executive Order N-79-20

EV Goal	EV Penetration Rate	Expected Year
#1	35%	2040
#2	68%	2045
#3	100%	2055

4.2.2 High Penetration EV Adoption with Level 2 and DC Fast Charging

This section will discuss the reasoning behind the development of each EV scenario and the detailed configuration as well as penetration rate of all involved charging events.

With California's 2025 State ZEV goal [121][122], a combination of different types and levels of charging is planned to take place in the OVMG [16]. The eventual goal of EV adoption in CA is 100% replacement of current vehicle market with EVs. In the foreseeable future, with more charging infrastructure available to the public, charging will no longer be mainly at home [123]. As a matter of fact, California policy should eventually favor workplace charging for coincidence of EV charging demand with grid supply of mostly solar primary energy, as expected by the California Air Resources Board [50]. To analyze the impact of EV adoption in

OVMG with charging other than Level 1 charging, several EV scenarios of high penetration rate are developed. A summary of discussed EV scenarios is depicted in Table 7. A summary of involved charger type and explanatory information are shown in Table 8.

Table 7. EV Scenario Summary

Scenario Name	EV Penetration Rate	Charger Type in Residential Area	Charger Type in C&I Area
1: 100% Residential LV 2	High	100% HL2	PL2, WL2, PDCF (default)
2: 100% Residential LV1/LV2	High	80% HL1, 20% HL2	PL2, WL2, PDCF (default)
3: 100% Residential LV1/LV2 +100% C&I LV2	High	80% HL1, 20% HL2	50% PL2, 50% WL2
4: 100% Residential LV2 +100% PDCF	High	100% HL2	100% PDCF

Table 8. Abbreviation of EV Charger Level and Power Level

Charger Type Abbreviation	Definition	Charger Power Level/KW
HL1	Home Level 1 EV Charger	1.4
HL2	Home Level 2 EV Charger	7.5
PL2	Public Level 2 EV Charger	11.4
WL2	Work Level 2 EV Charger	11.4
PDCF	Public DC Fast Charger	50

Originally derived from NREL's EVI-Pro program [124], a set of scaled-down OVMG EVSE charging load profiles is shown in Figure 19. This figure serves as a reference, and it is assumed that in later simulations that the peak power of individual charging of each of the charging types strictly follows the limits of Figure 19 whenever used. The charging power of all Level 2 charging is 10KW while Public DC Fast charging is 50KW.

Based on previous work done by the author [16], charger count of different types are acquired via a clustering method that is represented in Table 9. This scenario is designed based on CEC's projection of EV infrastructure projection to state's 2025 Zero-Emission-Vehicle deployment goals [121].

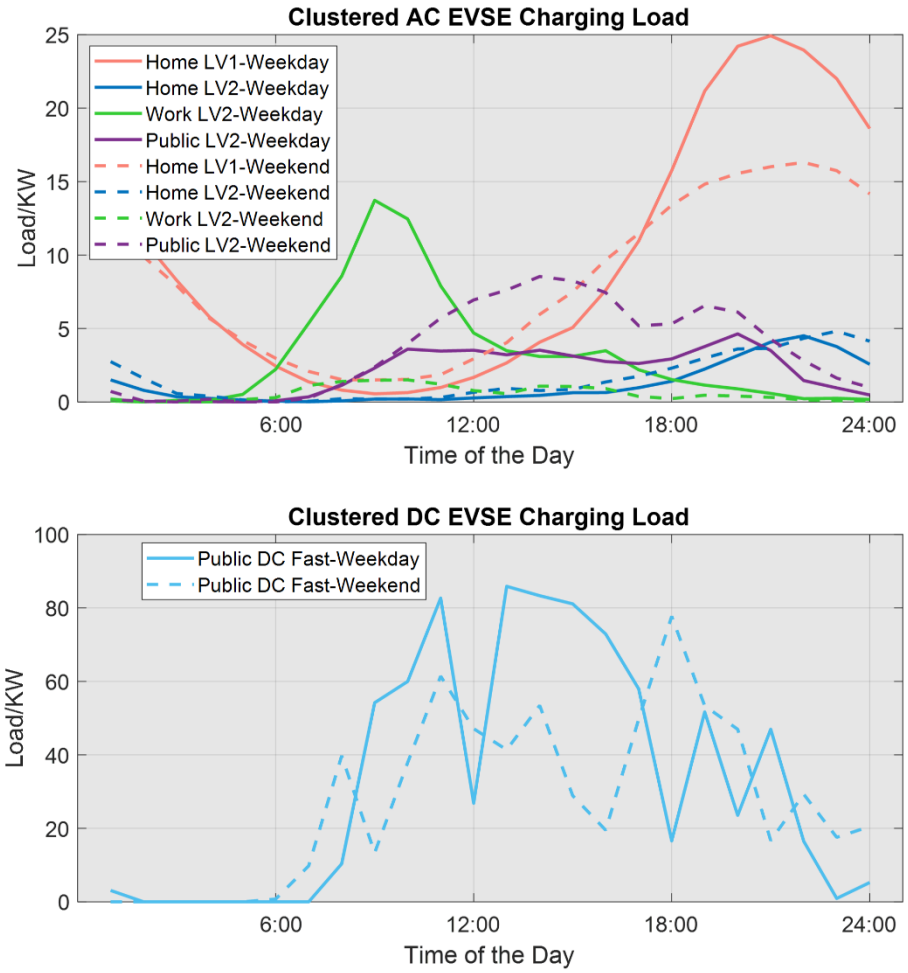

Figure 19. Hourly PEV Charging Profile for EVSE clusters: Home L1, Home L2, Work L2, Public, L2, and DC Fast charging. Solid lines represent charging demand on weekdays. Dashed lines represent charging demand on weekends.

Table 9. Details about chargers of different levels deployed in the Oak View Community sufficient for the 100% EV penetration scenario.

Charging Power Level	Transformer Count	EVSE count	Clusters
Home L1	9	394	10 clusters of 40
Home L2	1		
Work L2	5	19	5 clusters 4
Public L2	3	21	3 clusters of 7
Public DC Fast	1	5	1 cluster of 5

4.2.2.1 *Scenario 1: 100% Residential EV Penetration with LV2 Charging*

Similar to the previous LV1 discreet scenario, we now develop a LV2 charging scenario for residential vehicle electrification and charging. In this scenario, Level 2 chargers supplant their Level 1 counterparts, representing a boundary or spanning case wherein advancements in charger technology have precipitated the widespread affordability of Level 2 Home chargers among the demographic of utility consumers within the OVMG community. This evolution is underpinned by a customer preference for expeditious and more controllable charging experiences (e.g., to match charging with cheapest electricity rates) at residential premises, eclipsing the conventional reliance on Level 1 charging infrastructure.

A similar Monte Carlo process of LV2 and Public DC Fast charging profiles is extrapolated, with all algorithm parameters being the same, which mirrors a prototypical scenario of 100% LV2 EV charging deployment within the residential domain. The only difference lays in charging rate which results in different charging time and charging profiles.

The charging infrastructure within the C&I sector encompasses a range of charger types, including WL2 PL2, and PDCF chargers. These chargers adhere to the default operational configurations as delineated in the seminal work of L. Novoa et al. [125]. An example siting of different chargers is depicted in Figure 20.

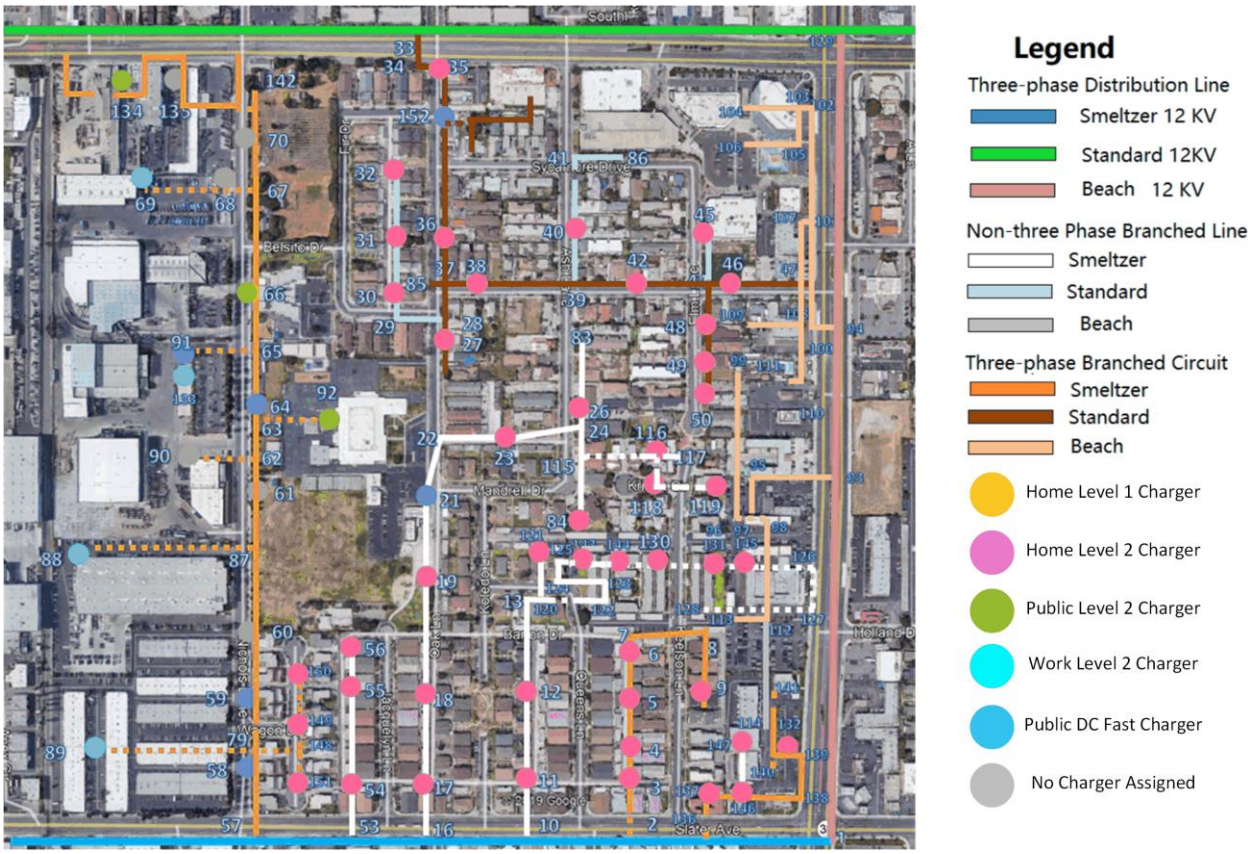

Figure 20. Position of different types of chargers in Scenario 3. Note that all chargers associated with each particular active distribution transformer shown in all sectors of the graph represent the situation where all affiliated utility customers connected to that transformer use the same type of charger.

4.2.2.2 Scenario 2: 100% Residential EV Penetration with LV1/LV2 Charging

This scenario delineates a transition from a moderate penetration of EVs within the C&I sector of the in OVMG Community compared to Scenario 1 and a more mixed adoption of LV1 and LV2 chargers in the residential sector. In residential areas, prior to the technological advancement of Level 2 charger systems to a degree where significant price reductions on individual purchases are feasible, it is pragmatic to posit that a blend of Level 1 and Level 2 charging infrastructure would likely prevail in the event of a complete 100% EV conversion.

Level 2 chargers predominantly find placement in newly developed residential buildings that are fully electric, exemplified by the Soltaros Apartment Homes, constituting a 20% share of the residential charging landscape. The remaining 80% of residential charging is exclusively facilitated by Level 1 chargers. The percentage of LV1 and LV2 charging used here are considered by NREL as most probable average shares in 2050 [126]. Concurrently, the same number and deployment of Level 2 chargers and Public DC Fast chargers are integrated into the C&I sector, with their deployment contingent upon factory/facility dimensions and hosting capacity, as delineated by the findings of L. Novoa et al. [125].

The Monte Carlo algorithm is employed for the stochastic selection and deployment of LV1 and LV2 chargers within the residential sector. Maintaining a fixed ratio of 80% LV1 chargers and 20% LV2 chargers per stochastic iteration, the allocation process initiates by randomly selecting residential units for LV1 charger installation until the 80% threshold is achieved. Subsequently, the remaining 20% of residential units are automatically designated for LV2 charger installation. An example siting of different chargers is depicted in Figure 21.

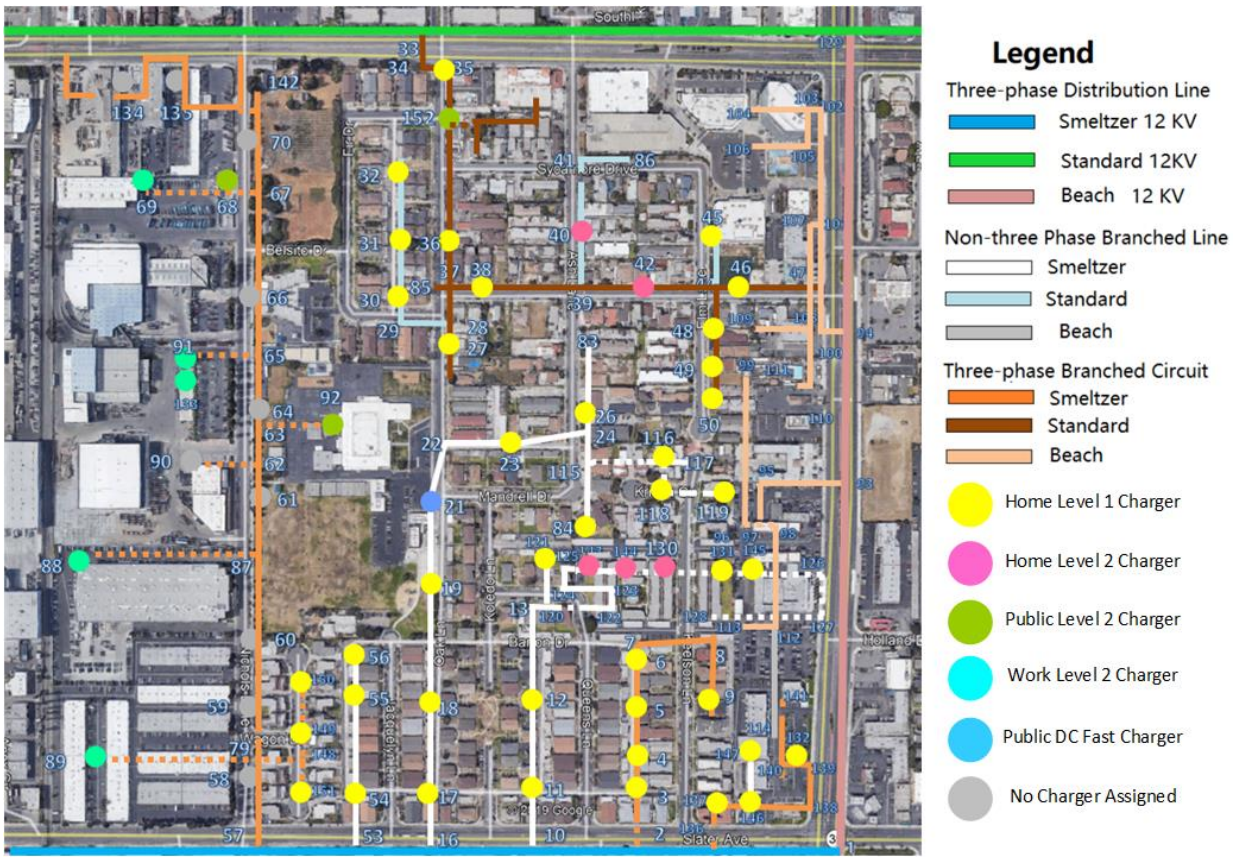

Figure 21. Position of different types of chargers in Scenario 2. Note that all chargers associated with each particular active distribution transformer shown in all sectors of the graph represent the situation where all affiliated utility customers connected to that transformer use the same type of charger.

4.2.2.3 Scenario 3: 100% Residential EV Penetration and 100% C&I Section EV Penetration with LV2 Charging

This scenario builds upon Scenario 2 by achieving a LV2 100% EV penetration rate within the Commercial and Industrial sector, symbolizing a complete conversion of EV adoption throughout the OVMG Community. This transition to full vehicle electrification, employing cutting-edge charging technologies within each sector, serves as a pivotal step towards fulfilling the goal of 100% community electrification.

A substantial and equitable deployment of Public Level 2 and Work Level 2 chargers is implemented within the C&I zone, informed by recommendations from the EVI-PRO framework [126]. The Monte Carlo Algorithm is once again utilized for the allocation of both types of LV2 chargers within the residential sector, with an 80% and 20% distribution of LV1 and LV2 chargers, respectively.

Figure 22 illustrates a sample layout depicting the distribution of various charger types across different settings.

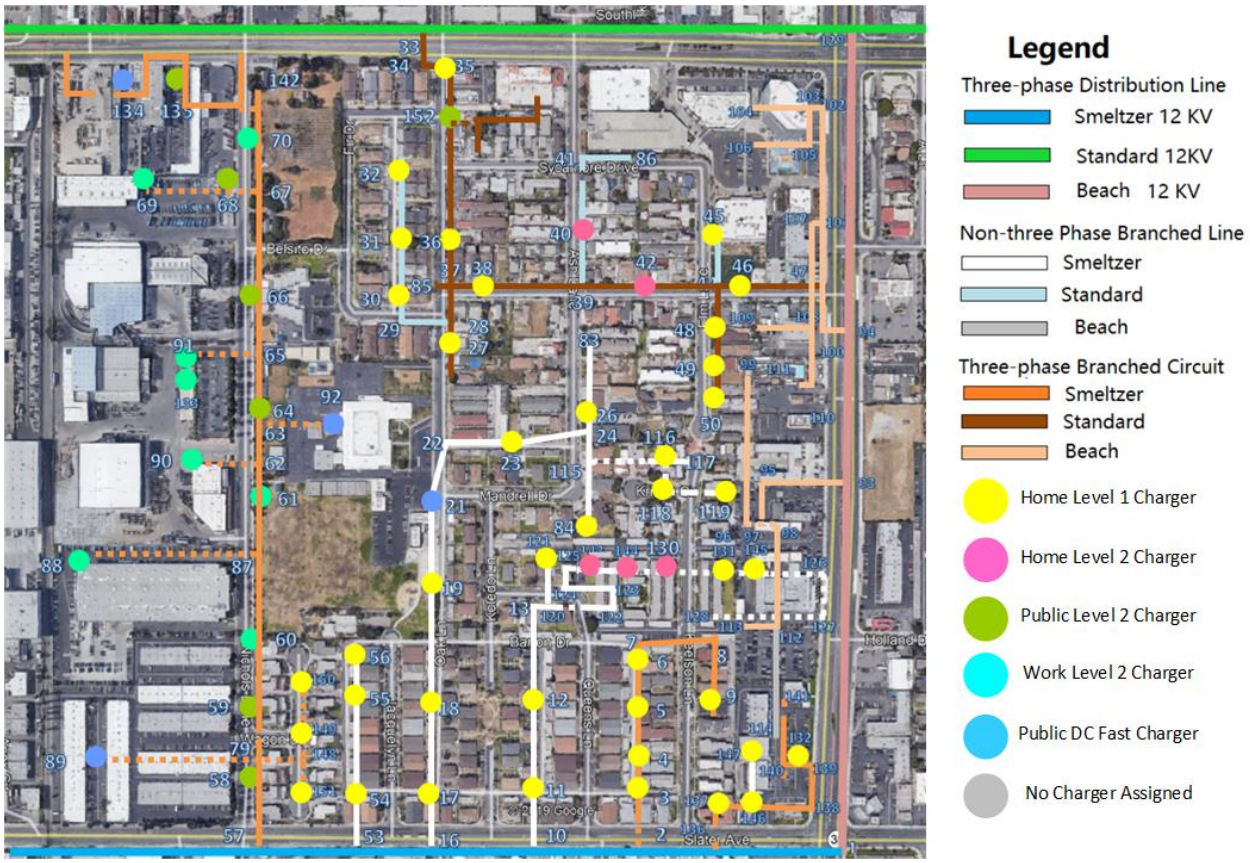

Figure 22. Position of different types of chargers in Scenario 3. Note that all chargers associated with each particular active distribution transformer shown in all sectors of the graph represent the situation where all affiliated utility customers connected to that transformer use the same type of charger.

4.2.2.4 *Scenario 4: 100% Residential EV Penetration with LV2 charging and 100% C&I PDCF Charging*

This scenario represents another spanning set of conditions for achieving 100% EV conversion within the OVMG Community, with all customers provided access to fast charging (LV2 at home and DC fast charging at work). By ensuring an ample quantity of chargers to accomplish the swiftest charging capabilities accessible to all members of the community, this scenario delineates a very advanced and successful prospective EV market. Within this scenario, all utility customers residing in residential zones are presumed to exclusively utilize Home Level 2 chargers for EV charging purposes, while those in C&I sectors rely exclusively upon Public DC Fast chargers. The placement of each set of chargers is delineated in Figure 23, as associated with each distribution transformer in the microgrid model.

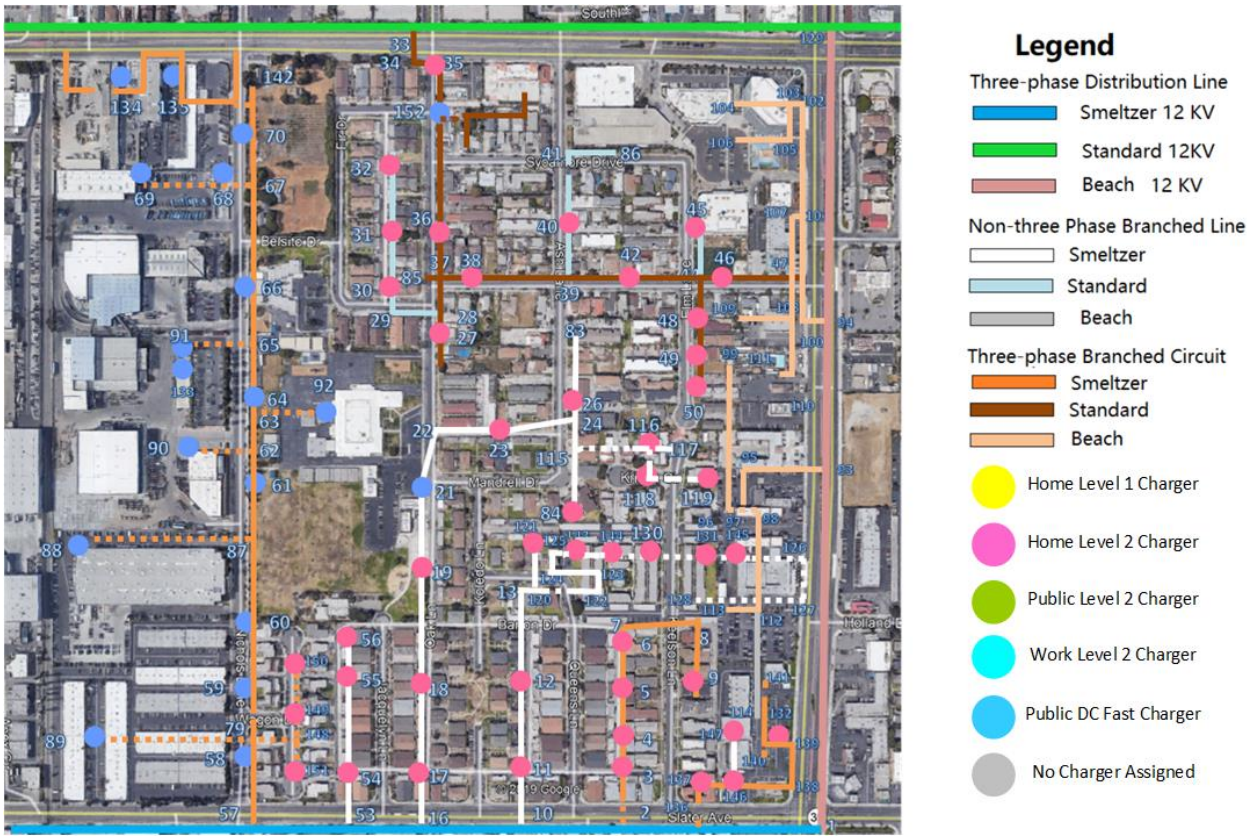

Figure 23. Position of different types of chargers in Scenario 3. Note that all chargers associated with each particular active distribution transformer shown in all sectors of the graph represent the situation where all affiliated utility customers connected to that transformer use the same type of charger.

4.3 Bulk Vehicle Electrification in Southern California

4.3.1 SCE Service Territory Scenarios

Given the author's prior work on the quantification of empirical transformer degradation model [127], it is advantageous to extend the simulation to the county level, specifically for the regional substations. This endeavor has been facilitated through the utilization of SCE's Distribution Resources Plan External Portal (DRPEP) [109] and Power Site Search Tool (PSST) [128]. These tools have enabled the comprehensive recording of load profiles for each

operational distribution substation, along with their respective ratings. The geographical distribution of these transformers and population served by each set of distribution substation transformers is illustrated in Figure 24.

To incorporate the aggregate electric vehicle charging load profiles into individual substations, we employed NREL's Electric Vehicle Infrastructure Projection Tool (EVI-Pro) [126]. This tool offers anticipated EV charging loads based on user-defined population parameters. The median commuting distance of each SoCal County has been used here as a reference for standard EV travel distance and stays the same for all substations in the same county. The individual EV charging profiles derived from EVI-Pro for each county is presented in in Figure 19. However, ascertaining the population served by each substation requires a preliminary estimation, as illustrated in Figure 25. Although the population serviced by each substation is not publicly accessible, the total load, or the comprehensive projected load on DRPEP, can be determined. It is posited that the former is directly proportional to the latter. Summing up the populations of all substations yields a total population of 15 million individual meters within SCE's operational domain. Subsequently, individual substation populations are determined by assigning fractions of the total population to each substation in proportion to the respective load ratios (i.e., substation load/total SCE load). The meteorological profile for each substation is sourced from the National Weather Service (NWS). Figure 24 also illustrates the population density corresponding to each substation. SCE's capacity expansion plan [109] was used to increase each of the substation transformer capacities for the power flow simulations and degradation analysis for the entire SCE service territory. That is, we assumed that each specific

year's simulation uses the upgraded planned total capacity as the actual substation transformer ratings.

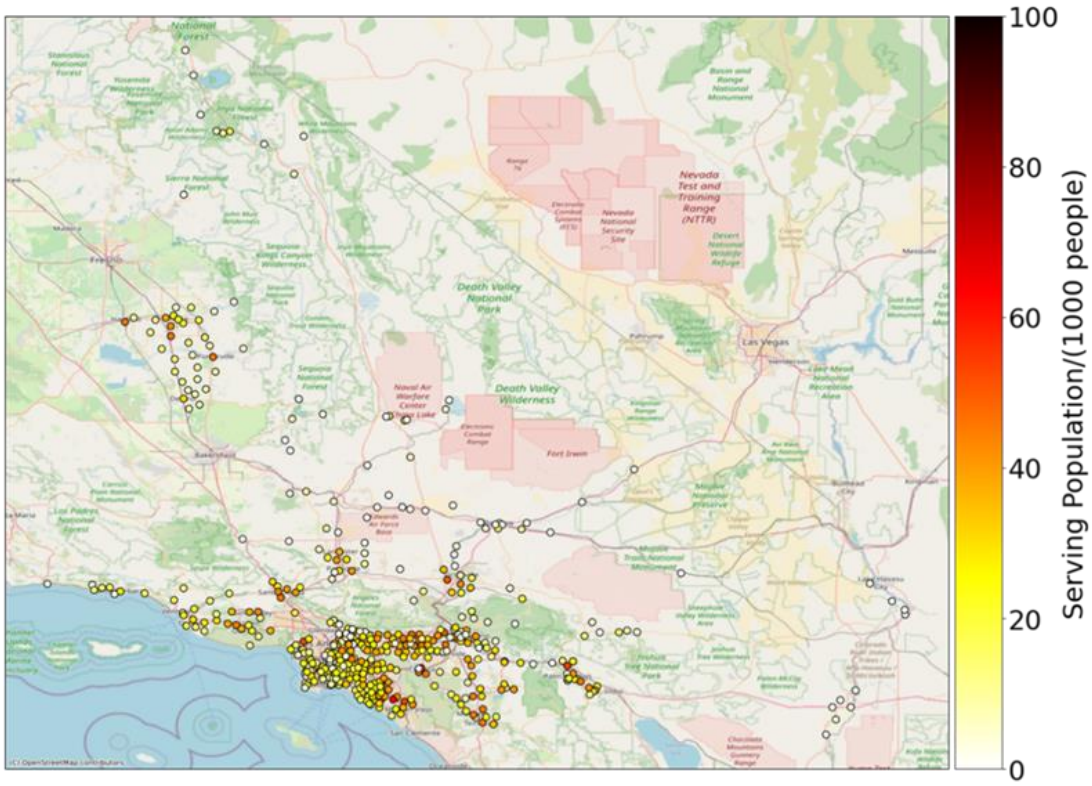

Figure 24. Population served by every set of SCE distribution substation transformers.

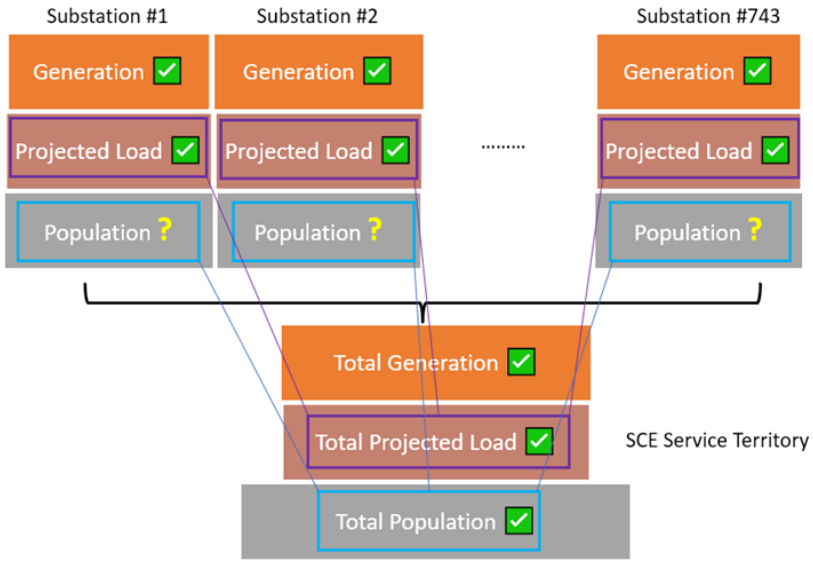

Figure 25. The process of estimating each substation's serving population with the ratio of known substation projected load.

4.3.2 The Oceanview Substation Special Analysis

Of all the substations shown in Figure 25, one substation, the Oceanview substation, can be further analyzed. The Oceanview substation serves a multitude of local communities, including the Oak View Community, and the author was able to check the overall layout in person during one of the fields trips for the OVMG project. Due to the fact that the Oak View Community and neighboring local communities also powered by the Oceanview Substation are electrically, socially, and economically similar, it is reasonable to assume that a scaled-up load level from the Oak View Community for different EV scenarios would represent the overall level of increased electric demand imposed on the Oceanview Substation. The details of the analysis will be expanded upon in later sections.

The analysis for this very substation will be further expanded to substation bus, protection relay and related common electronics and switchgear used for protection purposes. In this case the popular analysis platform for substation ETAP (Electrical Transient Analyzer Program) is used.

The Oceanview Substation, a 230kV/13.8kV substation, is modeled in ETAP 16.00 with utility system equivalent, overhead transmission line, power transformer, underground cable, substations bus, feeder loads, and protective relays. The equivalent feeder load is the direct result from the previous scaled-up estimation using the load level from the Oak View Community by population. The length of the transmission lines and cables is from the SCE's DRPEP toolkit [109]. The substation bus and protection relays settings are modeled with observed facts during one field trip for OVMG project, where one high side and low side

transformer respectively were spotted to connect with one circuit breaker each. The protection mechanism is believed to be differential protection with multiple current transformers.

The parameters to build the Oceanview Substation ETAP model are listed in Table 10. Most parameters are acquired either through direct observation during OVMG field trips or from most common utility practical standardized procedures. A few parameters, such as the load power factor, have been configured with OVMG project assumptions. The ETAP model is illustrated in Figure 26.

Table 10. Oceanview Substation ETAP model parameters

Category	Parameter Type	Parameter Value	Parameter Source
Feeder Loads	Load Nominal Voltage	13.9KV	SCE DRPEP
	Load Power Factor	0.9	OVMG Assumption
	Connection	Delta	Field Trip Observation
Utility System Equivalents	Utility Nominal Voltage	220KV	SCE DRPEP
	3LG Fault Current	5000A, X/R=10	Practical Industrial Standard
	SLG Fault Current	7000A, X/R=12	Practical Industrial Standard
Transmission Line	Length	0.21 miles	SCE DRPEP
	R/X/C	Pelican	OVMG Assumption
Substation Transformer	Primary Nominal Voltage	220KV	Field Trip Observation
	Secondary Nominal Voltage	13.8KV	Field Trip Observation
	Rated OA Apparent Power	100	Field Trip Observation

	Impedance	9.5%	Practical Industrial Standard
	X/R	35	Practical Industrial Standard
	Tap Setting	Nominal on Both Side	OVMG Assumption
	Connection	Dyn1	Field Trip Observation
Underground Cable	Size	1000 kcmil	Practical Industrial Standard
	Length	500 ft	OVMG Assumption
	Conductor per Phase	16	OVMG Assumption
	Rated Voltage	15KV	Practical Industrial Standard
	Type/material	Aluminum	Practical Industrial Standard
Relay	Transformer Relay	Schweizer 487E	OVMG Assumption

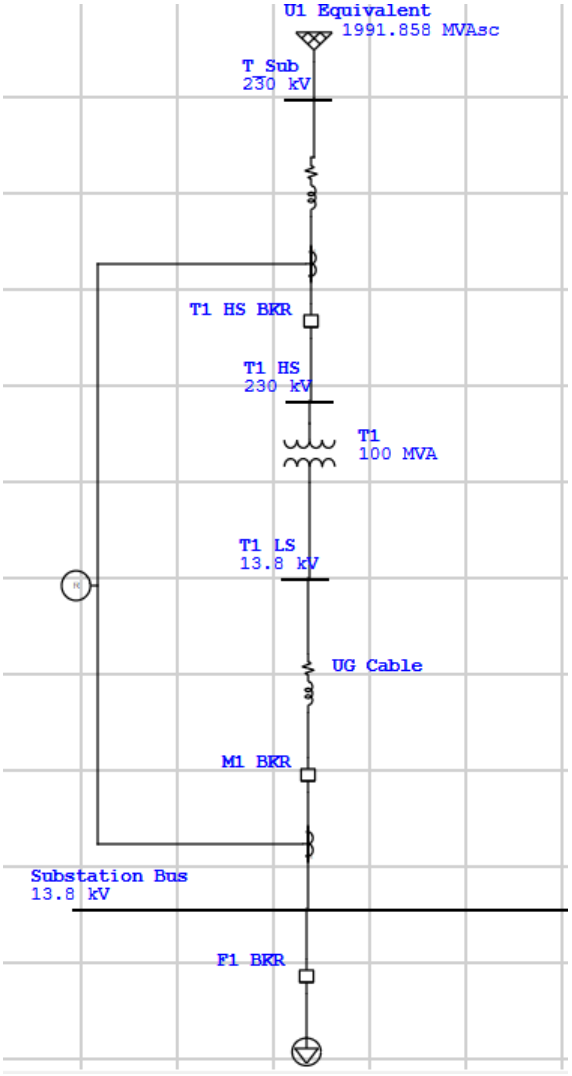

Figure 26. ETAP model of the Oceanview Substation with transformer, protection relay scheme and related switchgear.

5 Renewable and Clean Energy Systems Adoption in Novel Operational Scenarios

In recent years natural disasters have severely impacted the reliability of electric grids to power communities. From extreme weather conditions such as high winds to abnormal climate phenomenon such as hurricanes, super storms and even drought, the weather cuts off power

or operators are forced to cut off electricity supply on an increasingly frequent basis, in PSPS events. In the meantime, new concepts and technologies have been reshaping the way people use electricity, especially with much higher use of electricity for meeting transportation demands and increasingly electrifying buildings. To help mitigate the climate consequences from global warming, microgrids have been used to power communities with high use of distributed resources and also to keep powering the communities through emergencies such as PSPS events. In this section several topology designs based upon the original OVMG are first proposed, each tested in the ACPF model and will then be analyzed for their impacts on the community and on the macro grid.

It has been quite a while since EV was first introduced to the market, and one new technology derived from EV use has been proposed and discussed— vehicle-to-grid, or V2G. With bidirectional charging of EV to or from the microgrid, EV can serve in many helpful roles in grid and microgrid control. In this section a V2G peak shaving application in the OVMG will also be developed and analyzed.

The openness toward energy trading has also created new challenges for and complicated the reliable operation of microgrids. Methods to handle excess clean energy from DER by mainly harnessing ESS have now been expanded with individuals selling back their surplus power to the grid for credit, mostly through Net Metering or Co-Metering programs. Currently in California, with NEM 3.0 replacing the NEM 2.0, different adoption rates of NEM qualifying systems will have different impacts on a microgrid and its reliability. Therefore, a case study applied with NEM 3.0 users active in the OVMG will be analyzed with multiple scenarios. Details about each scenario are shown in Table 11. Two sets of scenarios are developed, one being

NEM 3.0 with infrastructure degradation constraints, one without. Details of NEM scenarios will be shown in Section 5.3.

Table 11. NEM Scenario Summary

Scenario	NEM System
1	NEM 3.0 without constraints
2	NEM 3.0 with constraints

5.1 Topology Design for Better Islanded Operations During Grid Interruptions

Global climate change has led to numerous challenges across Californian electrical distribution systems [132]. Extreme weather events, like heat waves, high winds, wildfires, and Public Safety Power Shutoff events, and flooding have reduced electric distribution grid resiliency, particularly in rural areas in California. Microgrids with distributed energy resources (DERs), can operate in islanded mode, increasing resiliency against these unexpected climate-inducted power failures [132]. However, reliable microgrid islanding operation has multiple challenges, including local power balance, power quality control, equipment protection coordination [133]. Therefore, microgrid design, topology, and control topics must be taken into consideration to cope with those challenges.

A balance between load and demand has been required since the creation of the 1st circuit, which is a major focus of research on microgrids. In recent years, research has been performed on microgrid design to address these challenges. In [134] a micro-CHP device used as an islanding generator was incorporated into household load/demand balancing. A methodology for isolated grid operation power balance is further demonstrated in [135]. Additional types of

energy management for microgrid islanding design are studied in [20,77,136–138]. Some studies advance the design of microgrid topology based on power quality optimization, such as in [139] and [140]. A few other studies evaluate the possibility of microgrid power quality control with the use of Vehicle-to-grid (V2G) techniques [20,70,73,76,141]. Many topology design methods have been proposed. Based on survivability schemes, one topology design reconnects small microgrid network through optimized utilization of renewable energy sources [23]. Topology design in [24] and [25] efficiently combines graph partitioning algorithm with MILP to reach local energy equilibrium when generating islands and remaking connections for mesh circuits. Multi-Objective Substrate Layer Coral Reefs Optimization Algorithm was applied to decide distribution of DERs and optimal connection of different nodes in [26] A viable restructuring of existing microgrids was used with phase angle measurements of the swing equations based on multivariate Wiener filtering to reconstruct operating radial power grids in [27]. While most of the above address different goals in grids under islanding operation mode, very few bring about such goals based on existing topology, and usually a significant amount of effort on or even a complete reconstruction of grid system is needed to implement the algorithms proposed. Also, very few propose designs considering more than one goal such as local power balance focus and electric power quality (PQ) control and very few are experienced under real-life electrification scenarios.

This section continues previous works on topological optimization for distribution circuit power balance in islanded operation without considering existing powerlines [24] by adapting into forms that are appropriate for radially developed community scale circuits with an

emphasis on power balance ability as well as power quality control while keeping as much of the original distribution system infrastructure as possible as applied in a real-life scenario.

5.1.1 Development of Graph-partitioning-based Loop Planning

Our work builds upon a graph partitioning algorithm presented in [24] that designed the optimal microgrid topology for a given set of nodes with loads and generation. Our main contribution to this algorithm are modifications to this algorithm that design microgrid topologies across preexisting electric distribution systems. A standard multilevel graph partitioning algorithm consisting of three phases-- the Coarsening, Partitioning and Uncoarsening. The graph-partitioning-based island distribution circuit topology algorithm determines which nodes should form a microgrid during a utility interruption, and indicates how these nodes should be connected. Similar to the classic three-phase approach, our modified variant of these phases is aimed at achieving a more equitable distribution of power, ultimately enhancing the power balance in the generated islands. The primary objective of our graph partitioning methodology is twofold: first, to produce islands with a well-balanced power distribution, and second, to adhere to the stipulated power quality requirements.

The topology of the baseline scenario chosen for analysis is shown in Figure 27. The community is supplied with power through two 12 kV 3-phase distribution lines. Pad-mounted and pole-mounted transformers are indicated with blue squares and yellow circles, respectively. The determination of cable connections and transformer placements was established through a hybrid approach that combines on-site field observations with maps of distribution circuits [109]. Building loads serviced through this infrastructure is based on work

in [142][16] [143]. It should be noted that all ensuing examples will be executed on distinct segments of the Oak View Community grid topology or encompass the entire grid network. New potential infrastructure is highlighted using dashed cyan blue lines. These new lines were selected based on proximity of different distribution branch circuits and the potential to install new powerlines located on public or city owned land.

Difference from original topology design will be pointed out below.

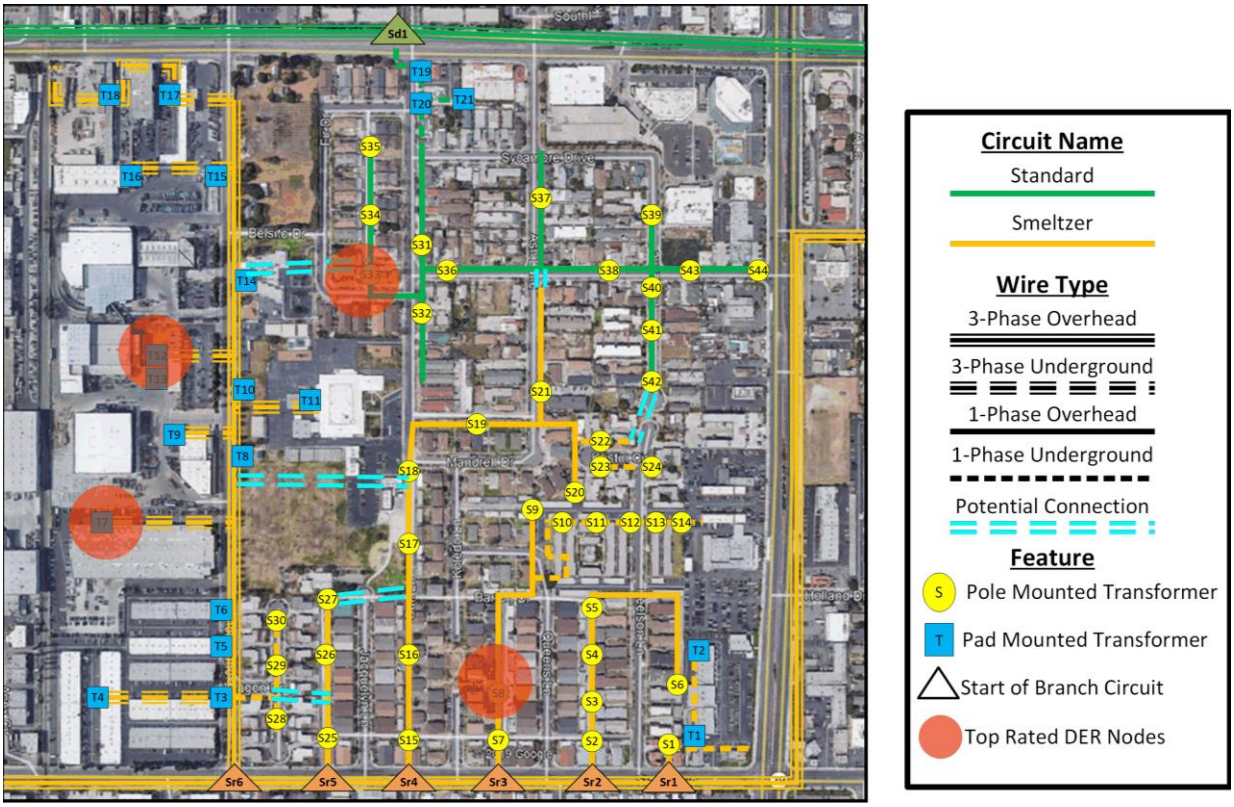

Figure 27. Oak View Community topology. All the marked nodes in yellow and blue are existing transformers.

5.1.1.1 Phases of Topology Design

5.1.1.1.1 Phase 1--Coarsening

Phase 1 is coarsening, where the graph is simplified into several node sets that are regarded as single nodes in phase 2 partitioning. Heavy edge matching (HEM) is used here. The basic idea

of HEM is to have neighbor nodes join the given adjacent node to form a single node that has relatively high-weight edges. HEM is commonly seen in communication network problems. In our case, HEM is slightly modified to cluster nodes based on proximity – closer nodes have a higher weight. The following modified HEM steps are followed:

a) Initialize the set of matching as M0= ∅; i=0;

b) Randomly select a vertex (V_m) in Gi that is not yet associated with the matching Mi;

c) Among edges adjacent to V_m select the minimal length edge (maximal-weight edge) (E_{mn});

d) Join vertices V_m and V_n to form a new vertex in Gi + 1; associate V_m and V_n with matching Mi;

e) If half of the total nodes are included in the coarsened graph, which is the criteria we chose) then stop; otherwise, set i=i+1 and go back to Step b.

5.1.1.1.2 Phase 2--Partitioning

After coarsening, a greedy graph growing partitioning (GGGP) algorithm is applied to group nodes together based on balancing loads and generation at each group of nodes. In contrast to initiating the phase with random nodes, our proposed algorithm takes a more targeted approach by commencing with nodes exhibiting the most significant power imbalances. This strategic initiation is designed to enhance the partitioning process's effectiveness. Similar to Phase-1, the Phase-2 partitioning process continues to adhere to a weight-based approach. However, in order to align the partitioning strategy more closely with our specific objectives, we introduce modifications to the weight and gain considerations, taking local power balance into account, as elaborated in step (b). It is noteworthy that our partitioning approach considers

not only nodes with pre-existing connections but also nodes with the potential for connection, even if such connections do not exist in the original network. In our particular case, we recognize all horizontal connections between nodes from nearby branch circuits as potential connections, as illustrated in Figure 27. The following steps are followed:

a) Each loop (V1) starts to grow from one of selected imbalanced nodes

b) Vertex (V_m) in V1's boundary (V2) that has maximal Gain is inserted to V1. The Gain is defined as:

$$Gain(V_1) = 1 - |PM(V_m)| \quad (7)$$

$$where,\ PM(V_j) = \int_t^{\square} \frac{DG(V_m) - D(V_m)}{D(V_m)} \times 100\%, \quad (8)$$

and PM(V_m) is the power mismatch in loop V_m when V_m's closest first-order outside neighbor node Vj is inserted ; DG and D are the dynamic DER capacity and load at the a given time t respectively.

c) The first-order neighbors of V_m previously belong to V3 are moved to V2;

d) If half or more of all nodes are included in different V1 then stop; otherwise, go back to Step-b.

5.1.1.1.3 Phase 3--Uncoarsening

Phase-3 is specially modified. Our criteria for doing swap testing, apart from keeping down generation/load unbalance, also focus on inviting nodes from branched circuit that are from different distribution circuit. The following steps are followed:

a) Swap testing: randomly select a pair of boundary nodes and test if their swap can improve the current partition (e.g., successful or failed swap);

Revised the swap testing (step a) criterion:

λm,n=$\sum_{m,n}\{|PM(V_i) - PM(V_i) ** |\}$ ×Distline_weight (9)

Distline_weight= 1 if i is from different distribution line of m or n,2 otherwise. The double superscript ** denotes the desired value, which is defined manually based on design requirement.m and n denote two adjacent loop systems.

b) Only perform the successful swaps where λ is reduced;

c) Once a vertex is tested, it will be fixed (excluded from any future swap testing);

d) If a given condition is satisfied (e.g., there are n successive cancelled swaps where n is a predefined number), then stop; otherwise, go back to Step-a.

then stop; otherwise, go back to Step-a.

5.1.2 Real-life Examples Using Proposed Islanding Method and Reference Scenarios

Four configurations of island topology design are used for comparison. The first configuration replicates the Oak View Community topology by disconnecting each branch circuit from the primary 12-kV distribution line for simplicity of implementation. The second one creates two islands based on distribution line origin. The third one applied the microgrid formation algorithm to the Oak View community but does not allow for supplementary connections. The last configuration involves employing the algorithm when allowing supplementary connections. Quantitative analysis will be conducted to compare the

effectiveness of these four topology design algorithms in maintaining local power balance, including quantified power balance analysis and power quality comparison after islanding.

The real-life power flow model for the Oak View Community is used to demonstrate the islanding algorithm described above Both islanded operation mode with and without the extra connections in the Oak View Community were considered, where the latter serves as a close reference. Selection of the starting point for each island for both scenarios under islanded operation mode is shown as red dots in Figure 27.

The details and comparison of four topology designs are depicted in Table 12.

Table 12. Topology Design Method Summary for OVMG

Topology Design	Design Goal	involved Algorithm	Addition of extra connections
Branch Islanding	Easiness to implement	None	N/A
12 KV Distribution Line Islanding	Common Engineering Islanding Solution	None	N/A
Optimal Design w/o Extra Connection	Local Power Demand and Supply Balance	Multilevel Graph Partitioning, MILP	No
Optimal Design w/ Extra Connection	Potential Better Local Power Demand and Supply Balance with Extra Energy Routes	Multilevel Graph Partitioning, MILP	Yes

After conducting a yearly power flow analysis on each island employing distinct methods as delineated in in the previous section, the ensuing section embarks on a thorough examination of four islanding methodologies. Therein, all islanding outcomes derived from various scenarios employing two of the basic islanding algorithms, alongside comparative analyses of scenarios with and without supplementary connections using the proposed optimized islanding algorithm, shall be expounded upon.

5.1.2.1 *Topology Design 1: Branch Islanding*

This scenario exemplifies the implementation of a basic islanding technique, wherein each radially developed branch is regarded as an independent island during an islanding event. This design scenario functions as a reference, offering the most straightforward method to island the OVMG, which is characterized by radial development. Notably, this particular islanding technique yields seven distinct islands, as depicted in Figure 28.

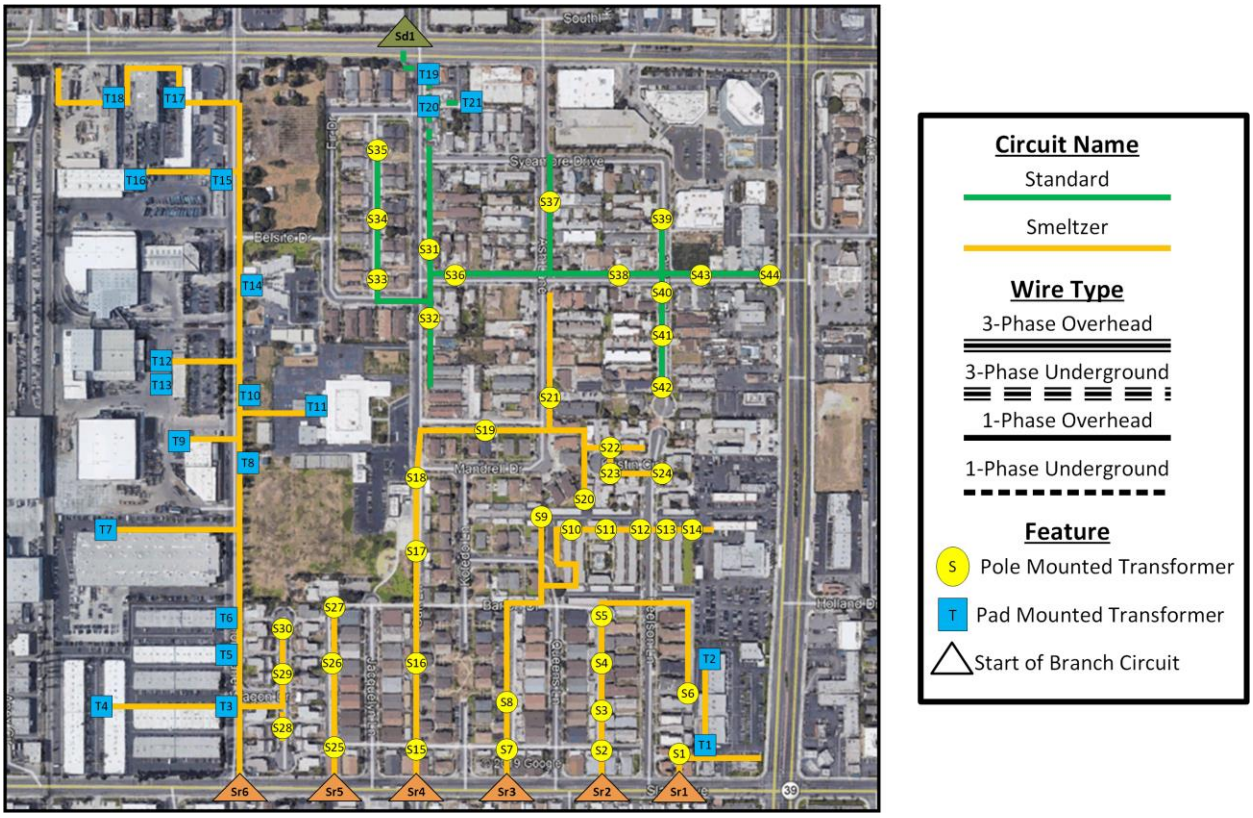

Figure 28. Final islanding result by islanding each branch circuit. In this case seven different islands are generated.

5.1.2.2 *Topology Design 2: 12 KV Distribution Line Islanding Scenario*

The concept underlying this islanding scenario involves the deliberate segregation of primary branch circuits according to their respective 12 KV distribution lines. The islanding outcome is visualized in Figure 29. All branch circuits originating from the Standard distribution

line were composed into a singular island, depicted in Figure 29 as the ensemble of green branch circuits (top island). Conversely, branch circuits originating from the Smeltzer distribution line form a distinct island, portrayed in Figure 29 as the collective of yellow branch circuits (bottom island).

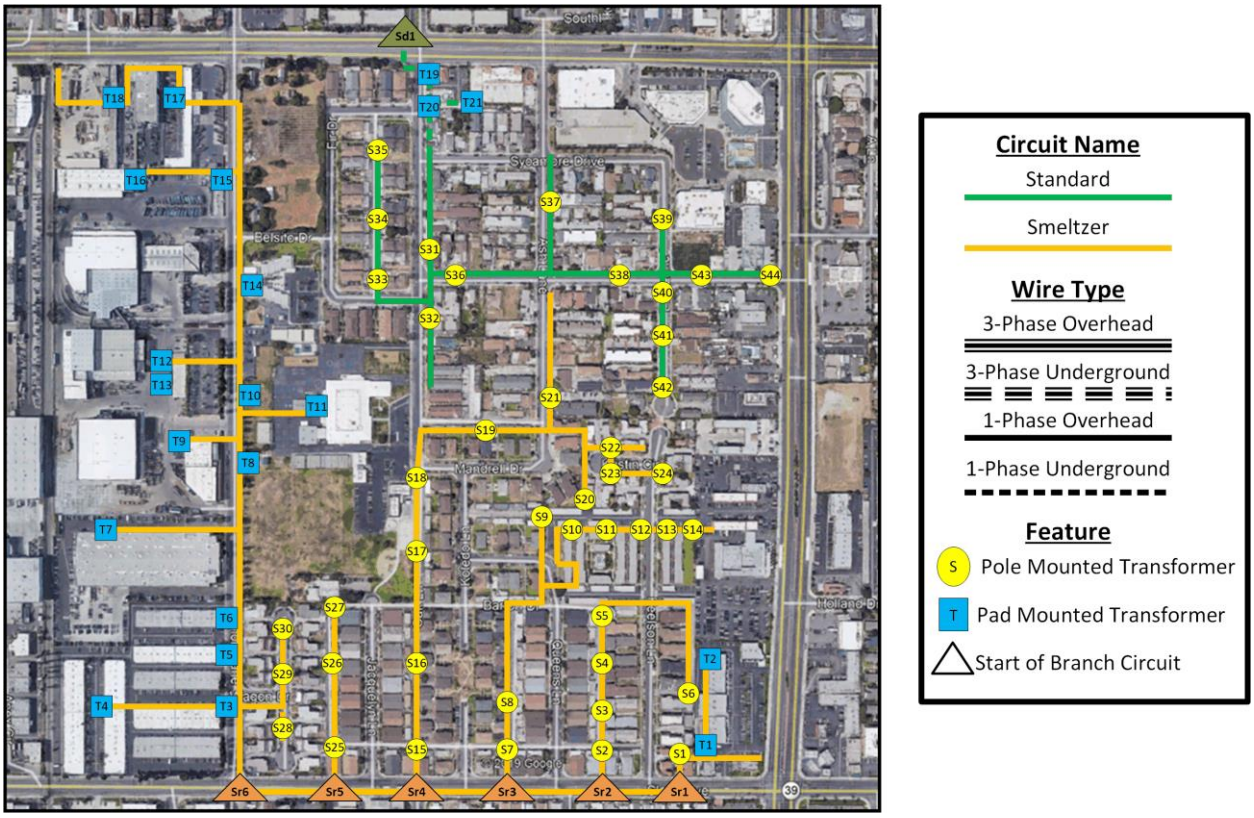

Figure 29. Final islanding result by islanding based on 12 KV Distribution Line Origin. In this case two different islands are generated.

5.1.2.3 Topology Design 3: Optimal Design without Extra Connection

In accordance with the aforementioned topology design methodology, which integrates MILP algorithms, the initial configurations of the OVMG Baseline Scenario are depicted in Figure 30. Pursuing the overarching objective of optimally aligning local DER generation with electric demand within each microgrid, this design approach concurrently evolves and refines five distinct microgrid configurations from five distinct starting points.

The ultimate outcome of the topology design process is illustrated in Figure 31, where individual microgrids are delineated by distinct colors. While it is believed that optimal local power balance has been achieved within each microgrid, it is possible that this may not represent the overall power balance optimum, as physical barriers have hindered inter-microgrid energy exchange, potentially thwarting a more balanced solution. Consequently, an alternative topology design accommodating additional interconnections to better balance local power distribution is proposed and elaborated upon below.

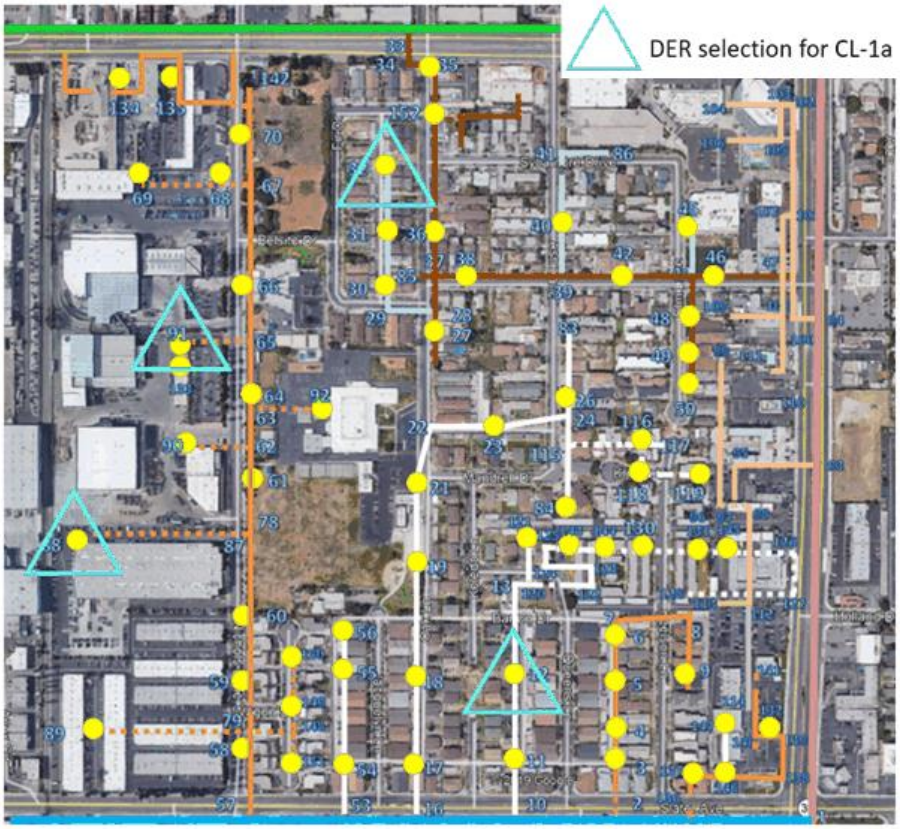

Figure 30. Starting points of OVMG ACPF model based on Baseline Scenario. The starting points are marked in light blue color.

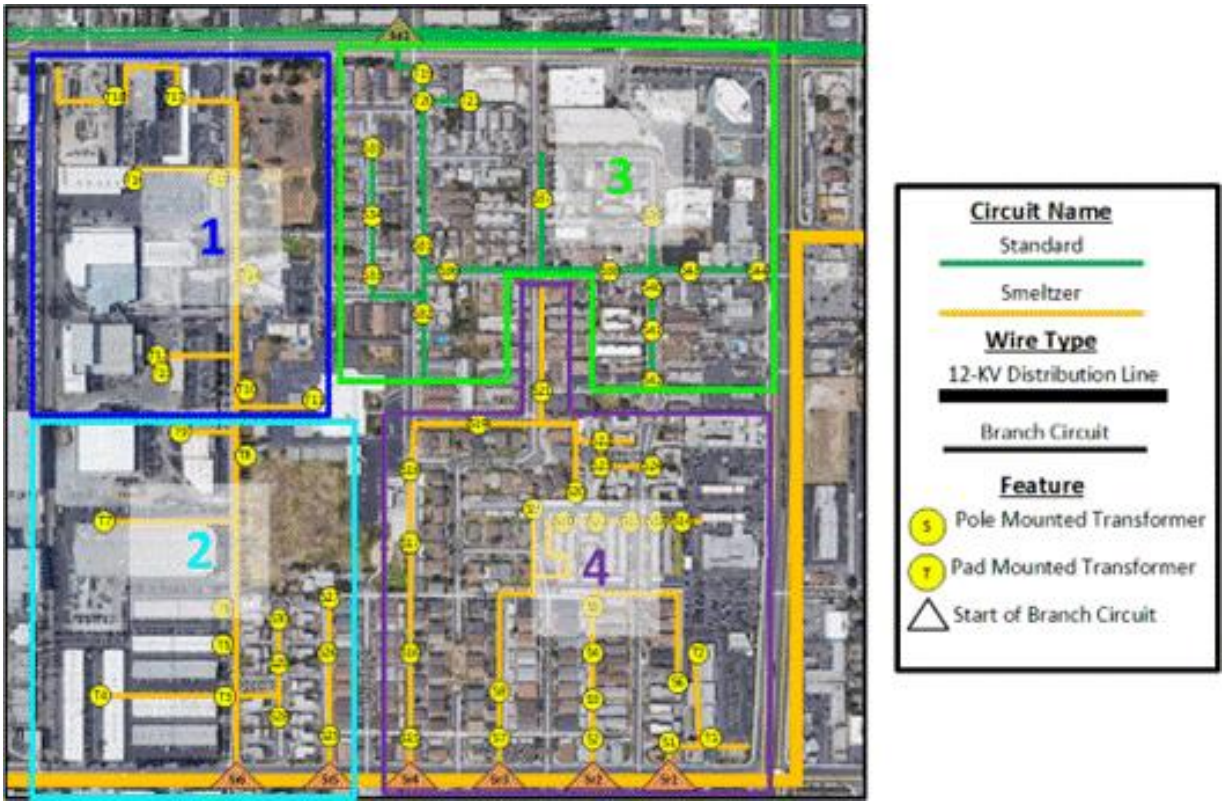

Figure 31. Final islanding result without extra connections. In this case four different islands are generated. Different islands are circled in different colors.

5.1.2.4 Topology Design 4: Optimal Design with Extra Connection

The final result of the proposed topology design process, shown in Figure 32, only involves two big islands. This islanding method best represents the case where optimal local power balance has been achieved within each microgrid throughout the microgrid, and quantified results showing the effectiveness of the algorithm will be described in Section 6.

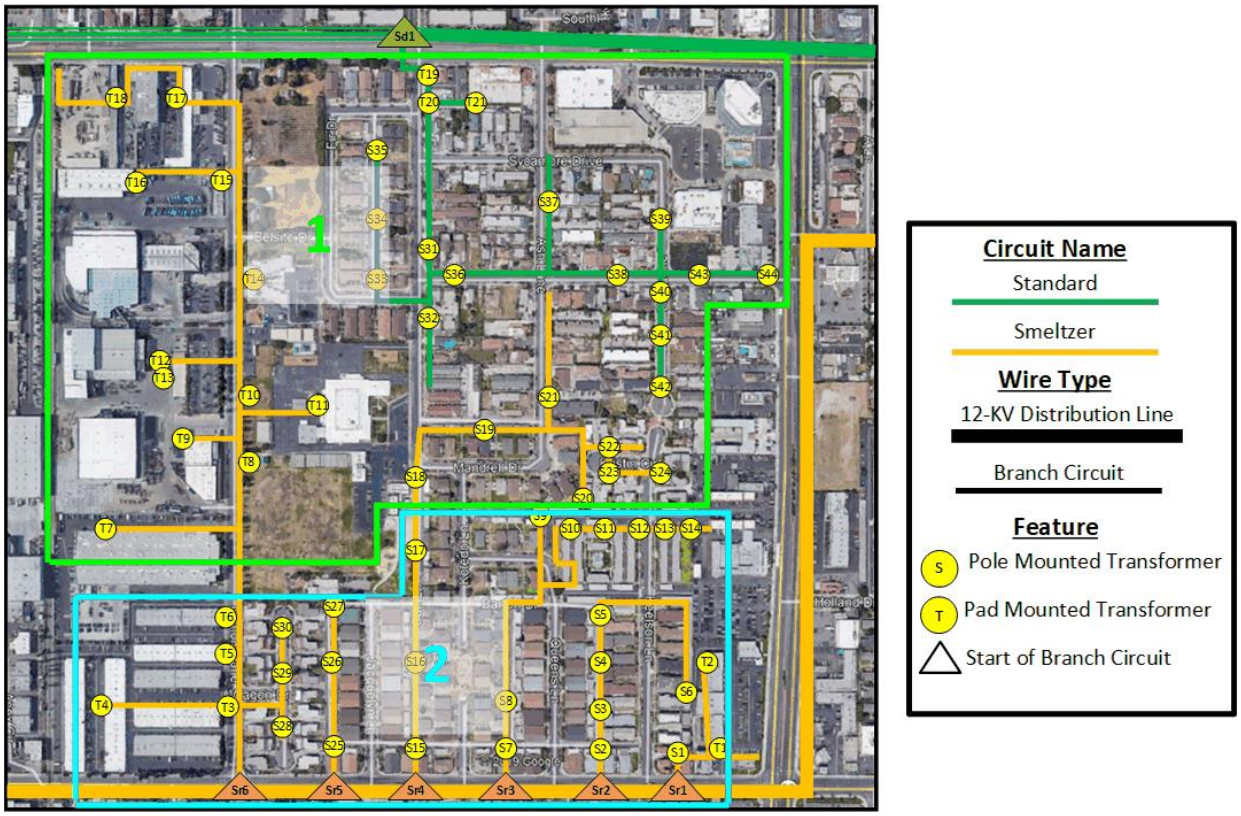

Figure 32. Final islanding result with extra connection permitted. Note that only two islands are generated.

5.2 DER Alternative Solution

An alternative strategy to mitigate the adverse impacts associated with increased electricity demand from various electrification initiatives is to deploy DERs and ESSs. In this section, we propose a mixed-integer linear programming optimization model for determining the optimal size and placement of PV panels and battery storage systems throughout the OVMG community, which operates within a complex existing distribution grid infrastructure. The goal is to minimize overall NPV costs across the system's dynamic, time-sensitive operations over a representative year, incorporating established load and solar insolation profiles. This work expands upon previous studies by Flores et al. [125][144], namely the DERopt system, introducing a novel method to prevent distribution transformer overloads by leveraging prior

analyses on transformer degradation thresholds, with the option to consider California's NEM 3.0 rates.

5.2.1 Lowest Cost DER Deployment with Transformer Constraint

The lowest cost DER deployment is achieved by DERopt mentioned above and is achieved by MILP algorithm [108] . The platform was used to determine the lowest possible cost of solely using PV/ESS systems to meet the electric demand of various EV integration scenarios, which include all EV scenarios in Section 4.2. The results of DERopt include the total amount of DER and ESS to achieve lowest overall cost and will be shown in Chapter 6.

The objective function of DERopt is the sum of various individual cost components that the algorithm minimizes, including the cost of electricity purchased from the grid, demand charges, and the cost to purchase and operate DER, including capital and O&M costs. The objective function also captures the revenue generated by exporting excess electricity to the grid under both net energy metering (NEM 3.0 only) and wholesale rates. The objective function is shown in Figure 33. The detailed realization of each cost is included in Appendix C.

A novel transformer Electric Demand/Transformer Rating chart table has been developed based on previous studies by the author. Given the ambient temperature, transformer rating as well as calculated HST (Hot Spot Temperature, details of HST will be explained in Chapter 6), any dynamic electric Demand/transformer ratio that goes above the value shown in the table is considered dangerous with high risk of overloading and is not allowed in the DERopt MILP

calculation. A showcase table showing transformer rating from 25 KVA to 150 KVA from 50 °C to 100 °C in HST is shown in Table 13.

$$\begin{aligned} \textit{minimize} \sum_b \Bigg(& \sum_t C_{grid,t} e_{grid,t,b} + \sum_n C_{DC,n} P_{max,n,b} + \sum_m C_{on\ DC,m} P_{on\ max,m,b} \\ & + \sum_m C_{mid\ DC,m} P_{mid\ max,m,b} + \sum_k C_{cap\ PV,k} P_{max\ PV,k,b} \\ & + \sum_t C_{om\ PV} e_{PV\ elec,t,b} - \sum_t C_{NEM,t} e_{PV\ NEM,t,b} - \sum_t C_{wsale} e_{PV\ wsale,t,b} \\ & + C_{cap\ EES} E_{EES,b} + \sum_t C_{om\ EES\ dchrg} e_{EES\ chrg,t,b} \\ & + \sum_t C_{om\ EES\ chrg} e_{EES\ dchrg,b} + C_{cap\ REES} E_{REES,b} \\ & + \sum_t C_{om\ REES\ dchrg} e_{REES\ chrg,b} + \sum_t C_{om\ REES\ chrg} e_{REES\ dchrg,b} \\ & - \sum_t C_{NEM,t} e_{\ REES\ NEM\ dchrg,b} \Bigg)_b \end{aligned}$$

- $n \in N$: Set of all months
- $m \in M$: Set of all summer months ($M \subset N$)
- $t \in T_n$: Set of all hourly increments in month n
- $o \in O_m$: Set of all hourly increments during on-peak in summer month m ($O \subset T$)
- $p \in P_m$: Set of all hourly increments during mid-peak in summer month m ($P \subset T$)
- $k \in K$: Set of all generator types
- $b \in B$: Set of all buildings
- $i \in I$: Set of all transformers
- $j \in J_i$: Set of buildings that are connected to transformer i ($J \subset B$)
- $x \in X$: Set of electrical notes (x, x' notation used to indicate separate nodes)

Figure 33. Objective function of proposed MILP cost function.

Table 13. Electric Demand/Transformer Rating table for transformer with rating between 25KVA to 150 KVA from HST 50 ℃ to 100 ℃.

Transformer Rating/KVA	Actual Electric Demand/Transformer Rating											
	HST=50.0°C				HST=60.0°C				HST=70.0°C			
	θ_{ambi} = 15°C	θ_{ambi} = 20°C	θ_{ambi} = 25°C	θ_{amb} = 30°C	θ_{ambi} = 15°C	θ_{ambi} = 20°C	θ_{ambi} = 25°C	θ_{amb} = 30°C	θ_{ambi} = 15°C	θ_{ambi} = 20°C	θ_{ambi} = 25°C	θ_{amb} = 30°C
25	0.52	0.50	0.48	0.42	0.78	0.61	0.56	0.54	0.92	0.82	0.78	0.76
75	0.67	0.56	0.47	0.46	0.80	0.78	0.67	0.64	0.99	0.90	0.80	0.79
100	0.78	0.53	0.51	0.50	0.83	0.73	0.71	0.69	1.01	0.94	0.84	0.82
150	0.78	0.69	0.55	0.53	0.86	0.79	0.75	0.73	1.06	0.94	0.89	0.88
Transformer Rating/KVA	**Actual Electric Demand/Transformer Rating**											
	HST=80°C				HST=90°C				HST=100°C			
	θ_{ambi} = 15°C	θ_{ambi} = 20 °C	θ_{ambi} = 25°C	θ_{amb} = 30 °C	θ_{ambi} = 15°C	θ_{ambi} = 20 °C	θ_{ambi} = 25°C	θ_{amb} = 30 °C	θ_{ambi} = 15°C	θ_{ambi} = 20 °C	θ_{ambi} = 25°C	θ_{amb} = 30 °C
25	0.97	0.93	0.92	0.84	1.20	1.13	1.11	1.10	1.28	1.19	1.10	1.08
75*	1.01*	0.96*	0.93*	0.92	1.22	1.16	1.15	1.11	1.32	1.20	1.16	1.14
100	1.03	1.01	0.99	0.98	1.22	1.17	1.15	1.12	1.34	1.30	1.27	1.23
150	1.13	1.07	1.05	1.04	1.26	1.23	1.15	1.14	1.38	1.30	1.28	1.27

6 Impact Analysis

After the application of different types of renewable and clean energy systems in various scenarios as mentioned above, in this chapter the impacts of those measures are evaluated. The analysis consists of three parts: reliability and resiliency evaluation, degradation evaluation, cost and benefit evaluation.

The first evaluation includes the necessary index for reliability and resiliency. For all OVMG scenarios without islanding, a thorough electrical quality evaluation is achieved, which includes a per unit voltage assessment of distribution transformer and cable maximum ampacity to determine the viability, efficacy, capability, and stability of the entire grid system. For the islanding scenarios, a unique comparison of local power demand and supply balance is also completed.

The second evaluation quantifies the degradation of key infrastructure including distribution transformers and power cables in the community. A degradation model for key infrastructure is first developed, and all considered scenarios are implemented with the model to examine the degree of deterioration of infrastructure life.

The third evaluation tests each scenario's cost effectiveness. With different well-established analysis methods performed on each scenario, feasibility and practicality of different techniques or novel operational scenarios can be quantified for reference for possible energy efficiency, renewable and distributed energy program planning processes.

6.1 Key Infrastructure Degradation

Electrification and renewable distributed energy resources (DER) are key tools for fighting climate change [49]. However, both options potentially introduce accelerated electric distribution system degradation through increased electric imports or through high levels of energy backflow.

In recent years, efforts have been made to study these influences on grid infrastructure. Prior work has primarily focused on the degradation of distribution transformers, utilizing an empirical transformer degradation model developed by IEEE [145]. An empirical thermal degradation for oil-immersed transformers with various plug-in electric vehicles (PEV) scenarios was explored and applied in [146] . Accelerated aging of transformers under various DER appliances was studied in [147–149]. A degradation study of distribution transformers with an appliance combination of PEV and DER was discussed in [150] and [151]. Discussions of hazards and solutions of DER power back-feeding on grid infrastructure are present from [137,152–154] . While most studies above research degradation effect on distribution transformers under single electrification or high penetration DER scenario, few discuss the degradation of multiple electric infrastructure under a wider and more general electrification and DER appliance.

This section adds to the prior work presented in [146] by adding two features. First, the work by Razeghi et.al. is extended to address cable degradation by coupling material degradation results [155] with a simplified cable thermal energy balance [156]. Second, a simple, cost-optimal transformer and conductor sizing method is introduced to predict the costs of upgrading degraded electric distribution infrastructure. These models are tested using

a community scale energy model designed to capture the effects of building and vehicle electrification.

6.1.1 Cable Degradation

According to previous work by the author [155], the primary for of cable degradation occurs due to aging of insulation material on cable. The cable degradation model captures this by first predicting cable temperature, followed by determining insulation degradation. The insulation degradation model is based on XLPE due to recent work on this material. This model, however, could be adjusted to other insulation material provided sufficient experimental data is available.

Using our model, damage of cable life happens when a long-lasting overheating situation exists. Given the same environment variables and conductor ampacity, cables with smaller AWG decrease the chance of life loss by both increasing the wire diameter which reduces conductor joule heating generation and raising the temperature rating.

Assuming that the electricity carrying cable is operating at steady state, the steady-state energy balance for a power cable is [156]:

$$\mathrm{q_j} + \mathrm{q_s} = \mathrm{q_c} + \mathrm{q_r} \qquad (9)$$

where q_j is conductor joule heating, q_s is solar heat gain across the cable, q_c is convective heat transfer to air, q_r is radiation loss from the cable to the environment. These components are defined using equations (10)-(13):

$$q_j = R \cdot I_{cond}^{\ 2} \quad (10)$$

$$q_s = \delta \cdot D \cdot a_s \quad (11)$$

$$q_c = \pi \cdot h \cdot D \cdot (T_{con} - T_{env}) \quad (12)$$

$$q_r = \pi \cdot \sigma \cdot \varepsilon \cdot D \cdot (T_{cond}^4 - T_{env}^4) \quad (13)$$

where R represents electrical resistance, D represents cable diameter, I_{cond} stands for cable ampacity, T_{cond} is the temperature of the conductor, T_{env} is the ambient temperature, ε and a_s are the radiative emissivity and absorptivity of the conductor material, δ is the incident solar radiation, σ is the Stefan-Boltzmann constant, and h is the convective heat transfer coefficient. This coefficient is calculated in

$$h = 0.3 + \frac{0.62 \cdot (V \cdot D/v)^{1/2} \cdot Pr^{1/3}}{(1+(\frac{0.4}{Pr})^{2/3})^{1/4}} \cdot \left(1 + \frac{\left(V \cdot \frac{D}{v}\right)^{\frac{5}{8}}}{282{,}000}\right)^{\frac{4}{5}} \cdot k/D \quad (14)$$

where V is wind speed, v and k is dynamic viscosity and thermal conductivity of air respectively, Pr is Prandtl number.

Plugging ()-() equations into (9) yields a 4th order polynomial. This equation can be solved when both weather and cable ampacity I_{cond} are known.

Prior experimental work using XLPE insulated cables operating at less than 69 kV has shown that cable lifespan can be measured in days using Equation (15) [155].

$$t_{failure} = e^{\frac{19024}{T_{cond}} - 42.3} \quad (15)$$

Eventually, equivalent life loss per hour under certain cable temperature can be further written into the calculated by the ratio of cable full lifespan to cable expected lifespan (given all weather profiles are known). Table 14 describes AWG 4, 6 and 8 cable information, which are commonly found in community level and will be used in results and examples later.

Table 14. Specifications for 4,6 and 8 AWG cables

Wire Gauge	**75°C ampacity rating/A**	**Wire Diameter/mm**	**Resistance per unit length/mΩ/m**
4-gauge wire	95	5.2	0.82
6-gauge wire	55	4.1	1.30
8-gauge wire	40	3.3	2.1

6.1.2 Optimal Sizing of Distribution

Both the IEEE distribution transformer and cable degradation model provide estimates for when equipment will need to be replaced based on loading patterns and weather. In instances where component replacement is necessary due to failure, the new component would ideally be sized such that total cost is minimized. This work employs a simple optimization method that determines the optimal component size that accounts for system degradation and overall life.

The optimization method is based on available infrastructure improvement costs associated with the interconnection of DER [157], including the cost to upgrade distribution transformers ranging from 300 kVa to 2500 kVa, and to reconductor distribution circuits. Since the focus of this work is on a residential circuit described in Section 3, additional 75 kVa, 100 kVa, and 150

kVa transformers were included in the analysis. The cost for these equipment upgrades were estimated using the 6/10ths rule [158] using the 300 kVa transformer as the base cost.

Using these cost values, the component degradation models were exercised for each possible replacement component to determine how often each component would need to be replaced over 30 years. The net present value of these costs was taken using a discount rate of 9%. Using these values, the component with the lowest net present value was selected. Although this approach focused on a timeframe far less than desired distribution cable lifespans, the step increases in cable ampacity ratings typically resulted in a clear preference for cables that experience minimal to no degradation. However, additional care must be taken in instances where this optimization method yields cable lifespans between 30 and 50 years.

6.2 Renewable and Clean Energy System Integration

6.2.1 Vehicle Electrification

6.2.1.1 Simulation Results for Policy-driven EV Adoption Scenarios

6.2.1.1.1 EV Scenario #1 (33%) Result

This section presents the outcomes derived from the application of the 33% EV penetration goal, specifically targeting a 35% penetration rate within the tested scenario subsequent to the cessation of the Monte-Carlo algorithm. Average annual degradation for all iterations corresponding to each individual transformer, all recorded transformer Line-Neutral voltage as well as all recorded cable ampacity are shown in Figure 34. Various transformers exhibit varying degrees of degradation, as illustrated in Figure 34 on the left. Our analysis reveals that while the majority of transformers experience an approximate 10% reduction in service life, a subset

located in the northeastern region suffers a more substantial loss, ranging between 30% and 40%. Addressing these heavily degraded transformers necessitates a course of action, such as a rating upgrade or replacement. The degradation rate and electrical power quality analysis of the Oak View Community Baseline is included in Appendix A for reference.

In Figure 34 on the right shows the yearly simulation result of transformer voltage and cable ampacity. Adhering to the stipulated standard, a 5% deviation from the nominal voltage is considered acceptable. The lower and upper voltage limits are distinctly marked in the graphical representation of the results. All recorded cable ampacity results are also presented to show the degree of electric pressure on basic electric infrastructure. Although different ampacity ratings of electric conductor are highlighted according to AWG [111], all cables are believed to run safely if the maximum ampacity does not exceed the 2-gauge limit. Both voltage and ampacity results are demonstrated using box plots, where the x-axis of those figures indicates the start of branch circuits. Transformers and cables for each branch are shown in order of proximity to the start of branch circuit. The middle red line in each box plot indicates the median annual value. The 25th and 75th percentile values are shown at the bottom and top of each box, respectively. All regular data falls within the whiskers and extreme data points as red '+' markers. In Figure 34, it is evident that no significant breach of voltage rating limits is observed for all active transformers/nodes under the considered scenario.

While only a slight overall degree of infrastructure degradation and no power quality issues were found, failure to undertake the upgrade measures may still result in a disturbance to the stability of power usage.

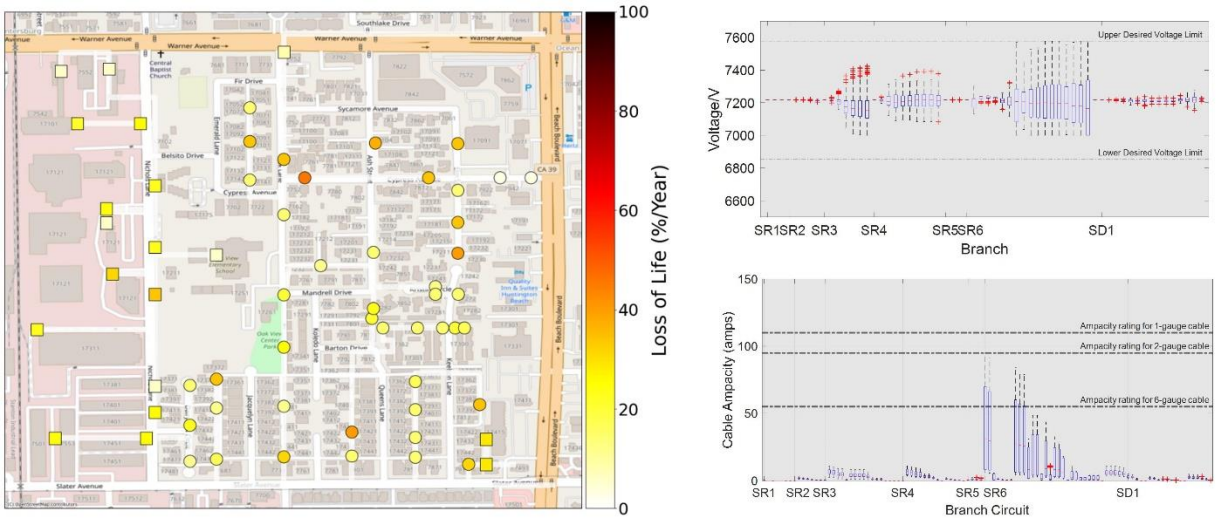

Figure 34. Yearly degradation result of cable and transformers, transformer Line-Neutral voltage and cable ampacity respectively in Oak View Community in 33%EV integration scenario. No cable degradation was found but transformers show different degrees of degradation, indicated by different colors on the left. The node voltage and circuit ampacity results are shown in box plots on the right.

6.2.1.1.2 EV Scenario #2 (66%) Result

This section delineates the results obtained through the implementation of the 66% EV penetration , with a particular focus on achieving a 66% penetration rate within the investigated scenario following the conclusion of the Monte-Carlo algorithm. Similar to the previous section, degradation of infrastructure, Line-Neutral voltage results, cable ampacity results are presented in Figure 35. Lower and upper voltage limits were marked in results with 5% threshold. Both voltage and ampacity results are again demonstrated using box plots. In Figure 35 on the left, it is clear that the annual degradation of the overall transformer system is escalating. The transformers exhibit an average degradation rate of 33%, with a maximum observed degradation rate of 56% within a single year.

Figure 35 on the right, illustrates that the overall voltage level experiences a marginal reduction, albeit remaining within permissible limits. It is noteworthy that nodes along branch

SR2 exhibit the most pronounced voltage decline. In Figure 35, it is evident that nearly all branches display outliers with an augmented ampacity level. Nevertheless, these increases are insufficient to induce significant disturbances.

The results underscore the imperative for upgrades to the transformer infrastructure to ensure the provision of power in a reliable and stable manner.

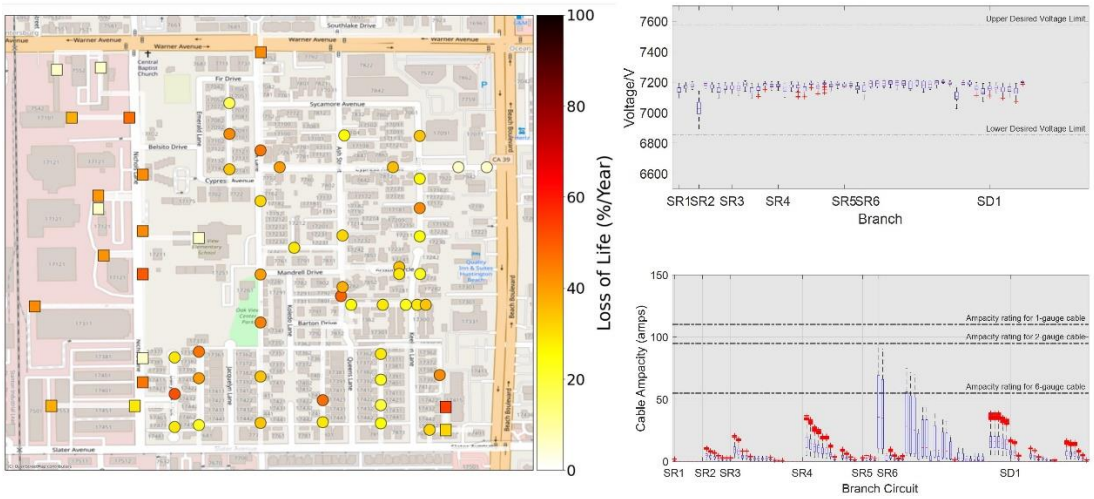

Figure 35. Yearly degradation result of cable and transformers, transformer Line-Neutral voltage and cable ampacity respectively in Oak View Community in 66% EV integration scenario. No cable degradation was found but transformers show different degrees of degradation, indicated by different colors on the left. The node voltage and circuit ampacity results are shown in box plots on the right.

6.2.1.1.3 EV Scenario #3 (100%) Result

This section presents the outcomes derived from the application of the 100% Electric Vehicle state goal to the test scenario. The results pertaining to degradation of infrastructure, Line-Neutral voltage results, cable ampacity results are presented in Figure 36. Both voltage and ampacity results are again demonstrated using box plots. Figure 36 on the left elucidates the annual degradation status of all active transformers. Evidently, a significant portion of transformers within the residential sector is anticipated to cease functioning before the

conclusion of the year, necessitating transformer rating upgrades. It is imperative to highlight that several cable segments originating from SR6 exhibit a noteworthy degree of degradation, warranting the imperative need for cable upgrades.

It is shown in Figure 36 on the right that serious breaching of voltage rating limit is found for branch SR2, with many outliers from several branches drawing close to the lower limit. This will cause serious power quality issues. Cable ampacity also have similar problems, with cable segments from SR4 and SR6 having the most serious problems.

It is safe to say that without proper upgrades on both distribute transformers and electric cables severe safety hazards will appear, likely within one year of operation.

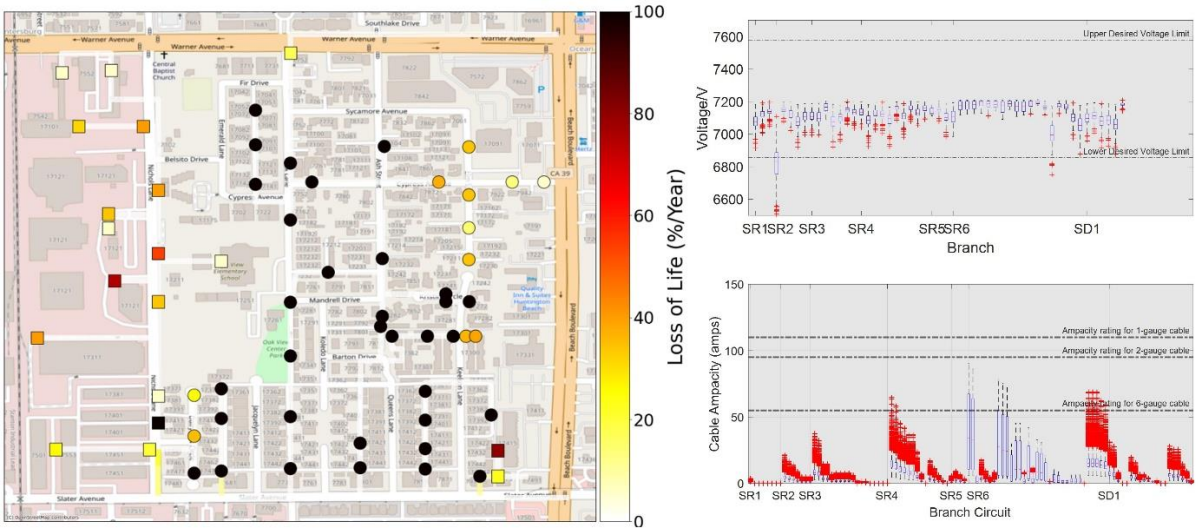

Figure 36. Yearly degradation result of cable and transformers, transformer Line-Neutral voltage and cable ampacity respectively in Oak View Community in 100% EV integration scenario. Slight degrees of cable degradation and different degrees of transformers degradation were found, indicated by different colors on the left. The node voltage and circuit ampacity results are shown in box plots on the right.

6.2.1.2 *Simulation Results for High Penetration EV Adoption with Level 2 and DC Charging*

6.2.1.2.1 Scenario 1 Result: 100% Residential EV Penetration with LV2 Charging

This section shows the outcomes derived from the implementation of 100% residential EV adoption exclusively employing Level 2 charging events, utilizing the default charger setup outlined in the Commercial and Industrial sector. Similar to the preceding section, findings pertaining to infrastructure degradation, Line-Neutral voltage characteristics, and cable ampacity are presented in Figure 37. Lower and upper voltage thresholds are delineated in the results with a 5% margin. Both voltage and ampacity outcomes are portrayed using box plots.

In Figure 37 on the left, the transformers within the residential sector demonstrate an average annual degradation rate of 76%. Interestingly, in comparison to 100% LV1 adoption, the observed degradation is notably less severe. This discrepancy may be attributed to the LV2 charging paradigm, characterized by higher charging ratings and reduced charging durations, thereby accruing an elevated Accumulated Aging Factor (AAF), consequently yielding a lower Loss of Life (LOL). Based on Table 13, the reduced overall degradation percentage can also be the reason that the high-capacity transformer is less sensitive to short-period overload issues with Hot Spot Temperature (HST) going up, which is positively correlated with higher peak level from Level 2 charging. While increased HST from increased charging demand peak increase the overall degradation rate of lower rated transformers (such as 25KVA, 50KVA, etc.) and thus increase the degradation cost of them, the higher rated transformers, especially those with a rating of 150 KVA and higher, actually benefit from the higher HST which increases their minimal overload percentage that start to cause significant degradation, and would likely not increase the degradation of those higher rated transformers and accordingly the upgrade cost

from it. If the theory is correct, then in 100% Level 1 EV penetration scenario the degradation rate and upgrade cost from higher rated transformers would both be higher compared to this scenario. Even though the increase charging level also increase the degradation of lower rated transformers, their upgrade cost is a lot smaller than their higher rated counterparts. Additionally, the initial segment of SR2 manifests a discernible degree of degradation owing to the heightened electric demand stemming from LV2 charging.

Figure 37 on the upper right describes the overall voltage profile, illustrating a prevalent issue similar to that observed in the case of 100% LV1 adoption, specifically, pronounced undervoltage scenarios with multiple instances of lower voltage limit violations. In Figure 37 on the lower right, a moderate degree of breaches in ampacity levels are identified. Although the overall scenario appears marginally improved compared to LV1 100% EV adoption, the increased electric demand from EV charging remains sufficient to induce cable over ampacity issue on SR2.

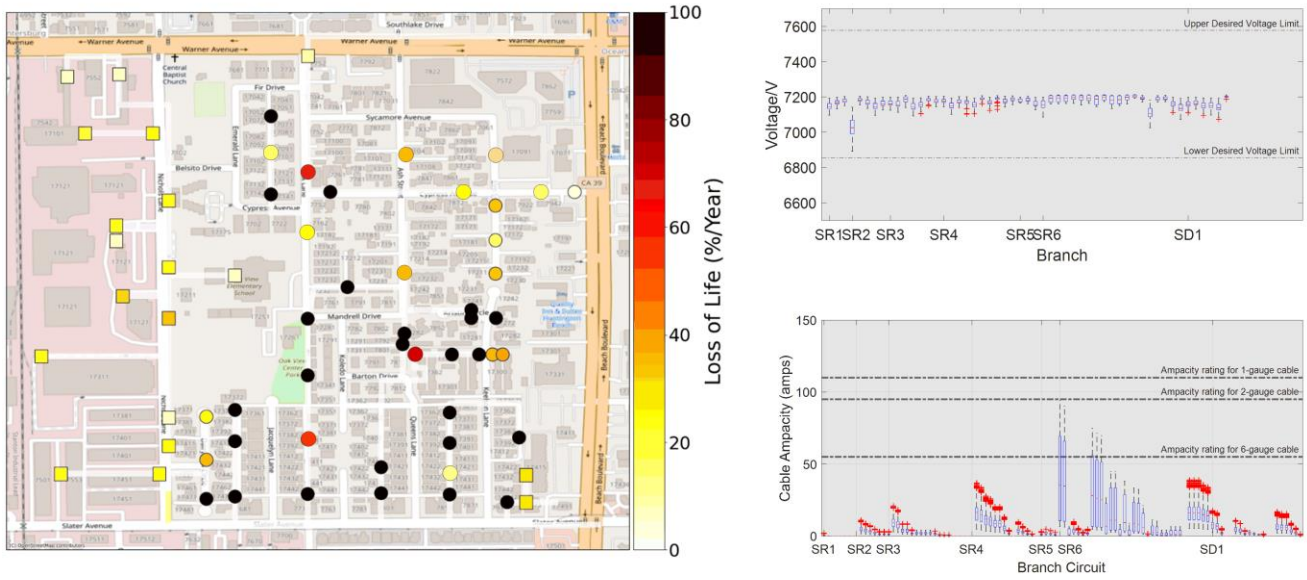

Figure 37. Yearly degradation result of cable and transformers, transformer Line-Neutral voltage and cable ampacity respectively in Oak View Community in 100% LV2 residential EV integration scenario. Slight degrees of cable degradation and severe degrees of transformers degradation were found, indicated by different colors on the left. The node voltage and circuit ampacity results are shown in box plots on the right.

6.2.1.2.2 Scenario 2 Result: 100% Residential EV Penetration with LV1/LV2 Charging

This section shows the outcomes derived from the comprehensive implementation of 100% residential EV adoption with both Level 1 and Level 2 charging events, utilizing the default charger setup delineated within the Commercial and Industrial sector. A predetermined ratio of 80% Level 1 chargers and 20% Level 2 chargers per stochastic iteration was employed. Same with the previous sections, findings pertaining to infrastructure degradation, Line-Neutral voltage characteristics, and cable ampacity are expounded upon, as illustrated in Figure 38. The delineation of lower and upper voltage thresholds within the results, accompanied by a 5% margin, provides a comprehensive understanding of the voltage-related observations. Furthermore, both voltage and ampacity outcomes are aesthetically depicted through the utilization of box plots.

Within Figure 38, depicted on the left, the transformers situated within the residential sector have an average annual degradation rate of 66%. Notably, the incorporation of Level 2 chargers with Level 1 chargers within the community exhibits a mitigating effect on overall degradation when compared with scenarios exclusively featuring 100% Level 1 EV charging adoption or Level 2 EV charging adoption alone. Nevertheless, significant degradation is observed along the first cable segment of SR2, resulting from the heightened electric demand attributed to LV1/LV2 charging.

Figure 38, situated on the upper right and lower right, depicts the overarching voltage profile and cable ampacity scenario. While an undervoltage condition persists, it is discernibly less severe compared to scenarios featuring either 100% LV1 or 100% LV2 EV adoption scenario. Conversely, the cable ampacity scenario mirrors that of the preceding scenario.

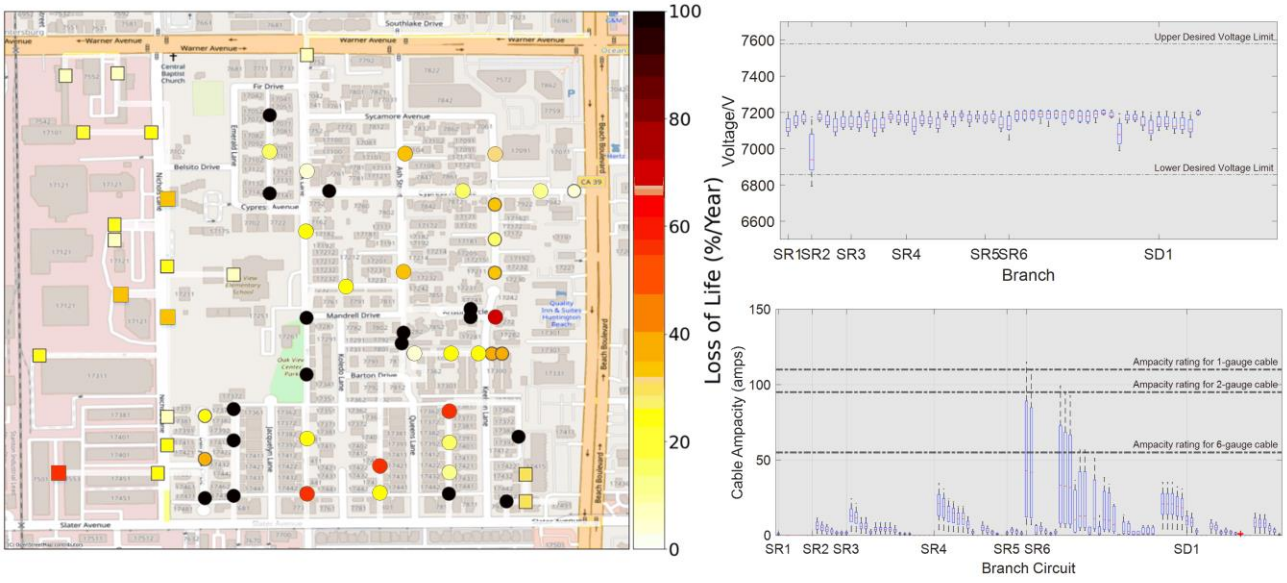

Figure 38. Yearly degradation result of cable and transformers, transformer Line-Neutral voltage and cable ampacity respectively in Oak View Community in 100% LV1/ LV2 residential integration scenario. A fixed ratio of 80% LV1 chargers and 20% LV2 chargers per stochastic iteration was used in the residential sector. The charger arrangement is in C&I section is by

default. Cable degradation and transformers degradation are indicated by different colors on the left. The node voltage and circuit ampacity results are shown in box plots on the right.

6.2.1.2.3 Scenario 3 Result: 100% Residential EV Penetration and 100% C&I Section EV Penetration with LV2 Charging

This section shows the outcomes derived from the implementation of 100% residential EV adoption with both Level 1 and Level 2 charging events and 100% C&I Level 2 charging events. This scenario is a direct development from the previous scenario, with 100% Level 2 charging events taking place at the shops and factories. This scenario represents the most possible future 100% EV adoption scenario, with people charging their EVs using a combination of Level 1 and Level 2 chargers in their houses, and in their workplace or publicly using Level 2 chargers. The ratio of Public Level 2 charging and Work Level 2 charging is assumed to be the same throughout the analysis for this very scenario.

Similar to the previous analyses, results on infrastructure degradation, including Line-Neutral voltage characteristics, and cable ampacity are shown in Figure 39. While the degradation in the residential sector remains the same as Scenario 2, the degradation in the C&I sector deteriorated due to a higher percentage of EV charging demand. On average, the transformers situated within the C&I sector have an average annual degradation rate of 35%. Significant degradation is observed along the first cable segment of SR2, same as the previous scenario.

The overarching voltage profile (as a function of branch circuit) and cable ampacities that result from this scenario are presented in the upper right and lower right of Figure 39. The results closely resemble the previous results in the residential sector but differ in that the power quality in C&I sector suffers more from the increase in EV charging demand.

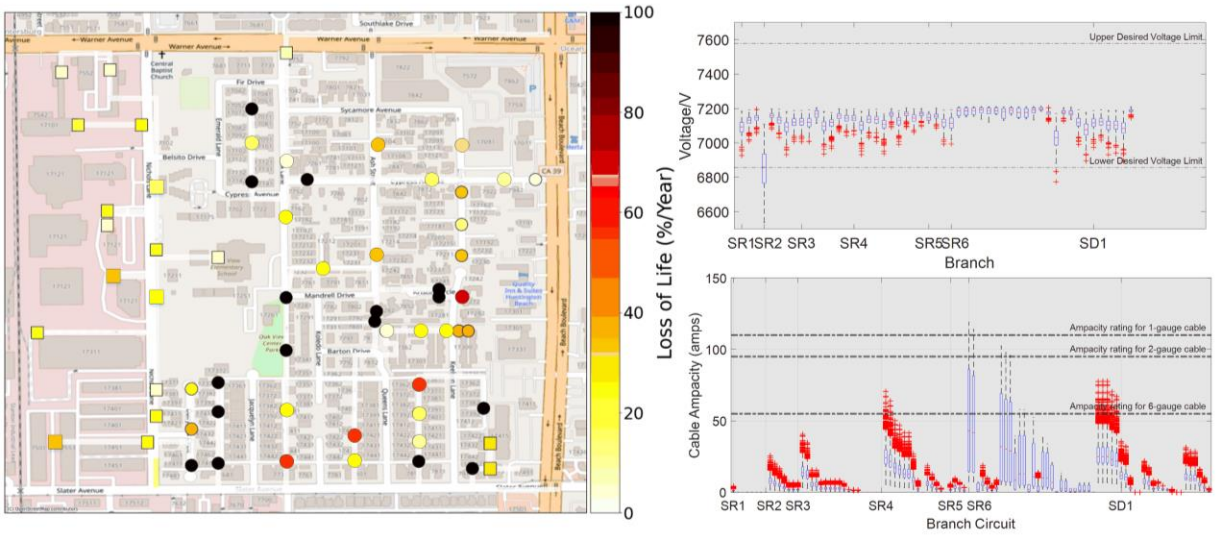

Figure 39. Yearly degradation result of cable and transformers, transformer Line-Neutral voltage and cable ampacity respectively in Oak View Community in 100% LV2 EV integration scenario. The charger is in both residential and C&I sectors are solely LV2. Cable degradation and transformers degradation are indicated by different colors on the left. The node voltage and circuit ampacity results are shown in box plots on the right.

6.2.1.2.4 Scenario 4 Results: 100% Residential EV Penetration with LV2 charging and 100% C&I PDCF Charging

This section shows the outcomes of implementation of 100% residential EV adoption with Level 2 charging events and 100% C&I Public DC Fast charging events. This scenario represents the ideal future scenario where people are able to afford and charge in the fastest way possible. The fastest charging technique currently available in the residential sector is Home Level 2 charging and Public DC Fast charging in the C&I sector. This scenario, with its most advanced charging techniques with highest charging voltage possible, will most likely put very serious pressure, if not the most, on key electric infrastructure.

Same with the previous analysis, results on infrastructure degradation, Line-Neutral voltage characteristics, and cable ampacity are shown in Figure 40. The degradation in the C&I sector is significantly worse than Scenario 2 and Scenario 3, but it is still better than when 100% LV1

charging takes place. The possible reason will be similar with why 100% LV2 charging caused less degradation on the transformers than 100% LV1 charging shown in Scenario 1, which is that the shortened charging time compensates for the impacts on AAF or EAF from higher charging voltage. The degradation in the residential remail the same with Scenario 1. On average, the transformers situated within the C&I sector have an average degradation rate of 43%. Significant degradation is observed along the first few cable segments of SR2, same as the previous scenario.

Figure 40 also depicts the overall voltage profile and cable ampacity scenario. While the results are the worst in the four High Penetration EV Adoption scenarios considered in this section, the power quality is less severe than when 100% LV1 charging dominates the entire Oak View Community.

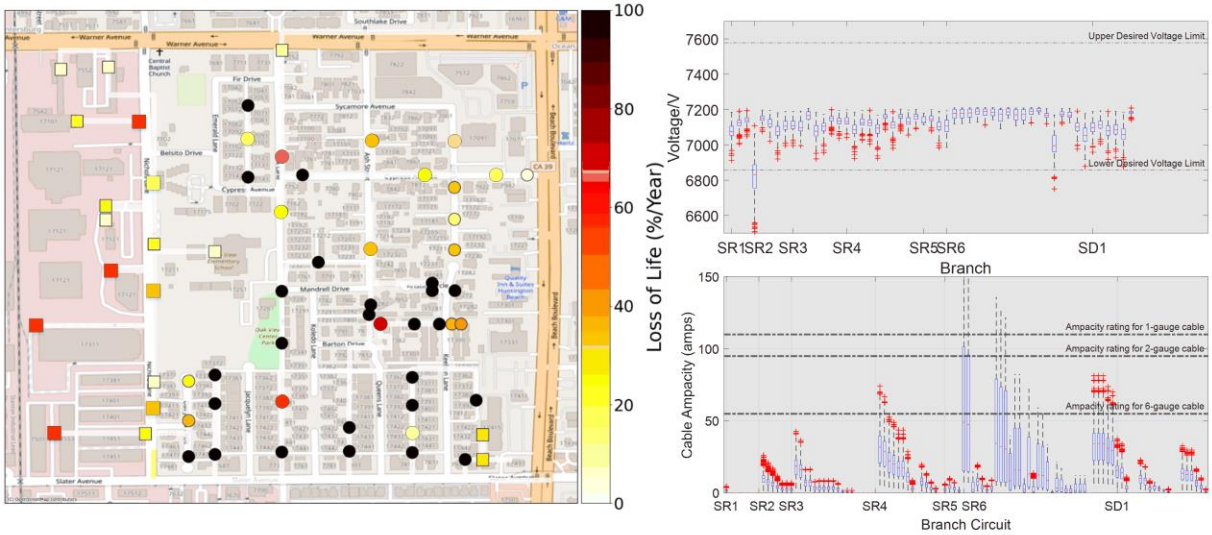

Figure 40. Yearly degradation result of cable and transformers, transformer Line-Neutral voltage and cable ampacity respectively in Oak View Community in 100% Residential LV2 and 100% Public DC Fast C&I EV integration scenario. Cable degradation and transformers degradation

are indicated by different colors on the left. The node voltage and circuit ampacity results are shown in box plots on the right.

6.2.1.3 Simulation Results for County and State Level EV Adoption

6.2.1.3.1 SCE Service Territory Scenarios

The annual degradation results of the entire SCE service territory's substation with required 33%, 66%, 100% EV penetration goals are shown in Figure 41, Figure 42, Figure 43, respectively. The zoomed-up versions of results of Orange County and most parts of Los Angeles County are also shown in the upper right corner of the figures. Compared to community level yearly degradation results in the previous section, it is obvious that a significant amount of substation transformers will not be able to withstand even the state EV goal of 2025 which is merely 33%. The percentage of substation transformers in 2025 CA EV scenario that shows more than 50% of yearly degradation is 56%, while the percentage increases to 78% in 2023 state goal scenario, with the worst being the 2035 EV scenario which reaches 89% in Figure 43.

While community rated transformers could potentially do well in 33% EV penetration goal or even 67% EV goal without serious upgrades, their higher rated substation counterparts likely may not. The degradation results of substations are under the assumption that electric load will stay the same from 2025-2035, which in reality is not possible given the state and local municipal effort to electrify building and industry sector. The smaller non-EV electric demand actually mitigates the seriousness of degradation impact from EV integration. It is also obvious that current SCE planned capacity expansion is far from enough, and a bigger overall upgrade is dearly needed.

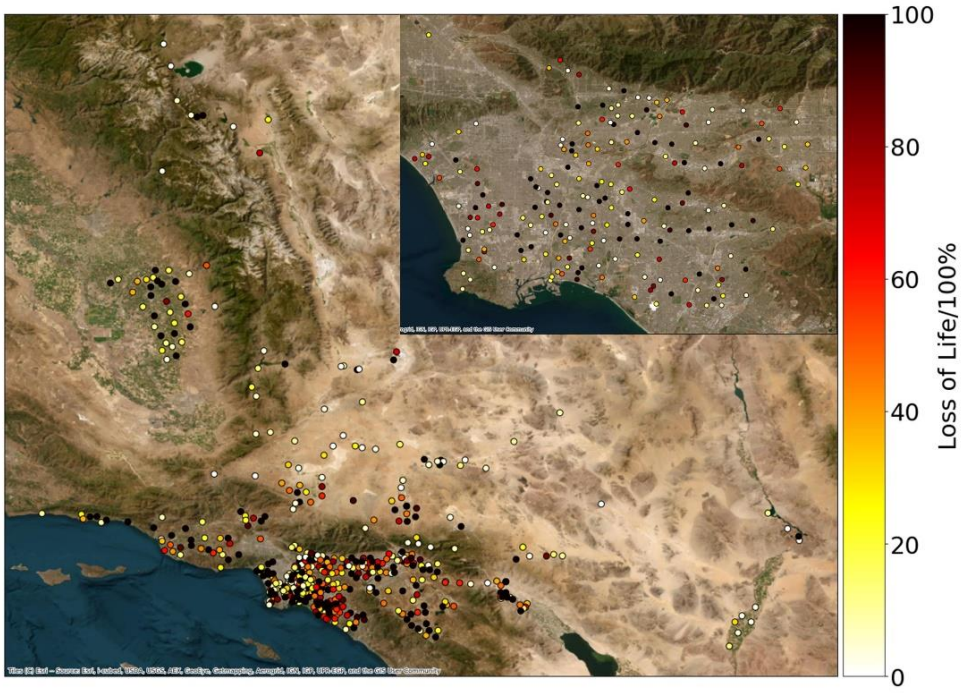

Figure 41. Yearly degradation result of transmission and distribution substation transformers in 33% EV integration scenario. Transformers degradation is indicated by different colors. The upper right graph shows a zoomed in detailed view of Orange County and Los Angeles County within SCE service territory.

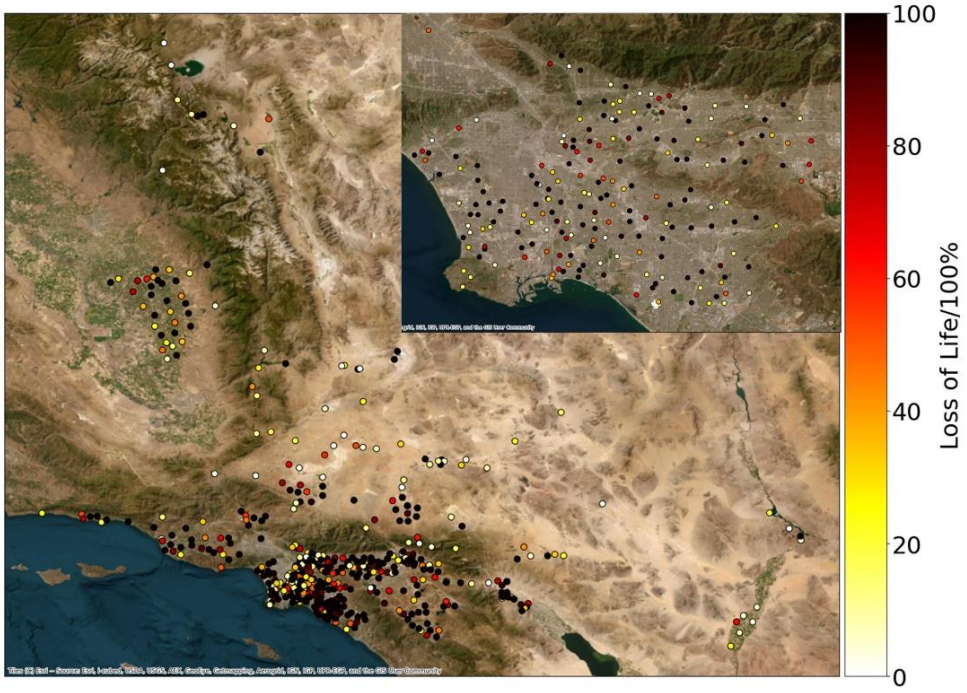

Figure 42. Yearly degradation result of transmission and distribution substation transformers in 66% EV integration scenario. Transformers degradation is indicated by different colors. The

upper right graph shows a zoomed in detailed view of Orange County and Los Angeles County within SCE service territory.

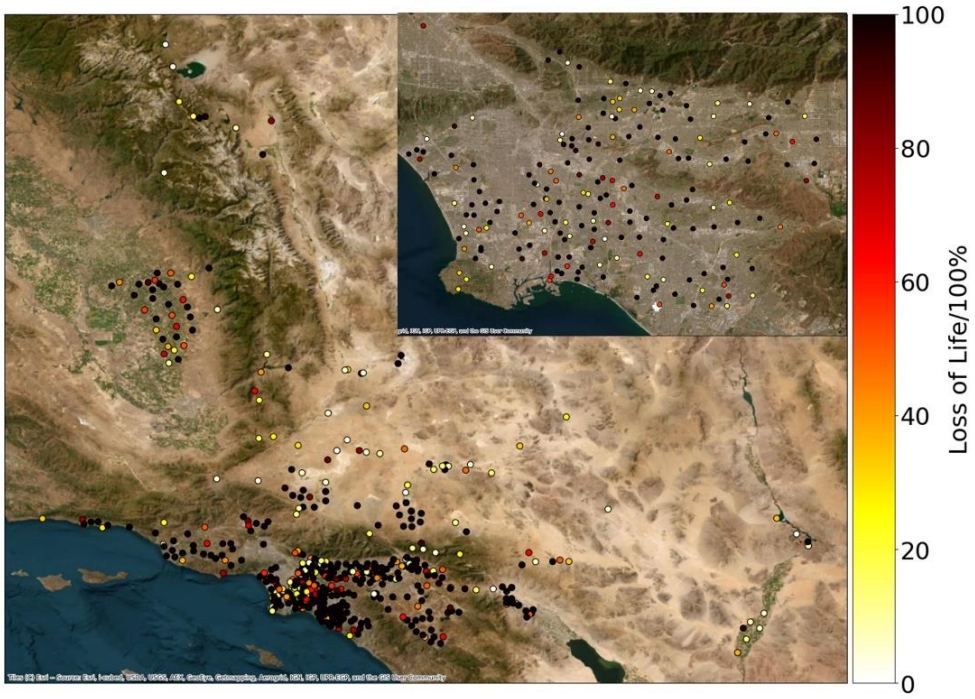

Figure 43. Yearly degradation result of transmission and distribution substation transformers in 100% EV integration scenario. Transformers degradation is indicated by different colors. The upper right graph shows a zoomed in detailed view of Orange County and Los Angeles County within SCE service territory.

6.2.1.3.2 The Oceanview Substation Special Analysis

As mentioned previously, the availability of estimated electric demand level of the substation and the layout of the substation allows the author to further analysis the electric impact from EV integration. The overload situation of the overhead transmission lines, power transformers, underground cables, substations bus, as well as the protective relays will be discussed in this section.

The Oak View Community has a population of 1100, while the Oceanview Substation serves a population of 3,3000 people based on our estimation. With an aggregated baseline load level

of 0.45 MVA in the Oak View Community, the aggregated baseline load level of the substation is 15MVA. The aggregated load level of each electrified level is calculated and is shown in Table 15.

Table 15. Aggregated load level of different EV integration scenarios.

Scenario		Load Level/MVA
Policy-driven Scenarios	33% EV LV1	27
	66% EV LV1	39
	100% EV LV1	56
High Penetration EV Scenarios	100% Residential EV LV2	49
	100% Residential EV LV1/LV2	50
	100% Residential w/ 100% LV2 C&I	51
	100% Residential LV2 w/ 100% PDCF C&I	55

The ETAP steady state ACPF simulation result is shown in Figure 44 and Figure 45 for all considered scenario. Figure 44 represents ACPF steady state simulation result for all policy-driven EV integration scenarios with discrete LV1 EV charging, while Figure 45 shows ACPF steady state simulation result for all high penetration EV integration scenarios with aggregated EV charging profiles from EVI-PRO. The warning report which consists of overload, overvoltage/undervoltage and over ampacity analysis by ETAP is shown in Figure 46.

The increased load level obviously falls short to put enough pressure on all considered equipment to cause overload, overvoltage or overcapacity problem, which we assume will cause minimal degradation as well.

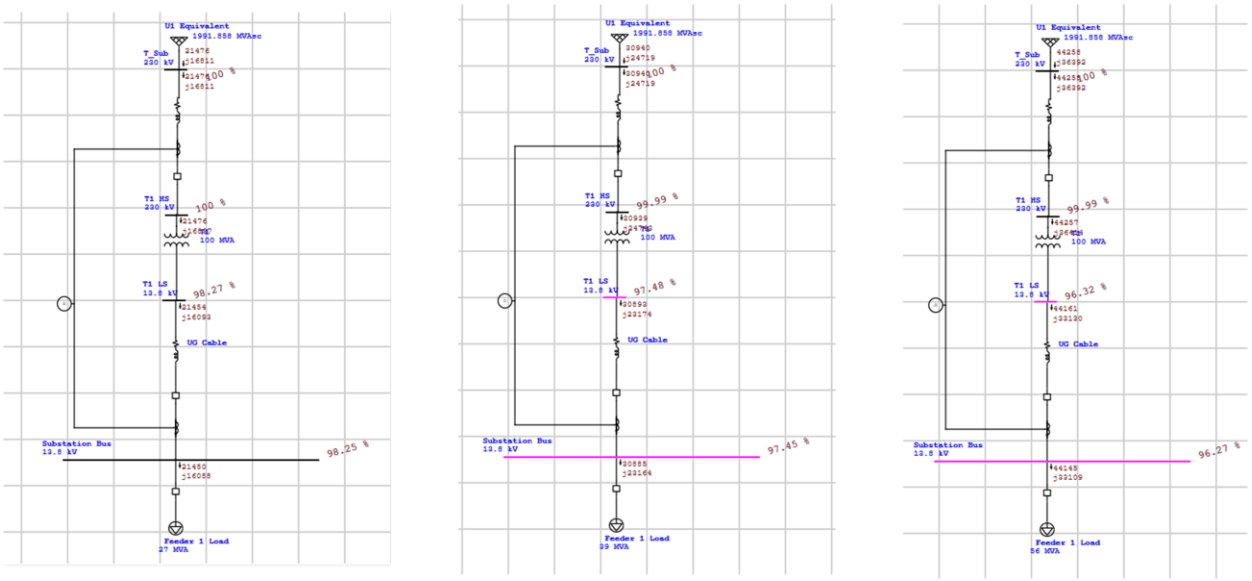

Figure 44. ETAP ACPF steady state simulation result for all policy-driven EV integration scenarios with discrete LV1 EV charging. From left to right: EV Scenario #1 (33%), EV Scenario #2 (66%), EV Scenario #3 (100%).

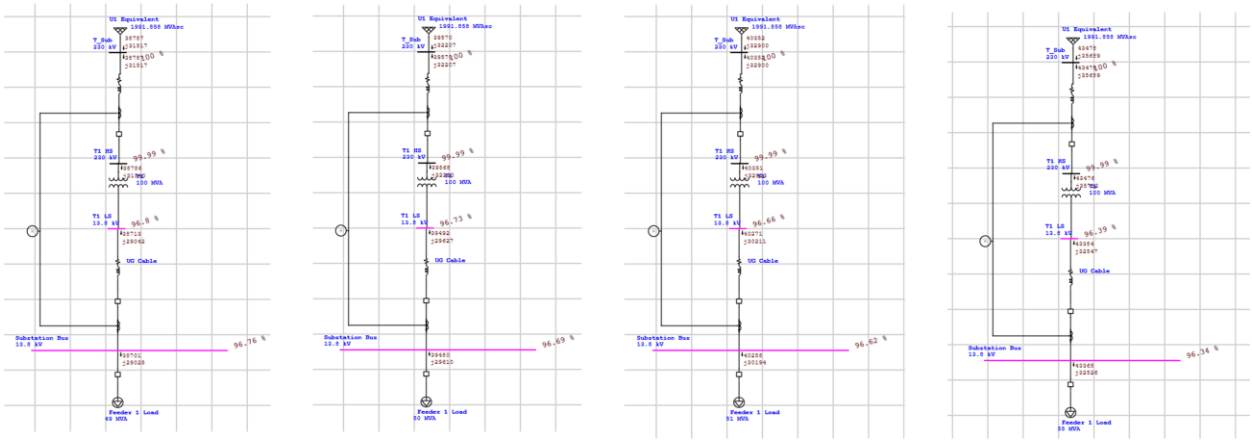

Figure 45. ETAP ACPF steady state simulation result for all high penetration EV integration scenarios with aggregated EV charging profiles from EVI-PRO. From left to right: Scenario 1, Scenario 2, Scenario 3, Scenario 4.

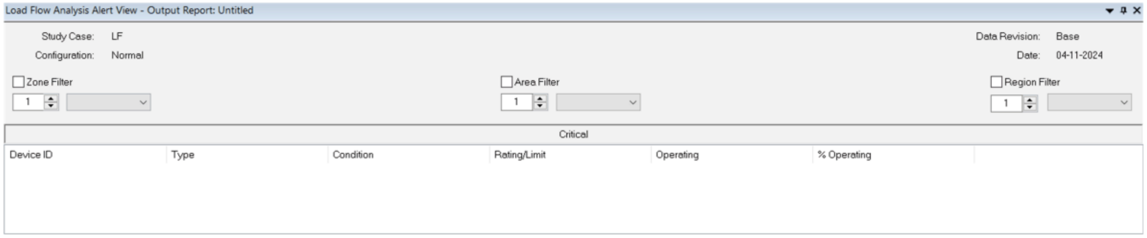
Load Flow Analysis Alert View - Output Report: Untitled
Study Case: LF
Configuration: Normal
Data Revision: Base
Date: 04-11-2024
Zone Filter
Area Filter
Region Filter
Critical
Device ID
Type
Condition
Rating/Limit
Operating
% Operating

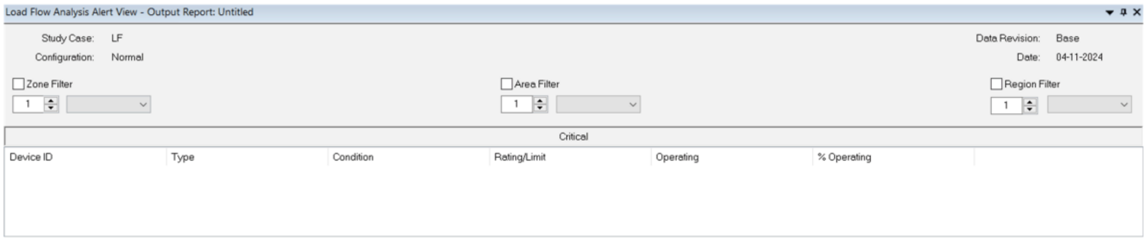
Load Flow Analysis Alert View - Output Report: Untitled
Study Case: LF
Configuration: Normal
Data Revision: Base
Date: 04-11-2024
Zone Filter
Area Filter
Region Filter
Critical
Device ID
Type
Condition
Rating/Limit
Operating
% Operating

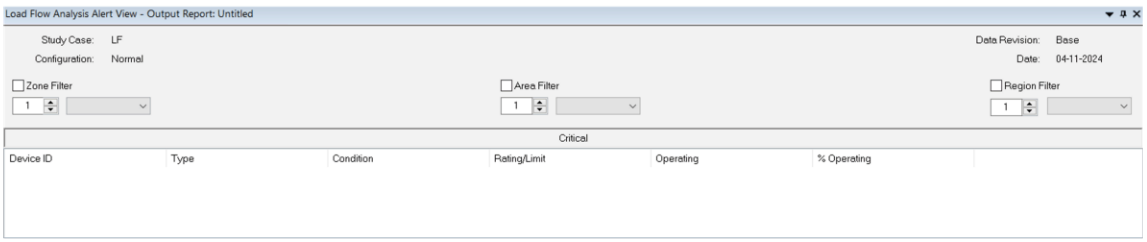
Load Flow Analysis Alert View - Output Report: Untitled
Study Case: LF
Configuration: Normal
Data Revision: Base
Date: 04-11-2024
Zone Filter
Area Filter
Region Filter
Critical
Device ID
Type
Condition
Rating/Limit
Operating
% Operating

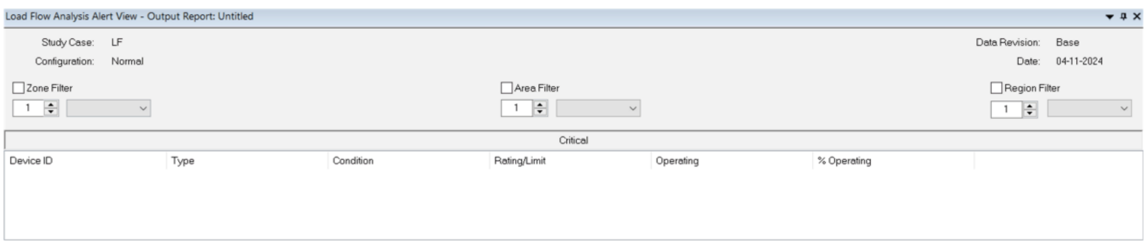
Load Flow Analysis Alert View - Output Report: Untitled
Study Case: LF
Configuration: Normal
Data Revision: Base
Date: 04-11-2024
Zone Filter
Area Filter
Region Filter
Critical
Device ID
Type
Condition
Rating/Limit
Operating
% Operating

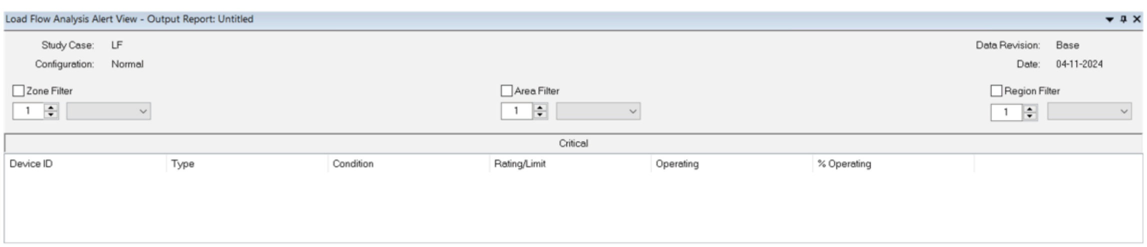
Load Flow Analysis Alert View - Output Report: Untitled
Study Case: LF
Configuration: Normal
Data Revision: Base
Date: 04-11-2024
Zone Filter
Area Filter
Region Filter
Critical
Device ID
Type
Condition
Rating/Limit
Operating
% Operating

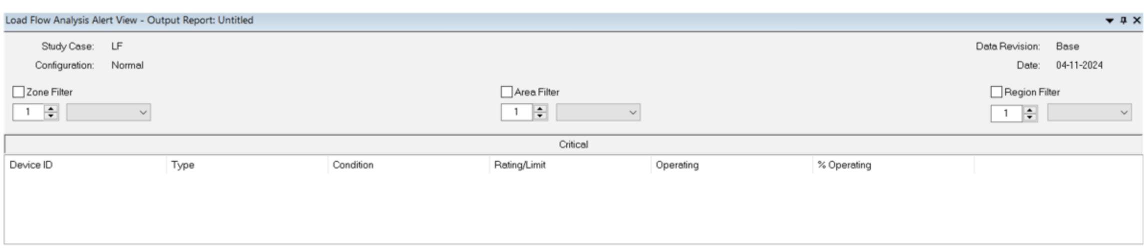
Load Flow Analysis Alert View - Output Report: Untitled
Study Case: LF
Configuration: Normal
Data Revision: Base
Date: 04-11-2024
Zone Filter
Area Filter
Region Filter
Critical
Device ID
Type
Condition
Rating/Limit
Operating
% Operating

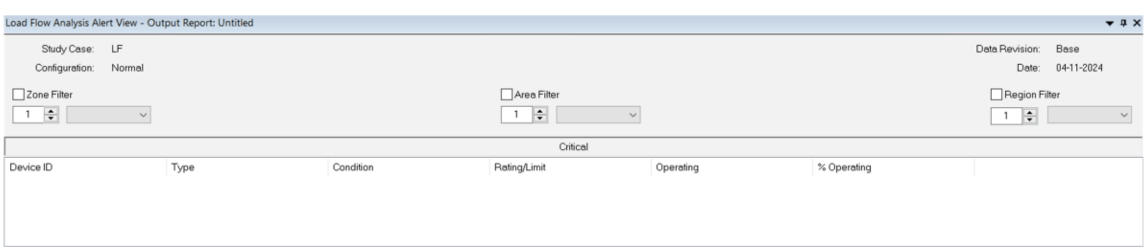
Load Flow Analysis Alert View - Output Report: Untitled
Study Case: LF
Configuration: Normal
Data Revision: Base
Date: 04-11-2024
Zone Filter
Area Filter
Region Filter
Critical
Device ID
Type
Condition
Rating/Limit
Operating
% Operating

Figure 46. ETAP critical warning report for all 7 considered scenarios. From top to bottom: Policy-driven EV Integration Scenarios: EV Scenario #1 (33%), EV Scenario #2 (66%), EV Scenario #3 (100%); High Penetration EV scenarios: Scenario 1, Scenario 2, Scenario 3, Scenario 4.

6.2.2 Upgrades and Cost Estimation

Due to the unavailability of pricing data pertaining to transmission transformers and cables exceeding 12KV voltage ratings, the analysis of upgrade and replacement costs will be focused on scenarios derived from the Oak View Community.

The predominant portion of upgrade expenditure pertains to transformers and cable/lines. Within electric distribution systems serving communities such as Oak View Community, the primary components necessitating upgrades comprise distribution transformers, as well as underground and overhead distribution circuit cables. On a broader scale encompassing county-level and statewide simulations, upgrade initiatives encompass substation transformers (both distribution and transmission varieties) and overhead transmission cables. The assessment of upgrade costs hinges upon the 30-year net present value (NPV) encompassing the comprehensive expenses associated with optimally selected transformers, as previously delineated. For all transformers deemed essential for rating upgrades, a systematic iteration process is conducted, wherein various options of higher-rated transformers are evaluated until the cumulative NPV cost reaches a minimum sum. The financial valuation of transformers is sourced from publications by the authors [127]. Concerning cable upgrades, segments identified as experiencing accelerated degradation are subjected to enhancements utilizing conductors of reduced gauge, thereby mitigating potential issues. The cost estimation for cable upgrades is derived from the 2021 SCE Per Unit Cost Guide.

The total upgrade cost for the Oak View Community with discrete EV charging profiles is depicted in Figure 47. From the figure, we learn that a community with a population of merely 1100 people can yield a high amount of upgrade charges due to high penetration EV adoption. Considering that utility infrastructure costs are typically amortized over expected equipment lifetime, this translates to an increased cost of service of $27.0 to $84.8 per year per utility customer when 33% to 100% EV adoption rates are implemented.

Figure 47. Cost estimation of EV integration scenarios with discrete EV charging events.

The upgrade cost status of High Penetration EV Charging Scenarios with LV2 and PDCF is shown in Figure 48. It is evident that exclusive deployment of Level 2 EV charging infrastructure within the residential sector results in decreased degradation and upgrade expenses compared to relying solely on Level 1 EV charging. This variance can be attributed to the Level 2 charging paradigm, distinguished by augmented charging capacities and reduced charging durations, consequently leading to an escalated Accumulated Aging Factor and thereby mitigating Loss of Life. Additionally, an observation can be made regarding Public DC Fast charging in the Commercial and Industrial sector, wherein despite its notably swifter charging pace,

degradation levels and associated upgrade costs surpass those of Level 2 charging alone. This phenomenon arises potentially due to the exceedingly high charging power ratings inherent in the PDCF methodology, whereby the abbreviated charging duration fails to offset the negative effects in terms of degradation stemming from such elevated power ratings.

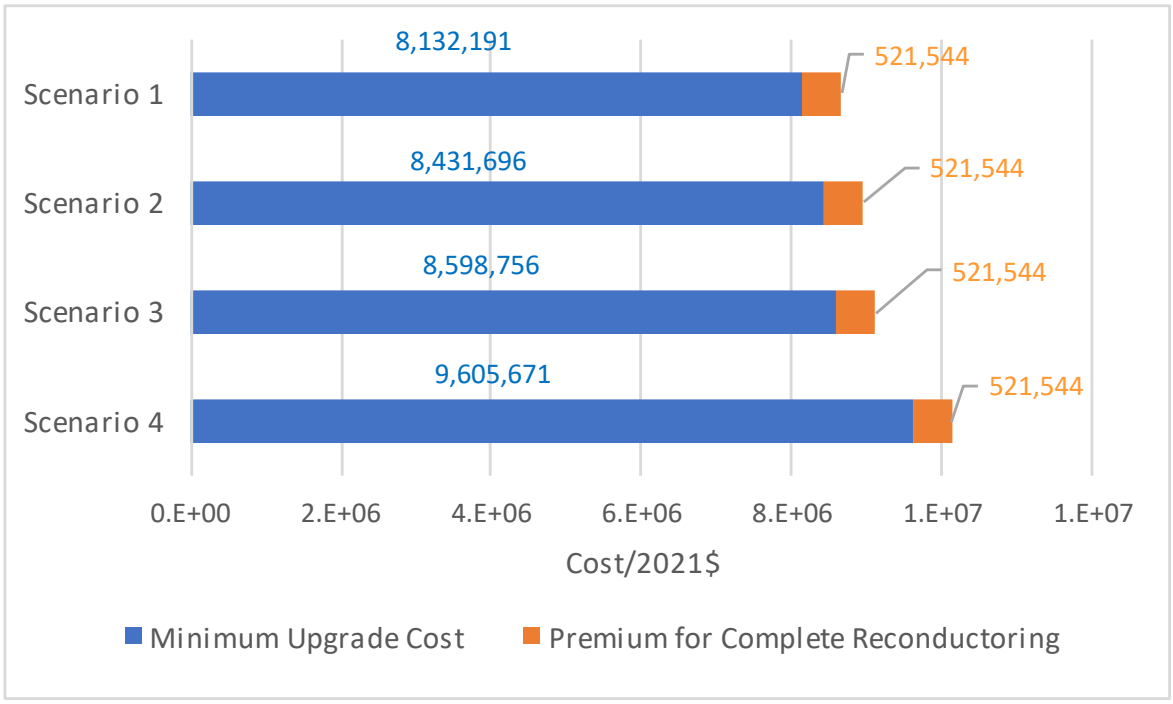

Figure 48. Yearly degradation loss of life status of vehicle electrification Scenario 1.

7 Optimal Renewable and Clean Energy System Adaption in Novel Operational Scenarios

7.1 Optimal Topology Design for Islanded Operations

The islanding results are analyzed from two perspectives. Firstly, a comprehensive annual analysis of electrical power quality is conducted, encompassing an evaluation of node Line-Neutral voltage and cable ampacity. Subsequently, an examination of the overall power equilibrium within each isolated island is performed, which includes a quantitative assessment

of yearlong island imbalance, considering both the cumulative absolute value and the frequency of high degree power imbalances. The primary objective of the first analysis is to ascertain the absence of any overvoltage or over-ampacity issues that may manifest in the isolated islands. The secondary analysis is geared towards testing and comparing the resilience of each individual island. This is achieved by assessing the disparities between their overall power generation and demand.

7.1.1 *Electrical Power Quality Analysis*

This section shows results from applying optimal topology design algorithm mentioned above to the test scenario. Line-Neutral voltage results are presented in Figure 49. A ±5% deviation from standard voltage is considered acceptable [159] and lower and upper voltage limit are marked in results. Cable ampacity results are also presented in Figure 50 to show the degree of pressure on the electric infrastructure. Although different ampacity ratings of electric conductor are highlighted according to AWG [111], all cables are believed to run safely if the maximum ampacity does not exceed the 2-gauge limit [16]. Both voltage and ampacity results are demonstrated using box plots, where the x-axis of those figures indicates the start of branch circuits. Transformers and cables for each branch are shown in order of proximity to the start of branch circuit. The middle red line in each box plot indicates the median annual value. The 25th and 75th percentile values are shown as the bottom and top of each box, respectively. All regular data falls within the whiskers and extreme data points as red '+' markers.

In Figure 49 it is shown that although no serious breaching of voltage rating limit is found for each islanding method, two reference islanding methods does show different degree of

undervoltage issues on several nodes in comparison, especially at the beginning of SR2. It is also shown that in Figure 50 our proposed islanding technique that allows extra connections is best in mitigating over ampacity problems.

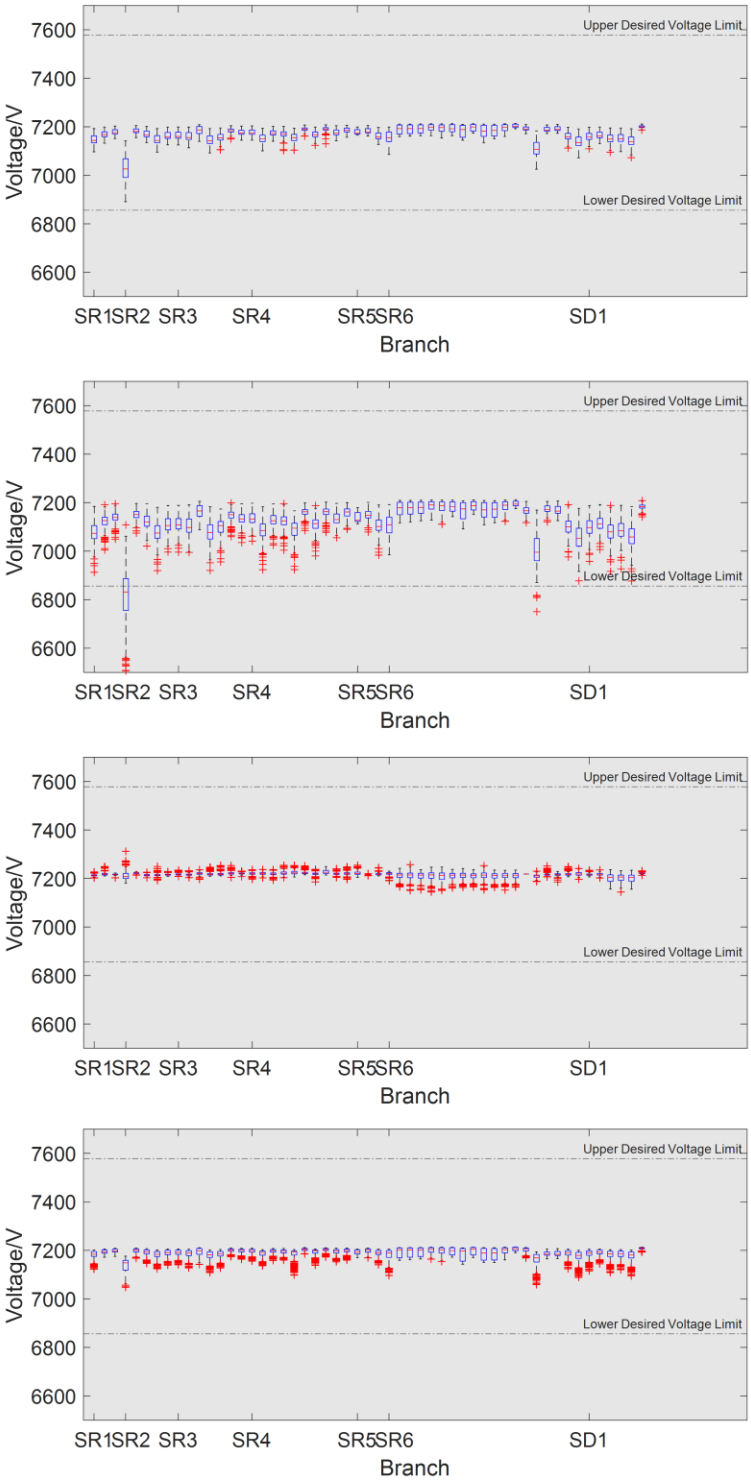

Figure 49. Line-Neutral yearly voltage of every active node in box plot. From top to bottom are voltage results of: Branch islanding, 12 kV Distribution Line Islanding, proposed islanding without extra connections, proposed islanding with extra connections.

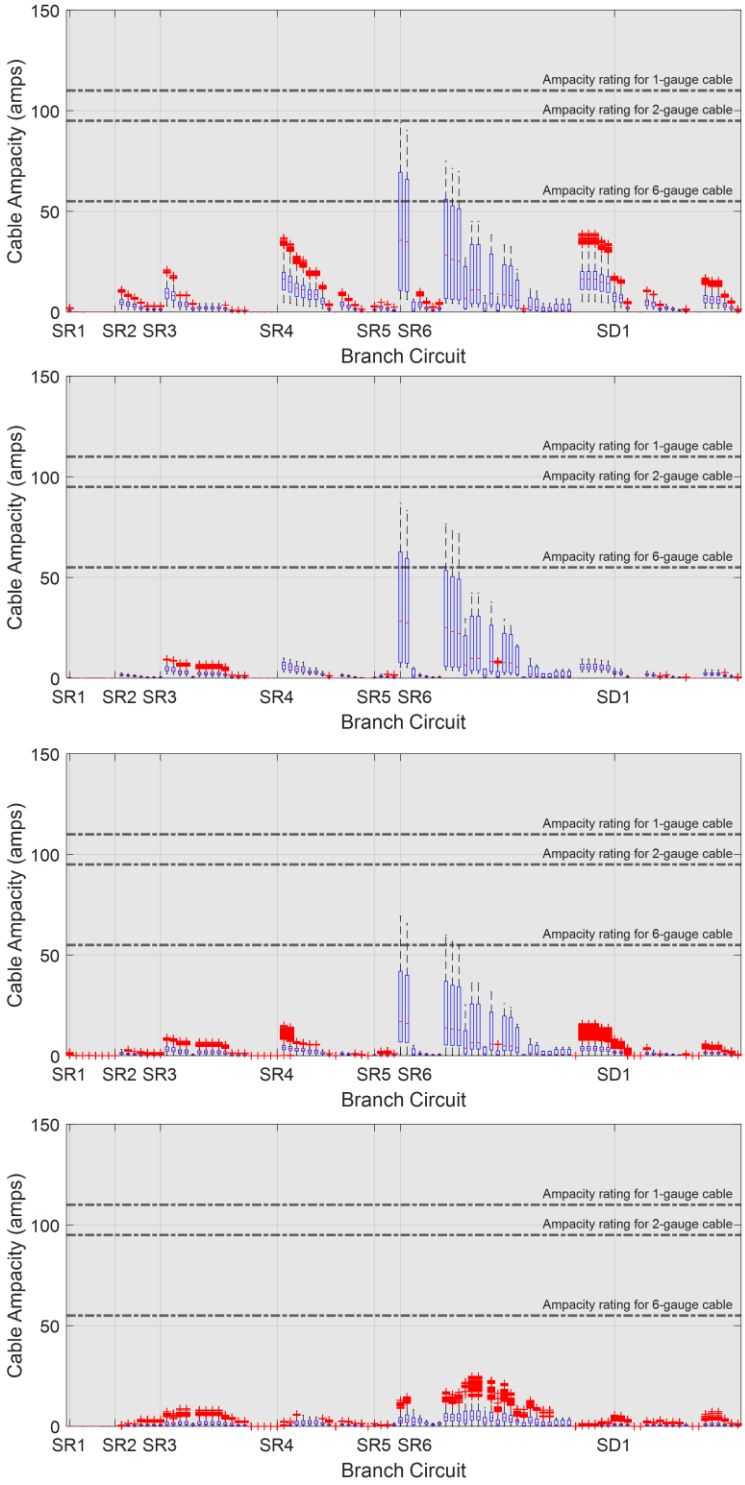

Figure 50. Yearly ampacity of all existing cables in box plot. From top to bottom are ampacity results of: Branch islanding, 12 KV Distribution Line Islanding, proposed islanding without extra connections, proposed islanding with extra connections. Lower and upper acceptable ampacity limit are marked.

7.1.2 Power Balance Analysis

The power balance is quantified through the computation of the annual sum of the absolute differences between the hourly power demand and DER generation for all active nodes within each island. As presented in Table 16, it becomes evident that the deployment of the proposed optimal topology design results in a notable mitigation of the overall power imbalance severity. This mitigation is reflected in the reduced maximum power imbalance observed within the existing islands. A further comparison of two optimal islanding designs also indicates that the introduction of additional connections facilitates a more effective balancing of power within the individual islands.

Figure 51 shows the magnitude of detailed power imbalance within each scenario, as represented by a histogram of the ratio of total hourly power imbalance of real-time DER capacity and load relative to transformer rating across all four considered scenarios. While no more than 30% of total power imbalance to transformer rating for all nodes for all scenarios is found, Figure 51 underscores the observation that the proposed optimal topology islanding technique is anticipated to exert the least disruptive influence on the stable operation of each island, manifesting 5% of power imbalance to transformer rating at most time.

Table 16. Average yearly power imbalance within each island for three tested islanding methods

	Optimal Islanding without extra connections				Optimal Islanding with extra connections		Branch Islanding							12 KV Distribution Line Islanding	
Island	Is1	Is2	Is3	Is4	Is1	Is2	SR1	SR2	SR3	SR4	SR5	SR6	SD1	Top Island	Bottom Island
Total Power Imbalance /KW	3.6	2.5	0.2	0.4	3.3	1.1	0.4	2.1	4.7	3.6	2.2	0.7	1.8	6.3	8.4

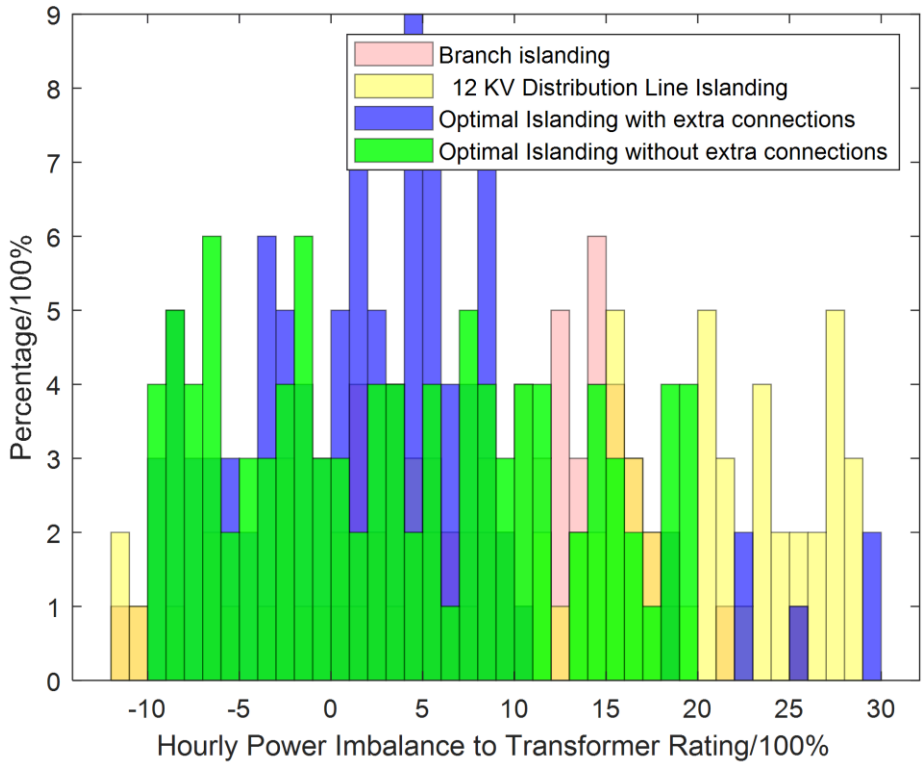

Figure 51. Histogram of total hourly absolute power imbalance to transformer rating for all considered scenarios.

7.2 DER Alternative Solution Capacity and Cost Results

The DER and ESS capacity for the lowest overall cost for all considered scenarios are listed in Table 17. From the results, it is shown that for each scenario, while the transformer overload constraint did not usually increase the PV capacity much, the necessary ESS capacity was usually elevated greatly. The PV and ESS capacity is then translated into a 30-year TDV cost [160]. Compared to the infrastructure upgrade cost in Section 6.2.2, the cost for even the lowest cost DER/ESS application to mitigate the electric stress from the increased EV charging demand for all scenarios is about 10 times on average compared to the highest average upgrade cost.

Table 17. Capacity of DER and ESS capacity for lowest cost deployment for all considered EV integration scenarios. The DER/ESS capacity is translated to TDV cost and is shown as well. The results also specify the difference of transformer constraint implementation.

Scenario	DER Capacity/KW		ESS Capacity/KWh		Cost/2021$	
	w/constraint	w/o constraint	w/constraint	w/o constraint	w/constraint	w/o constraint
35% LV1 EV	7,785	7,596	1,122	299	23,504,904	22,827,521
68% LV1 EV	15,831	15,367	2,007	453	47,759,803	46,163,275
100% LV1 EV	33,825	32,008	3,679	720	101,960,654	96,121,519
100% Residential LV 2	33,083	33,000	3,597	666	99,725,083	99,087,991
100% Residential LV1/LV2	34,013	33,780	3,761	714	102,536,704	101,436,127
100% Residential LV1/LV2 +100% C&I LV2	34,893	34,777	3,847	780	105,188,630	104,436,439
100% Residential LV2 +100% PDCF	35,021	34,799	3,796	753	105,565,298	104,497,675

8 Method Generalization

The need to integrate renewable and clean energy sources into our daily lives has intensified in recent years, spurred by the adverse impacts of climate change on the stability and sustainability of our power and energy supply infrastructure. Consequently, there has been a discernible trend towards the transformation of conventional power grid systems into microgrids. Therefore, the development of a comprehensive guideline framework for the integration of renewable energy into grid systems has become a necessity.

Researchers and scientists have come up with a few practical microgrid design frameworks integrating renewable and clean energy sources. Two categories of microgrid framework has been proposed. The first focus on operational optimization for reliable grid operation. [161] discusses the possibility of model-based analysis by rapid modeling environment construction. [162] focuses on the hierarchical control of grid components in microgrid framework, including three-level control algorithm of droop, voltage and power flow. [163] talks about optimization of energy management inside the frame using non-linear computational algorithms. A series of optimized control algorithms and methods within microgrid design frame have been proposed and developed by scientists in Pacific Northwest National Laboratory (PNNL) [164–171].

On the other hand, the second type of frameworks concentrates or involves mostly on socio-economic perspective when designing microgrid frameworks. [172] brings about the energy equity and economic feasibility into microgrid design framework. [173] demonstrates the possibility of including energy-related economic factors in optimization objectives of microgrid frameworks.

While the first category has considered a variety of modern and potentially very efficient optimization algorithms that help plan or organize grid operation and dispatching of renewable energy sources, it usually ignores the financial aspects of the analysis; on the other hand, the second category with a focus on socio-economy seldom involves optimization algorithms, especially on normal grid operation aspects, not to mention to enhance the reliability of the microgrid systems. In this section, we propose a novel microgrid design framework that balances both categories, derived and abstracted from the OVMG project.

8.1 Novel Analytical Frame for Renewable Energy Adoption

The process of novel microgrid framework design is shown in Figure 52.

Upon determining the research object/subject within the project's scope parameters, the initial endeavor would be the selection of optimal optimization algorithms. Should the project delineations specify algorithmic preferences, this procedural phase is skipped. If not, an evaluative process ensues, wherein algorithms are compared to ascertain the most effective solution. In the context of our OVMG project, aimed at facilitating discrete EV charging sessions within the Oak View Community, two algorithms were considered: the Monte Carlo Algorithm and the Neural Network Machine Learning (ML) algorithm. Due to lack of bulk charging data samples, the Monte Carlo Algorithm emerged as the preferred choice.

The subsequent phase entails the acquisition of necessary simulation data. In instances where data are provided by the project package, this stage may be skipped. Conversely, in their absence, the development of simulation data becomes imperative. Within the OVMG

framework, without foundational baseline and electrification load data, project participants undertook the development and estimation of datasets as shown in [110][143]. After data development, a validation process ensues, aimed at affirming data accuracy, where feasible. In the OVMG project context, baseline data underwent rigorous scrutiny as expounded upon in section 3.

Following data acquisition, the next step is modeling, which may range in scale from a localized community to expansive geographic regions such as counties or entire states. In the OVMG context, the modeling focus initially centered on the Oak View Community, a socioeconomically disadvantaged community comprising approximately 1,100 residents in Huntington Beach, California. Subsequently, the scope expanded to encompass the broader Southern California region for enhanced analysis of EV adoption trends, where millions of residents live, thereby necessitating commensurate modeling efforts.

Upon completion of modeling endeavors, a comprehensive, multifaceted analysis is undertaken, encompassing both technical and economic dimensions. Within our OVMG undertaking, various technical analyses were conducted, encompassing electrical power quality and degradation analysis. Concurrently, an economic assessment ensued, incorporating infrastructure upgrade cost projections and per capita electricity price escalation estimates. In instances where analysis outcomes reveal pronounced infeasibility, a reevaluation of optimization algorithm selection may ensue, and following steps are done again until viable outcomes are achieved.

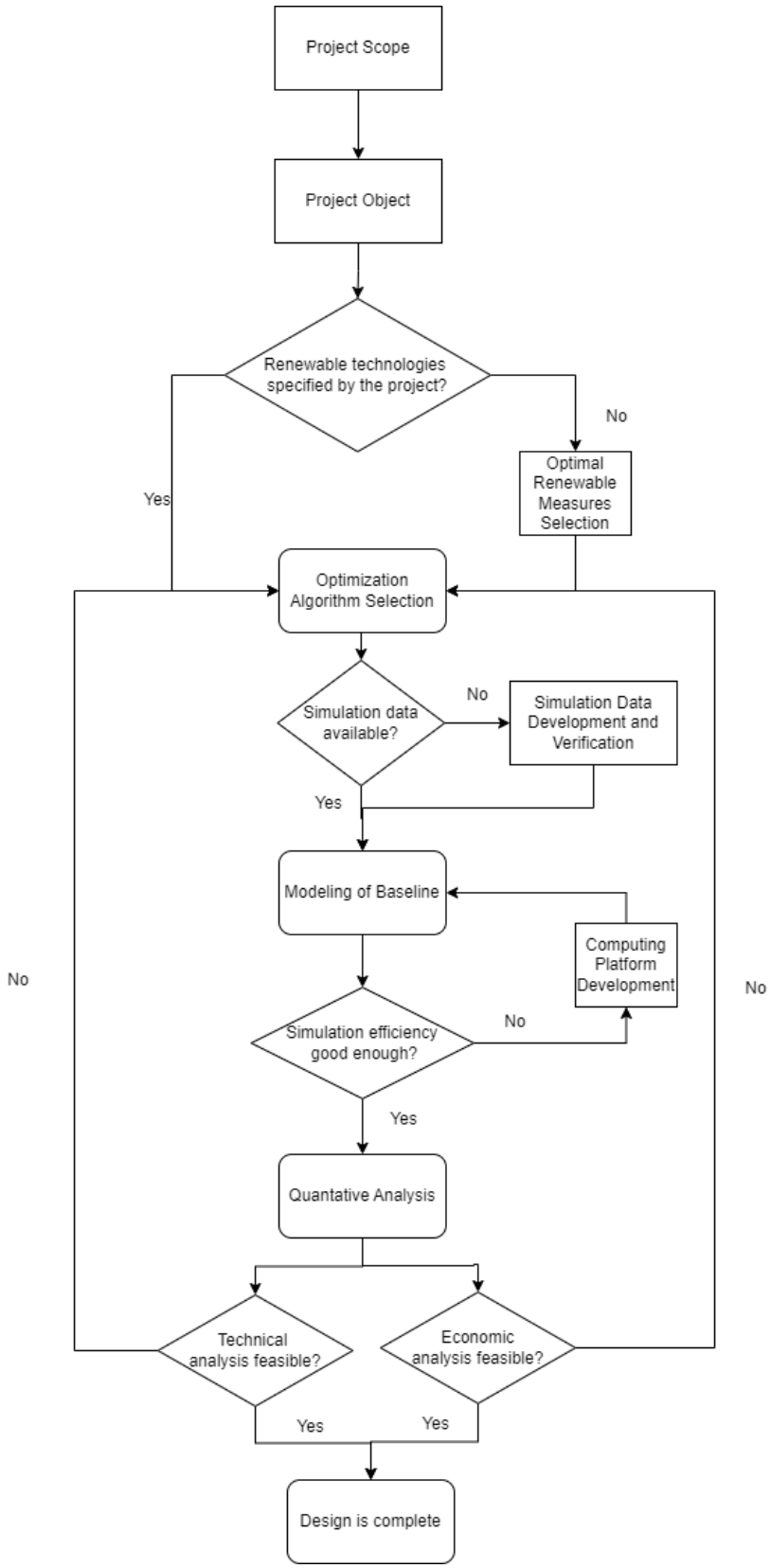

Figure 52. Novel microgrid design framework process in flowchart.

9 Conclusions, Summary and Future Work

This effort starts with building an AC Power Flow model for the Oak View Community microgrid system on OpenDSS for CEC's OVMG project. The modeling process involves three steps. The first step is to outline the general Oak View Community grid connection with SCE's DRPEP tool [109]. The second step is on-site inspections which were made to record and verify circuit topology, including connections, transformer types, ratings, locations and to revise them if necessary. The last step is to combine the outlined grid topology and information gained from field trips to make OpenDSS ACPF model. The model was supported with tuned electrical demand results from the Oak View community energy simulation developed in URBANopt [110].

The author's research then moves on to enhance the efficiency of power flow analysis of OpenDSS platform by building a MATLAB-OpenDSS interface. The interface greatly enhances the already powerful function of OpeenDSS's ACPF function by making the data input into OpenDSS easy and changing simulation parameters for different scenario settings more convenient. The OVMG baseline model is then tested with a cross-platform comparison of OpenDSS/DERopt platforms with same input to assure model accuracy. The comparison result indicates that the OpenDSS model is accurate.

Based on Oak View Community OpenDSS ACPF model, renewable and clean energy system was then integrated into the Oak View Community in several traditional and novel operational scenarios. The first operational scenario is EV adoption in the community. Initially, a stochastic methodology is introduced for generating discrete, dynamic Level 1 charging profiles for electric

vehicles, which are then allocated pseudo-randomly using the Monte Carlo algorithm. Subsequently, this methodology is applied to the load flow simulation of grid infrastructure in a disadvantaged community in Southern California typical of such communities in the region. A few theoretically high EV penetration scenarios with higher EV charging level using similar Monte Carlo process for different levels of EV charging load profiles are also developed. The LF and transformer degradation analysis is extended to the entire SoCal area with different levels of EV penetration in accordance with California policies. Power quality and degradation evaluations of crucial distribution infrastructure components are then completed. The simulation outcomes reveal that the electric infrastructure in Southern California, particularly distribution and transmission transformers, are ill-equipped to support the very high levels of EV market penetration stipulated by current California policies, with an estimated 12% to 39% increased yearly degradation rate under merely 33% of EV adoption rate. Addressing this challenge would require substantial investments in upgrading transformers and/or implementing additional measures for load management.

Following the EV charging load dynamics development mentioned above, the second operation scenario is then developed for a novel peak load shaving strategy, which involves changing the charging schedule of EVs to shift the load from peak to off-peak hours, thereby optimizing electricity costs. This optimization is achieved by prioritizing EV charging sessions to off-peak hours when electricity rates are lower. The electrical power quality analysis, infrastructure degradation analysis and electricity bill saving analysis are then carried out. It is shown that the proposed peak shaving strategy greatly alleviates the electrical pressure from added EV charging load demand in each considered scenario, thus easing the infrastructure

degradation as well. A comparison of the per customer amortized upgrade cost from EV adoption after peak shaving in each scenario and savings from electricity after shaving in each scenario indicates that the saving from electricity consumption may be able to cut the per customer upgrade cost by about 50% for most scenario, which further illustrates the effectiveness of the proposed peak load shaving strategy.

The next considered operational scenario is islanding during PSPS events. First, an optimal algorithm is developed based on multilevel graph partitioning techniques to island existing radially developed grid topology with added potential extra connections to consider based on known loads and DERs. The algorithm is further demonstrated with a real-life example of the Oak View Community consisting of residential, commercial, and industrial sectors. The simulation results preliminarily confirm that the algorithm further each island's resiliency and reliability by improving local energy balance while maintaining acceptable electrical power quality factors including bus voltage and cable ampacity. The quantified results shows that less than 5% of local power imbalance at all times is added for the proposed islanding technique.

The last considered operational scenario is to deploy DER for lowest cost with or without NEM 3.0 ratings. During the process, MILP algorithm is used to optimally size and dispatch the DERs while considering infrastructure degradation limits in DERopt. To mitigate the electric stress from the increased EV charging demand for all scenarios, DER/ESS solution with transformer limit constraint is about 10 times on average in cost compared to the highest average upgrade cost for infrastructure upgrade solution in Section 6.2.

Eventually, the author proposes a novel microgrid design framework derived and abstracted from the OVMG project that involves both efficient optimization algorithms and financial impacts analysis, which is unusual in tradition and popular microgrid framework with renewable energy integration.

Future work has been identified and listed as follows. Firstly, discrete EV charging generation technique can be further applied to more sophisticated EV charging scenarios, which will not only enable more accurate impact analysis of high penetration EV integration of various charging, but it can also further test the proposed peak shaving strategy's performance in various EV adoption scenarios. Also, more DER operation scenarios can be considered other than lowest cost and NEM 3.0 scenarios, such as a combination of NEM 2.0 and NEM 3.0. Last but not least, future analysis can consider partial or full fuel cell or hydrogen pipeline's influence on alleviating the existing electrical pressure from electrification.

References

[1] United States Congress. Energy Policy Act 1992 1992;102:357.

[2] United States Congress. Energy Policy Act 2005 2004;41:510–1.

[3] Biden-Harris Administration Announces $425 Million to Expand State Clean Energy Programs 2022.

[4] White House. Federal Sustainability Plan 2021.

[5] California S of. Senate Bill No. 1339 2020:1–4.

[6] Hurlbut D. State Clean Energy Practices: Renewable Portfolio Standards. Natl Renew Energy Lab 2008:1–15.

[7] Ali A, Li W, Hussain R, He X, Williams BW, Memon AH. Overview of current microgrid policies, incentives and barriers in the European Union, United States and China. Sustain 2017;9. https://doi.org/10.3390/su9071146.

[8] Public C, Commission U, Proposal S. Short-Term Actions to Accelerate the Deployment of Microgrids and Related Resiliency Solutions 2019;1339.

[9] Pickerel K. California city to establish residential solar microgrids with Electriq Power batteries 2022.

[10] Advanced Power and Energy Program (APEP). UCI Microgrid. n.d.

[11] Feng W, Jin M, Liu X, Bao Y, Marnay C, Yao C, et al. A review of microgrid development in the United States – A decade of progress on policies, demonstrations, controls, and software tools. Appl Energy 2018;228:1656–68. https://doi.org/10.1016/j.apenergy.2018.06.096.

[12] Ajit Niranjan. Renewable energy transition in 5 charts 2022.

[13] What is U.S. electricity generation by energy source? n.d.

[14] SCOTT MINOS. New Plug-in Electric Vehicle Sales in the United States Nearly Doubled from 2020 to 2021 n.d.

[15] Jeff S. Bartlett. More Americans Would Buy an Electric Vehicle, and Some Consumers Would Use Low-Carbon Fuels, Survey Shows n.d. https://www.consumerreports.org/hybrids-evs/interest-in-electric-vehicles-and-low-carbon-fuels-survey-a8457332578/.

[16] Wang W, Flores R, Razeghi G, Brouwer J. Quantifying Transformer and Cable Degradation in Highly Renewable Electric Distribution Circuits. IEEE PES Grid Edge Technol. Conf. Expo., 2023.

[17] Senate Bill No. 656 CHAPTER 369 An act to add Section 2827 to the Public Utilities Code, relating to public utilities. 1995.

[18] Sam Wigness. What is NEM 3.0 and How Will it Impact California Solar Owners? 2023. https://www.solar.com/learn/nem-3-0-proposal-and-impacts-for-california-homeowners/.

[19] US microgrid forecast H1 2020: Coronavirus delays projects and impacts origination. 2020.

[20] Xu Y, Zhang W, Hug G, Kar S, Li Z. Cooperative control of distributed energy storage systems in a

microgrid. IEEE Trans Smart Grid 2015. https://doi.org/10.1109/TSG.2014.2354033.

[21] Dorfler F, Simpson-Porco JW, Bullo F. Breaking the hierarchy: Distributed control and economic optimality in Microgrids. IEEE Trans Control Netw Syst 2016. https://doi.org/10.1109/TCNS.2015.2459391.

[22] Parisio A, Rikos E, Glielmo L. A model predictive control approach to microgrid operation optimization. IEEE Trans Control Syst Technol 2014. https://doi.org/10.1109/TCST.2013.2295737.

[23] Erol-Kantarci M, Kantarci B, Mouftah HT. Reliable overlay topology design for the smart microgrid network. IEEE Netw 2011. https://doi.org/10.1109/MNET.2011.6033034.

[24] Che L, Zhang X, Shahidehpour M, Alabdulwahab A, Al-Turki Y. Optimal Planning of Loop-Based Microgrid Topology. IEEE Trans Smart Grid 2017. https://doi.org/10.1109/TSG.2015.2508058.

[25] Cortes CA, Contreras SF, Shahidehpour M. Microgrid topology planning for enhancing the reliability of active distribution networks. IEEE Trans Smart Grid 2018. https://doi.org/10.1109/TSG.2017.2709699.

[26] Jiménez-Fernández S, Camacho-Gómez C, Mallol-Poyato R, Fernández JC, Del Ser J, Portilla-Figueras A, et al. Optimal microgrid topology design and siting of distributed generation sources using a multi-objective substrate Layer Coral Reefs Optimization Algorithm. Sustain 2018. https://doi.org/10.3390/su11010169.

[27] Talukdar S, Deka D, Materassi D, Salapaka M. Exact topology reconstruction of radial dynamical systems with applications to distribution system of the power grid. Proc. Am. Control Conf., 2017. https://doi.org/10.23919/ACC.2017.7963053.

[28] Arefifar SA, Mohamed YARI, El-Fouly THM. Optimum microgrid design for enhancing reliability and supply-security. IEEE Trans Smart Grid 2013. https://doi.org/10.1109/TSG.2013.2259854.

[29] Gazijahani FS, Salehi J. Robust Design of Microgrids with Reconfigurable Topology under Severe Uncertainty. IEEE Trans Sustain Energy 2018. https://doi.org/10.1109/TSTE.2017.2748882.

[30] Kirthiga MV, Daniel SA, Gurunathan S. A methodology for transforming an existing distribution network into a sustainable autonomous micro-grid. IEEE Trans Sustain Energy 2013. https://doi.org/10.1109/TSTE.2012.2196771.

[31] Sechilariu M, Wang BC, Locment F. Supervision control for optimal energy cost management in DC microgrid: Design and simulation. Int J Electr Power Energy Syst 2014. https://doi.org/10.1016/j.ijepes.2014.01.018.

[32] Nguyen DT, Le LB. Risk-constrained profit maximization for microgrid aggregators with demand response. IEEE Trans Smart Grid 2015. https://doi.org/10.1109/TSG.2014.2346024.

[33] Gazijahani FS, Salehi J. Game Theory Based Profit Maximization Model for Microgrid Aggregators with Presence of EDRP Using Information Gap Decision Theory. IEEE Syst J 2019. https://doi.org/10.1109/JSYST.2018.2864578.

[34] Tsao YC, Thanh V Van. Toward blockchain-based renewable energy microgrid design considering default risk and demand uncertainty. Renew Energy 2021. https://doi.org/10.1016/j.renene.2020.09.016.

[35] Qin M, Chan KW, Chung CY, Luo X, Wu T. Optimal planning and operation of energy storage

systems in radial networks for wind power integration with reserve support. IET Gener Transm Distrib 2016. https://doi.org/10.1049/iet-gtd.2015.1039.

[36] Dou C, Yue D, Guerrero JM, Xie X, Hu S. Multiagent System-Based Distributed Coordinated Control for Radial DC Microgrid Considering Transmission Time Delays. IEEE Trans Smart Grid 2017. https://doi.org/10.1109/TSG.2016.2524688.

[37] Almadhor A. Feedback-Oriented Intelligent Monitoring of a Storage-Based Solar Photovoltaic (PV)-Powered Microgrid with Mesh Networks. Energies 2018;11:1446. https://doi.org/10.3390/en11061446.

[38] Trivedi A, Singh M. L1 Adaptive Droop Control for AC Microgrid with Small Mesh Network. IEEE Trans Ind Electron 2018. https://doi.org/10.1109/TIE.2017.2772211.

[39] Lou G, Gu W, Wang J, Sheng W, Sun L. Optimal Design for Distributed Secondary Voltage Control in Islanded Microgrids: Communication Topology and Controller. IEEE Trans Power Syst 2019. https://doi.org/10.1109/TPWRS.2018.2870058.

[40] Simpson-Porco JW, Shafiee Q, Dorfler F, Vasquez JC, Guerrero JM, Bullo F. Secondary Frequency and Voltage Control of Islanded Microgrids via Distributed Averaging. IEEE Trans Ind Electron 2015. https://doi.org/10.1109/TIE.2015.2436879.

[41] Ashabani SM, Mohamed YARI. A flexible control strategy for grid-connected and islanded microgrids with enhanced stability using nonlinear microgrid stabilizer. IEEE Trans Smart Grid 2012. https://doi.org/10.1109/TSG.2012.2202131.

[42] Etemadi AH, Davison EJ, Iravani R. A generalized decentralized robust control of islanded microgrids. IEEE Trans Power Syst 2014. https://doi.org/10.1109/TPWRS.2014.2312615.

[43] Hossain MJ, Mahmud MA, Milano F, Bacha S, Hably A. Design of Robust Distributed Control for Interconnected Microgrids. IEEE Trans Smart Grid 2016. https://doi.org/10.1109/TSG.2015.2502618.

[44] Chen YK, Wu YC, Song CC, Chen YS. Design and implementation of energy management system with fuzzy control for DC microgrid systems. IEEE Trans Power Electron 2013. https://doi.org/10.1109/TPEL.2012.2210446.

[45] Kumar M, Singh SN, Srivastava SC. Design and control of smart DC microgrid for integration of renewable energy sources. IEEE Power Energy Soc. Gen. Meet., 2012. https://doi.org/10.1109/PESGM.2012.6345018.

[46] Unamuno E, Barrena JA. Hybrid ac/dc microgrids - Part I: Review and classification of topologies. Renew Sustain Energy Rev 2015;52:1251–9. https://doi.org/10.1016/j.rser.2015.07.194.

[47] Unamuno E, Barrena JA. Hybrid ac/dc microgrids - Part II: Review and classification of control strategies. Renew Sustain Energy Rev 2015;52:1123–34. https://doi.org/10.1016/j.rser.2015.07.186.

[48] Roggia L, Rech C, Schuch L, Baggio JE, Hey HL, Pinheiro JR. Design of a sustainable residential microgrid system including PHEV and energy storage device. Proc. 2011 14th Eur. Conf. Power Electron. Appl. EPE 2011, 2011.

[49] Gregus N. Why is Electrification Important? 2021. https://goenergylink.com/blog/why-is-

electrification-important/.

[50] California Energy Commission. Achieving 100 % Clean Electricity in California 2021.

[51] ZEV Action Plan History n.d. https://business.ca.gov/industries/zero-emission-vehicles/zev-action-plan/.

[52] Garwa N, Niazi KR. Impact of EV on Integration with Grid System - A Review. 2019 8th Int Conf Power Syst Transit Towar Sustain Smart Flex Grids, ICPS 2019 2019:1–6. https://doi.org/10.1109/ICPS48983.2019.9067587.

[53] Das HS, Rahman MM, Li S, Tan CW. Electric vehicles standards, charging infrastructure, and impact on grid integration: A technological review. Renew Sustain Energy Rev 2020;120. https://doi.org/10.1016/j.rser.2019.109618.

[54] Monteiro V, Gonçalves H, Afonso JL. Impact of electric vehicles on power quality in a Smart Grid context. Proceeding Int Conf Electr Power Qual Util EPQU 2011:660–5. https://doi.org/10.1109/EPQU.2011.6128861.

[55] Ucer E, Kisacikoglu MC, Cafer Gurbuz A. Learning EV Integration Impact on a Low Voltage Distribution Grid. IEEE Power Energy Soc Gen Meet 2018;2018-Augus:1–5. https://doi.org/10.1109/PESGM.2018.8586208.

[56] Schey S, Scoffield D, Smart J. A first look at the impact of electric vehicle charging on the electric grid in the EV project. World Electr Veh J 2012;5:667–78. https://doi.org/10.3390/wevj5030667.

[57] Ramanujam A, Sankaranarayanan P, Vasan A, Jayaprakash R, Sarangan V, Sivasubramaniam A. Quantifying the impact of electric vehicles on the electric grid - A simulation based case-study. E-Energy 2017 - Proc 8th Int Conf Futur Energy Syst 2017:228–33. https://doi.org/10.1145/3077839.3077854.

[58] Kapustin NO, Grushevenko DA. Long-term electric vehicles outlook and their potential impact on electric grid. Energy Policy 2020;137:111103. https://doi.org/10.1016/j.enpol.2019.111103.

[59] Awadallah MA, Singh BN, Venkatesh B. Impact of EV Charger Load on Distribution Network Capacity: A Case Study in Toronto. Can J Electr Comput Eng 2016;39:268–73. https://doi.org/10.1109/CJECE.2016.2545925.

[60] Van Der Burgt J, Vera SP, Wille-Haussmann B, Andersen AN, Tambjerg LH. Grid impact of charging electric vehicles; Study cases in Denmark, Germany and the Netherlands. 2015 IEEE Eindhoven PowerTech, PowerTech 2015 2015. https://doi.org/10.1109/PTC.2015.7232234.

[61] Hussain MT, Sulaiman DN Bin, Hussain MS, Jabir M. Optimal Management strategies to solve issues of grid having Electric Vehicles (EV): A review. J Energy Storage 2021;33:102114. https://doi.org/10.1016/j.est.2020.102114.

[62] Shahidinejad S, Filizadeh S, Bibeau E. Profile of charging load on the grid due to plug-in vehicles. IEEE Trans Smart Grid 2012;3:135–41. https://doi.org/10.1109/TSG.2011.2165227.

[63] Pashajavid E, Golkar MA. Non-Gaussian multivariate modeling of plug-in electric vehicles load demand. Int J Electr Power Energy Syst 2014;61:197–207. https://doi.org/10.1016/j.ijepes.2014.03.021.

[64] Cao Y, Tang S, Li C, Zhang P, Tan Y, Zhang Z, et al. An optimized EV charging model considering

TOU price and SOC curve. IEEE Trans Smart Grid 2012;3:388–93. https://doi.org/10.1109/TSG.2011.2159630.

[65] Xia Y, Hu B, Xie K, Tang J, Tai HM. An EV charging demand model for the distribution system using traffic property. IEEE Access 2019;7:28089–99. https://doi.org/10.1109/ACCESS.2019.2901857.

[66] Flores RJ, Shaffer BP, Brouwer J. Electricity costs for an electric vehicle fueling station with Level 3 charging. Appl Energy 2016;169:813–30. https://doi.org/10.1016/j.apenergy.2016.02.071.

[67] Bae S, Kwasinski A. Spatial and temporal model of electric vehicle charging demand. IEEE Trans Smart Grid 2012;3:394–403. https://doi.org/10.1109/TSG.2011.2159278.

[68] Wikipedia. Vehicle-to-grid n.d.

[69] Kisacikoglu MC, Kesler M, Tolbert LM. Single-phase on-board bidirectional PEV charger for V2G reactive power operation. IEEE Trans Smart Grid 2015;6:767–75. https://doi.org/10.1109/TSG.2014.2360685.

[70] Lund H, Kempton W. Integration of renewable energy into the transport and electricity sectors through V2G. Energy Policy 2008;36:3578–87. https://doi.org/10.1016/j.enpol.2008.06.007.

[71] Khan SU, Mehmood KK, Haider ZM, Rafique MK, Khan MO, Kim CH. Coordination of multiple electric vehicle aggregators for peak shaving and valley filling in distribution feeders. Energies 2021;14:1–16. https://doi.org/10.3390/en14020352.

[72] Mets K, Verschueren T, De Turck F, Develder C. Exploiting V2G to optimize residential energy consumption with electrical vehicle (dis)charging. 2011 IEEE 1st Int Work Smart Grid Model Simulation, SGMS 2011 2011:7–12. https://doi.org/10.1109/SGMS.2011.6089203.

[73] Wang Z, Wang S. Grid power peak shaving and valley filling using vehicle-to-grid systems. IEEE Trans Power Deliv 2013;28:1822–9. https://doi.org/10.1109/TPWRD.2013.2264497.

[74] Kempton W, Udo V, Huber K, Komara K, Letendre S, Baker S, et al. A Test of Vehicle-to-Grid (V2G) for Energy Storage and Frequency Regulation in the PJM System 2008;2008.

[75] Bishop JDK, Axon CJ, Bonilla D, Tran M, Banister D, McCulloch MD. Evaluating the impact of V2G services on the degradation of batteries in PHEV and EV. Appl Energy 2013;111:206–18. https://doi.org/10.1016/j.apenergy.2013.04.094.

[76] Yilmaz M, Krein PT. Review of benefits and challenges of vehicle-to-grid technology. 2012 IEEE Energy Convers Congr Expo ECCE 2012 2012:3082–9. https://doi.org/10.1109/ECCE.2012.6342356.

[77] Uddin M, Romlie MF, Abdullah MF, Abd Halim S, Abu Bakar AH, Chia Kwang T. A review on peak load shaving strategies. Renew Sustain Energy Rev 2018;82:3323–32. https://doi.org/10.1016/j.rser.2017.10.056.

[78] Li X, Cao X, Li C, Yang B, Cong M, Chen D. A Coordinated Peak Shaving Strategy Using Neural Network for Discretely Adjustable Energy-Intensive Load and Battery Energy Storage. IEEE Access 2020;8:5331–8. https://doi.org/10.1109/ACCESS.2019.2962814.

[79] Nikolovski S, Baghaee HR, Mlakic D. ANFIS-Based Peak Power Shaving/Curtailment in Microgrids Including PV Units and BESSs. Energies 2018;11. https://doi.org/10.3390/en11112953.

[80] Hwang JS, Fitri IR, Kim JS, Song H. Optimal ESS scheduling for peak shaving of building energy using accuracy-enhanced load forecast. Energies 2020;13. https://doi.org/10.3390/en13215633.

[81] Barzkar A, Hosseini SMH. A novel peak load shaving algorithm via real-time battery scheduling for residential distributed energy storage systems. Int J Energy Res 2018;42:2400–16. https://doi.org/10.1002/er.4010.

[82] Di Giorgio A, Liberati F, Lanna A, Pietrabissa A, Priscoli FD. Model Predictive Control of Energy Storage Systems for Power Tracking and Shaving in Distribution Grids. IEEE Trans Sustain Energy 2017;8:496–504. https://doi.org/10.1109/TSTE.2016.2608279.

[83] Karmiris G, Tengnér T. PEAK SHAVING CONTROL METHOD FOR ENERGY STORAGE n.d.:1–6.

[84] Danish SMS, Ahmadi M, Danish MSS, Mandal P, Yona A, Senjyu T. A coherent strategy for peak load shaving using energy storage systems. J Energy Storage 2020;32:101823. https://doi.org/10.1016/j.est.2020.101823.

[85] Hong Z, Wei Z, Li J, Han X. A novel capacity demand analysis method of energy storage system for peak shaving based on data-driven. J Energy Storage 2021;39:102617. https://doi.org/10.1016/j.est.2021.102617.

[86] Nasir T, Bukhari SSH, Raza S, Munir HM, Abrar M, Muqeet HAU, et al. Recent Challenges and Methodologies in Smart Grid Demand Side Management: State-of-the-Art Literature Review. Math Probl Eng 2021;2021. https://doi.org/10.1155/2021/5821301.

[87] Adika CO, Wang L. Smart charging and appliance scheduling approaches to demand side management. Int J Electr Power Energy Syst 2014;57:232–40. https://doi.org/10.1016/j.ijepes.2013.12.004.

[88] Yao E, Samadi P, Wong VWS, Schober R. Residential Demand Side Management Under High Penetration of Rooftop Photovoltaic Units. IEEE Trans Smart Grid 2016;7:1597–608. https://doi.org/10.1109/TSG.2015.2472523.

[89] Bhattacharjee A, Samanta H, Ghosh A, Mallick TK, Sengupta S, Saha H. Optimized Integration of Hybrid Renewable Sources with Long-Life Battery Energy Storage in Microgrids for Peak Power Shaving and Demand Side Management under Different Tariff Scenario. Energy Technol 2021;9:1–10. https://doi.org/10.1002/ente.202100199.

[90] Saffari M, de Gracia A, Fernández C, Belusko M, Boer D, Cabeza LF. Optimized demand side management (DSM) of peak electricity demand by coupling low temperature thermal energy storage (TES) and solar PV. Appl Energy 2018;211:604–16. https://doi.org/10.1016/j.apenergy.2017.11.063.

[91] Jo J, Park J. Demand-Side Management with Shared Energy Storage System in Smart Grid. IEEE Trans Smart Grid 2020;11:4466–76. https://doi.org/10.1109/TSG.2020.2980318.

[92] Lizondo D, Araujo P, Will A, Rodriguez S. Multiagent model for distributed peak shaving system with demand-side management approach. Proc - 2017 1st IEEE Int Conf Robot Comput IRC 2017 2017:352–7. https://doi.org/10.1109/IRC.2017.50.

[93] Shirazi E, Jadid S. Cost reduction and peak shaving through domestic load shifting and DERs. Energy 2017;124:146–59. https://doi.org/10.1016/j.energy.2017.01.148.

[94] Abbasi A, Khalid HA, Rehman H, Khan AU. A Novel Dynamic Load Scheduling and Peak Shaving Control Scheme in Community Home Energy Management System Based Microgrids. IEEE Access 2023;11:32508–22. https://doi.org/10.1109/ACCESS.2023.3255542.

[95] Debnath B, Biswas S, Uddin MF. Optimization of Electric Vehicle Charging to Shave Peak Load for Integration in Smart Grid. 2020 IEEE Reg 10 Symp TENSYMP 2020 2020:483–8. https://doi.org/10.1109/TENSYMP50017.2020.9231029.

[96] Leemput N, Geth F, Claessens B, Van Roy J, Ponnette R, Driesen J. A case study of coordinated electric vehicle charging for peak shaving on a low voltage grid. IEEE PES Innov Smart Grid Technol Conf Eur 2012:1–7. https://doi.org/10.1109/ISGTEurope.2012.6465656.

[97] Gerards MET, Hurink JL. Robust peak-shaving for a neighborhood with electric vehicles. Energies 2016;9. https://doi.org/10.3390/en9080594.

[98] Singh M, Thirugnanam K, Kumar P, Kar I. Real-time coordination of electric vehicles to support the grid at the distribution substation level. IEEE Syst J 2015;9:1000–10. https://doi.org/10.1109/JSYST.2013.2280821.

[99] Erdogan N, Erden F, Kisacikoglu M. A fast and efficient coordinated vehicle-to-grid discharging control scheme for peak shaving in power distribution system. J Mod Power Syst Clean Energy 2018;6:555–66. https://doi.org/10.1007/s40565-017-0375-z.

[100] Yao Y, Gao W, Li Y. Optimization of PHEV charging schedule for load peak shaving. IEEE Transp Electrif Conf Expo, ITEC Asia-Pacific 2014 - Conf Proc 2014:1–6. https://doi.org/10.1109/ITEC-AP.2014.6940718.

[101] Ramadan H, Ali A, Nour M, Farkas C. Smart Charging and Discharging of Plug-in Electric Vehicles for Peak Shaving and Valley Filling of the Grid Power. 2018 20th Int Middle East Power Syst Conf MEPCON 2018 - Proc 2018:735–9. https://doi.org/10.1109/MEPCON.2018.8635173.

[102] Ghotge R, Snow Y, Farahani S, Lukszo Z, van Wijk A. Optimized scheduling of EV charging in solar parking lots for local peak reduction under EV demand uncertainty. Energies 2020;13. https://doi.org/10.3390/en13051275.

[103] Van Kriekinge G, De Cauwer C, Sapountzoglou N, Coosemans T, Messagie M. Peak shaving and cost minimization using model predictive control for uni- and bi-directional charging of electric vehicles. Energy Reports 2021;7:8760–71. https://doi.org/10.1016/j.egyr.2021.11.207.

[104] Net metering n.d.

[105] Customer-Sited Renewable Energy Generation n.d. https://www.cpuc.ca.gov/industries-and-topics/electrical-energy/demand-side-management/net-energy-metering.

[106] Net Energy Metering: Understanding Your Bill n.d. https://www.sce.com/residential/generating-your-own-power/net-energy-metering/Understanding-Your-Bill.

[107] Dugan R. The Open Distribution System Simulator(OpenDSS). Sourceforge 2020:1–218.

[108] Novoa L, Flores R, Brouwer J. Optimal renewable generation and battery storage sizing and siting considering local transformer limits. Appl Energy 2019;256:113926. https://doi.org/10.1016/j.apenergy.2019.113926.

[109] Southern California Edison. Southern California Edison DRPEP 2019.

[110] Flores R, Houssainy S, Wang W, Joseph R, Cu KN, Polly B, et al. Developing and Tuning a Community Scale Energy Model for a Disadvantaged Community. Energy Build 2023:112861. https://doi.org/10.1016/j.enbuild.2023.112861.

[111] American wire gauge n.d. https://en.wikipedia.org/wiki/American_wire_gauge#cite_note-resperlength-11.

[112] MATLAB n.d. https://en.wikipedia.org/wiki/MATLAB.

[113] The MathWorks Inc. User ' s Guide R 2016 b 2016.

[114] Rebecca Linke. The real barriers to electric vehicle adoption 2017. https://mitsloan.mit.edu/ideas-made-to-matter/real-barriers-to-electric-vehicle-adoption.

[115] Barriers to Electric Vehicle Adoption in 2022 2022. https://www.exro.com/industry-insights/barriers-to-electric-vehicle-adoption-in-2022.

[116] NREL, CEC, Bedir A, Crisostomo N, Allen J, Wood E, et al. California Plug-In Electric Vehicle Infrastructure Projections: 2017-2025. 2018. https://doi.org/CEC-600-2018-001.

[117] National Household Travel Survey 2017. https://nhts.ornl.gov/.

[118] CNCDA. Comprehensive Information on the California Vehicle Market. vol. 19. 2023.

[119] Wang B, Hu B, Qiu C, Chu P, Gadh R. EV charging algorithm implementation with user price preference. 2015 IEEE Power Energy Soc Innov Smart Grid Technol Conf ISGT 2015 2015. https://doi.org/10.1109/ISGT.2015.7131895.

[120] Zero-Emission Vehicles Over the Years 2024. https://business.ca.gov/industries/zero-emission-vehicles/zev-timeline/.

[121] NREL, CEC, Bedir A, Crisostomo N, Allen J, Wood E, et al. California Plug-In Electric Vehicle Infrastructure Projections: 2017-2025. 2018.

[122] California ISO. Energy and environmental goals drive change. Tech Rep 2016:4.

[123] Nicholas M, Hall D, Lutsey N. Vehicle Charging Infrastructure Gap Across U.S. Markets. ICCT White Pap 2019. https://doi.org/10.13140/RG.2.2.22077.92647.

[124] California Energy Commission, NREL. CEC EVI-Pro 2019.

[125] Novoa L, Flores R, Brouwer J. Optimal DER allocation in meshed microgrids with grid constraints. Int J Electr Power Energy Syst 2021;128:106789.

[126] NREL. CEC EV Infrastructure Projection Tool (EVI-Pro) 2022. https://maps.nrel.gov/cec/?aL=0&bL=cdark&cE=0&lR=0&mC=36.87962060502676%2C-116.35620117187499&zL=6.

[127] Wang W, Flores R, Razeghi G, Brouwer J. Quantifying Transformer and Cable Degradation in Highly Renewable Electric Distribution Circuits. 2023 IEEE PES Grid Edge Technol. Conf. Expo. Grid Edge 2023, IEEE; 2023, p. 1–5. https://doi.org/10.1109/GridEdge54130.2023.10102733.

[128] Power Site Search Tool (PSST) n.d. https://www.sce.com/partners/consulting-services/power-requests.

[129] SCE. Time-Of-Use Residential Rate Plans n.d. https://www.sce.com/residential/rates/Time-Of-Use-Residential-Rate-Plans.

[130] DOE U. Electric Vehicle Registrations by State Last updated : June 2024 2024:2024.

[131] Zero-Emission Vehicle Sales Remain Strong in California 2024. https://www.energy.ca.gov/news/2024-05/zero-emission-vehicle-sales-remain-strong-california.

[132] Microgrids 2024. https://climate.mit.edu/explainers/microgrids.

[133] Paul Pabst. Challenges of Microgrid Deployment 2017. https://smartgrid.ieee.org/bulletins/february-2017/challenges-of-microgrid-deployment.

[134] Molderink A, Bakker V, Hurink JL, Smit GJM. Algorithms for balancing demand-side load and micro-generation in islanded operation. Proc 19th Int Conf Syst Eng ICSEng 2008 2008:115–20. https://doi.org/10.1109/ICSEng.2008.50.

[135] Lopes JAP, Moreira CL, Madureira AG. Defining control strategies for analysing microgrids islanded operation. 2005 IEEE Russ Power Tech, PowerTech 2005;21:916–24. https://doi.org/10.1109/PTC.2005.4524548.

[136] Chen C, Duan S, Cai T, Liu B, Hu G. Smart energy management system for optimal microgrid economic operation. IET Renew Power Gener 2011;5:258–67. https://doi.org/10.1049/iet-rpg.2010.0052.

[137] Foggia G, Christophe B, Conq P, Metivier N, Passelergue JC, Muscholl M, et al. Distributed control architecture for effective Distributed Energy Resources Management. CIGRE Sess 46 2016;2016-Augus.

[138] Pavan Kumar Y V., Bhimasingu R. Renewable energy based microgrid system sizing and energy management for green buildings. J Mod Power Syst Clean Energy 2015;3:1–13. https://doi.org/10.1007/s40565-015-0101-7.

[139] Wang C, Mei S, Dong Q, Chen R, Zhu B. Coordinated Load Shedding Control Scheme for Recovering Frequency in Islanded Microgrids. IEEE Access 2020;8:215388–98. https://doi.org/10.1109/ACCESS.2020.3041273.

[140] Vandoorn TL, Renders B, Degroote L, Meersman B, Vandevelde L. Active load control in islanded microgrids based on the grid voltage. IEEE Trans Smart Grid 2011;2:139–51. https://doi.org/10.1109/TSG.2010.2090911.

[141] Drude L, Pereira Junior LC, Rüther R. Photovoltaics (PV) and electric vehicle-to-grid (V2G) strategies for peak demand reduction in urban regions in Brazil in a smart grid environment. Renew Energy 2014;68:443–51. https://doi.org/10.1016/j.renene.2014.01.049.

[142] Flores R, Houssainy S, Wang W, Robertson J, Cu KN, Polly B, et al. Developing and Tuning a Community Scale Energy Model for a Disadvantaged Community. Submitt to Appl Energy 2022.

[143] Flores R, Houssainy S, Wang W, Cu KN, Nie X, Woolfolk N, et al. Addressing Building Related Energy Burden, Air Pollution, and Carbon Emissions of a Low-Income Community in Southern California. Adv Appl Energy 2024;14:100169. https://doi.org/10.1016/j.adapen.2024.100169.

[144] Flores RJ, Brouwer J. Optimal design of a distributed energy resource system that economically reduces carbon emissions. Appl Energy 2018;232:119–38.

https://doi.org/10.1016/j.apenergy.2018.09.029.

[145] IEEE C57.91™-2011. IEEE Guide for Loading Mineral-Oil-Immersed Transformers and Step-Voltage Regulators - Redline. vol. 2011. 2012.

[146] Razeghi G, Zhang L, Brown T, Samuelsen S. Impacts of plug-in hybrid electric vehicles on a residential transformer using stochastic and empirical analysis. J Power Sources 2014;252:277–85. https://doi.org/10.1016/j.jpowsour.2013.11.089.

[147] Kumar K, Kumbhar GB. A review on impact of distributed generation and electrical vehicles on aging of distribution transformer. 2017 3rd Int Conf Cond Assess Tech Electr Syst CATCON 2017 - Proc 2018;2018-Janua:283–8. https://doi.org/10.1109/CATCON.2017.8280229.

[148] Kumar K, Kumbhar GB. The effect of solar power injection on aging of a distribution transformer. 2017 6th Int Conf Comput Appl Electr Eng - Recent Adv CERA 2017 2018;2018-Janua:242–6. https://doi.org/10.1109/CERA.2017.8343334.

[149] Godina R, Rodrigues EMG, Matias JCO, Catalão JPS. Effect of loads and other key factors on oil-transformer ageing: Sustainability benefits and challenges. vol. 8. 2015. https://doi.org/10.3390/en81012147.

[150] Gray MK, Morsi WG. On the impact of single-phase plug-in electric vehicles charging and rooftop solar photovoltaic on distribution transformer aging. Electr Power Syst Res 2017;148:202–9. https://doi.org/10.1016/j.epsr.2017.03.022.

[151] El-Bataway SA, Morsi WG. Distribution Transformer's Loss of Life Considering Residential Prosumers Owning Solar Shingles, High-Power Fast Chargers and Second-Generation Battery Energy Storage. IEEE Trans Ind Informatics 2019;15:1287–97. https://doi.org/10.1109/TII.2018.2845416.

[152] Singh P, Meena NK, Yang J, Vega-Fuentes E, Bishnoi SK. Multi-criteria decision making monarch butterfly optimization for optimal distributed energy resources mix in distribution networks. Appl Energy 2020;278:115723. https://doi.org/10.1016/j.apenergy.2020.115723.

[153] Palmintier B, Krishnamurthy D, Wu H. Design flexibility for uncertain distributed generation from photovoltaics. 2016 IEEE Power Energy Soc Innov Smart Grid Technol Conf ISGT 2016 2016. https://doi.org/10.1109/ISGT.2016.7781196.

[154] Fei W, Moses P. Fault current tracing and identification via machine learning considering distributed energy resources in distribution networks. Energies 2019;12:1–12. https://doi.org/10.3390/en12224333.

[155] Abdulsalam S. Alghamdim RKD. A study of expected lifetime of XLPE insulation cables working at elevated temperatures by applying accelerated thermal ageing 2020. https://doi.org/10.1016/j.heliyon.2019.e03120.

[156] Bartos M, Chester M, Johnson N, Gorman B, Eisenberg D, Linkov I, et al. Impacts of rising air temperatures on electric transmission ampacity and peak electricity load in the United States. Environ Res Lett 2016;11. https://doi.org/10.1088/1748-9326/11/11/114008.

[157] California Energy Commission. CA Rule 21 Smart Inverter Update 2014.

[158] Whitesides RW. Process Equipment Estimating by Ratio and Proportion. Course Notes, PDH

Course G 2012;127:1–8.

[159] National Fire Protection Association. 1965 NFPA Advance Report Volume 2. Poult Sci 1965;54:2138. https://doi.org/10.3382/ps.0542138b.

[160] How much do solar panels cost in 2024? 2024. https://www.consumeraffairs.com/solar-energy/how-much-do-solar-panels-cost.html.

[161] Zhu W, Shi J, Liu S, Abdelwahed S. Development and application of a model-based collaborative analysis and design framework for microgrid power systems. IET Gener Transm Distrib 2016;10:3201–10. https://doi.org/10.1049/iet-gtd.2015.1295.

[162] Wang Y, Liu P, Liu D, Deng F, Chen Z. Enhanced Hierarchical Control Framework of Microgrids with Efficiency Improvement and Thermal Management. IEEE Trans Energy Convers 2021;36:11–22. https://doi.org/10.1109/TEC.2020.3002670.

[163] Silani A, Yazdanpanah MJ. Distributed Optimal Microgrid Energy Management With Considering Stochastic Load. IEEE Trans Sustain Energy 2019;10:729–37. https://doi.org/10.1109/TSTE.2018.2846279.

[164] Taft J. Electric Grid Resilience and Reliability for Grid Architecture. Pacific Northwest Natl Lab 2017:16.

[165] Taft JD. Advanced Networking Paradigms for High-DER Distribution Grids 2016:18.

[166] Taft JD. Architectural Basis for Highly Distributed Transactive Power Grids: Frameworks, Networks, and Grid Codes 2016.

[167] Taft JD. Architectural Framework for Variable Structure Grids 2021.

[168] Taft J. Control of Embedded Bulk Electric Storage Networks for Operational Flexibility and Grid Resilience 2021.

[169] Taft J, Kristov L, De Martini P. A Reference Model for Distribution Grid Control in the 21st Century 2015.

[170] Huang R. Distribution Storage Networks 2017.

[171] De Martini P, Taft J. Value Creation Through Integrated Networks and Convergence 2015.

[172] Santos AQ, Ma Z, Olsen CG, Jørgensen BN. Framework for microgrid design using social, economic, and technical analysis. Energies 2018;11. https://doi.org/10.3390/en11102832.

[173] Gao K, Wang T, Han C, Xie J, Ma Y, Peng R. A review of optimization of microgrid operation. Energies 2021;14:1–39. https://doi.org/10.3390/en14102842.

Appendix A

Transformer ratings required for stable and reliable electrical distribution service across the Oak View community.

Transformer Name	Transformer Rating (kVa)	Transformer Name	Transformer Rating (kVa)	Transformer Name	Transformer Rating (kVa)
S1	75	S24	50	T2	50
S2	25	S25	37.5	T3	150
S3	25	S26	25	T4	150
S4	50	S27	25	T5	150
S5	25	S28	50	T6	75
S6	75	S29	50	T7	1500
S7	50	S30	50	T8	25
S8	50	S31	25	T9	150
S9	50	S32	25	T10	100
S10	100	S33	100	T11	300
S11	100	S34	50	T12	50
S12	50	S35	50	T13	350
S13 & S14	150	S36	25	T14	75
S15	50	S37	100	T15	50
S16	100	S38	50	T16	150
S17	25	S39	50	T17	25
S18	112.5	S40	25	T18	300
S19	50	S41	25	T19	25
S20	37.5	S42	50	T20	300
S21	50	S43	25	T21	150
S22	50	S44	112.5		
S23	50	T1	50		


Warner Avenue
Southlake Drive
Fir Drive
Sycamore Avenue
Belsito Drive
Cypress Avenue
Mandrell Drive
Barton Drive
Slater Avenue
Beach Boulevard
Central Baptist Church
Major Fox Orthodontics
Quality Inn & Suites Huntington Beach
CA-39
100
80
60
40
20
0
Loss of Life (%/Year)

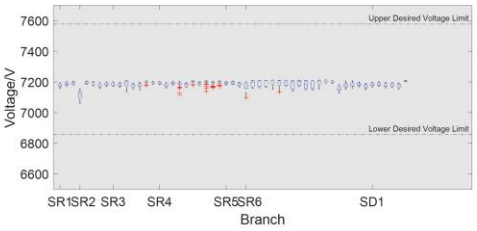
Upper Desired Voltage Limit
Lower Desired Voltage Limit
Voltage/V
7600
7400
7200
7000
6800
6600
SR1
SR2
SR3
SR4
SR5
SR6
SD1
Branch

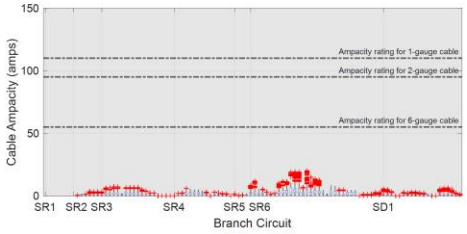
Ampacity rating for 1-gauge cable
Ampacity rating for 2-gauge cable
Ampacity rating for 6-gauge cable
Cable Ampacity (amps)
150
100
50
0
SR1
SR2
SR3
SR4
SR5
SR6
SD1
Branch Circuit

Appendix B

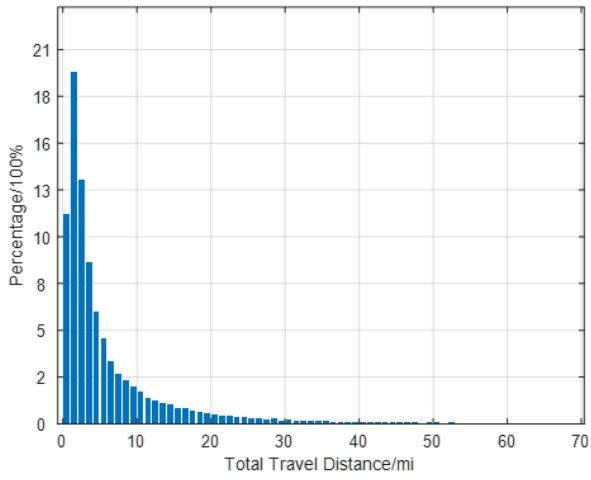

Weekday

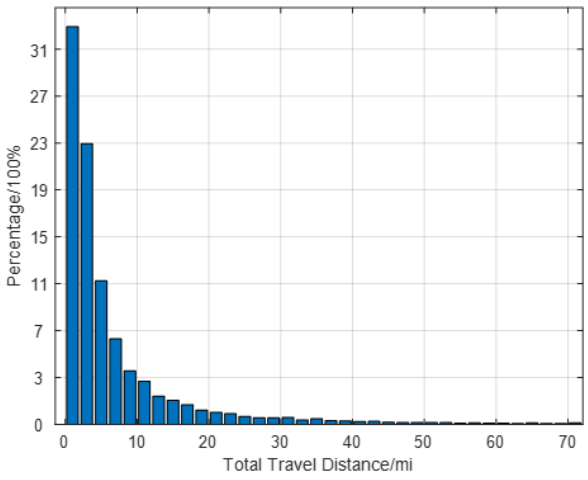

Weekend

EV traveling distances for weekdays and weekend. The figure is generated with data acquired from NHTS.

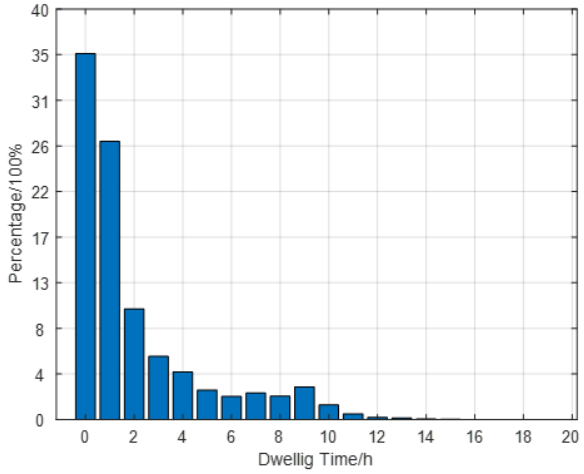

Weekday

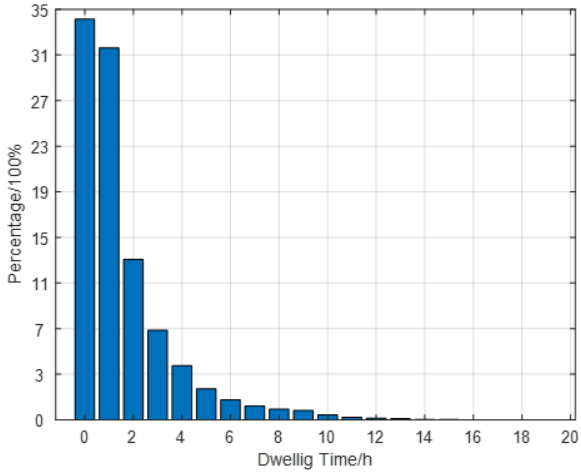

Weekend

EV dwelling time at the destination for weekdays and weekend. The figure is generated with data acquired from NHTS.

Appendix C

$P_{Import,t,b} + P_{PVelec,t,b} + P_{EES\ dch,t,b} + P_{REES\ dch,t,b} = P_{BLDG\ elec,t,b} + P_{EES\ ch,t,b}$ $Q_{Import,t,b} = Q_{BLDG,t,b} = P_{BLDG\ elec,t,b} \tan(PF)$	**Energy balance (Active and Reactive Power) within each building *b***
$P_{Import,t,b} \leq P_{max,n,b}$ $P_{Import,o,b} \leq P_{on\ max,m,b}$ $P_{Import,p,b} \leq P_{mid\ max,m,b}$ • $n \in N$: Set of all months • $m \in M$: Set of all summer months ($M \subset N$) • $t \in T_n$: Set of all hourly increments in month n • $o \in O_m$: Set of all hourly increments during on-peak in summer month m ($O \subset T$) • $p \in P_m$: Set of all hourly increments during mid-peak in summer month m ($P \subset T$) • $k \in K$: Set of all generator types • $b \in B$: Set of all buildings	**Non-TOU and TOU demand charges**
$P_{Import,t,b} + P_{PV\ elec,t,b} + P_{PVwsale,t,b} + P_{PV\ NEM,t,b} + P_{REES\ chrg,t,b} \leq \sum_k P_{solar,t}\ P_{max\ PV,k,b}$ $\sum_k P_{max\ PV,k,b}/\eta_{PV,k} \leq P_{max,n,b}$	**Solar PV adoption**
$e_{EES\ SOC,t,b} = \alpha_{EES} e_{EES\ SOC,t-1,b} + \eta_{EES\ chrg} e_{EES\ chrg,t,b} - \frac{P_{EES\ dchrg,t,b}}{\eta_{EES\ dchrg}}$ $\underline{\delta}_{EES} E_{EES,b} \leq e_{EES\ SOC,t,b} \leq \bar{\delta}_{EES} E_{EES,b}$ $P_{EES\ dchrg,t,b} \leq \bar{\mu}_{EES} E_{EES,b}$ $P_{EES\ chrg,t,b} \leq \underline{\mu}_{EES} E_{EES,b}$	**EES/REES adoption**
$\sum_t C_{NEMt,b} * (P_{PV\ NEM,t,b} + P_{REES\ NEM\ dchrg,t,b}) \leq \sum_t C_{grid,t,b} * P_{Import,t,b}$	**NEM revenue constraint**
$\sum_{t,b} P_{PV\ NEM,t,b} + P_{PV\ NEM,t,b} + P_{REES\ NEM\ dchrg,t,b} \leq \sum_{t,b} P_{Import,t,b}$	**Zero-Net Energy**

DERopt calculations. Source: RJF